

UCSF

UC San Francisco Electronic Theses and Dissertations

Title

Characterizing Magnetic Resonance Relaxation Times in the Extracellular Matrix in Osteoarthritis and Degenerative Disc Disease

Permalink

<https://escholarship.org/uc/item/4sh1n81r>

Author

Blumenkrantz, Gabrielle

Publication Date

2009

Peer reviewed|Thesis/dissertation

**Characterizing Magnetic Resonance Relaxation Times in the Extracellular
Matrix in Osteoarthritis and Degenerative Disc Disease**

by

Gabrielle Blumenkrantz

DISSERTATION

Submitted in partial satisfaction of the requirements for the degree of

DOCTOR OF PHILOSOPHY

in

Bioengineering

in the

GRADUATE DIVISION

of the

UNIVERSITY OF CALIFORNIA, SAN FRANCISCO

AND

UNIVERSITY OF CALIFORNIA, BERKELEY

Copyright 2009

by

Gabrielle Blumenkrantz

Acknowledgements

I would like to express my deepest gratitude to my advisors, Dr. Sharmila Majumdar and Dr. Thomas Link. It has been a privilege to learn from you both and to be a part of your research group.

I would like to thank Dr. Sharmila Majumdar for being my mentor and my inspiration. I am grateful for your wisdom, knowledge, continuous support, and friendship.

I would like to thank Dr. Thomas Link for his insightful guidance, encouragement, and cheerful enthusiasm. Thank you for believing in me.

I would like to thank Dr. Dan Vigneron for being an incredible qualifying exam chair. Your advice and insight were invaluable for my project.

I would like to thank Dr. Sarah Nelson for being my graduate advisor. Thank you for guidance and support on my project and for helping me choose classes.

I would like to thank Dr. Xiaojuan Li for being my teacher and friend. I was only able to learn T_{1p} through her insightful discussions.

I would like to thank Dr. Julio Carballido-Gamio for helping me prepare for my qualifying exam and for his hard work on all of our projects together. His work ethic and dedication is incredibly inspiring.

I would like to thank Dr. Janet Goldenstein for being an amazing friend and research partner. Thank you for working with me on our problem sets and classwork, for being my quals-partner, for listening and sharing with me, and for being a fellow Blumen-girl.

I would like to thank my lab group, especially Dr. Roland Krug, Dr. Galateia Kazakia, Dr. Suchandrima Banerjee, Andy Burghardt, Miki Sode, Karl Saldanha, Ana

Rodriguez, Rich Souza, Radu Bolbos, Dimitrios Karampinos, and Jin Zuo for helping me with my projects and for making day-to-day research life enjoyable.

I would like to thank Dr. Ying Lu, Dr. Chuck McCulloch, and Dr. John Kornak for their guidance with statistical analysis.

I would like to thank Dr. Steve Conolly for being an inspiring teacher and mentor.

I would like to thank Niles Bruce and Greg Corrales all their help with MR scanning.

I would like to thank my best friends Laura Perlin, Michal Shein, and Mabel Zelaya for always being there for me. I am incredibly grateful for having such wonderful and caring friends.

I would like to thank my parents, Azary and Clara Blumenkrantz, and my brother, Mark Blumenkrantz, for their loving support, for teaching me the value of hard work, teaching me how to think for myself, and inspiring me to be the best I can be.

I would like to thank my fiancé, Josh Joseph, for his unconditional love and support. Thank you for standing by me, making me smile, encouraging me, challenging me, understanding me, and believing in me. I love you.

Grant funding for this thesis was provided by NIH grants F31 EB006708, R01 AG17762, and RO1 AR 46905.

Characterizing Magnetic Resonance Relaxation Times in the Extracellular Matrix in Osteoarthritis and Degenerative Disc Disease

Gabrielle Blumenkrantz

Abstract

The extracellular matrix (ECM) is a network of extracellular macromolecules that is present in both cartilage and intervertebral disc tissues. While both cartilage and intervertebral disc tissues are comprised of an ECM, their form and structure vary. Likewise, each tissue has unique characteristics during degeneration. This project will investigate the non-invasive detection of early degenerative changes of cartilage and disc tissues in osteoarthritis (OA) and intervertebral disc degeneration (IVDD) using novel magnetic resonance imaging methods.

OA is a debilitating disease causing pain, stiffness, and loss of mobility to approximately 14% of the adult population. IVDD is the leading cause of pain and disability in adults in the United States. Despite the high prevalence of OA and IVDD worldwide, diagnosis in the early stages of symptomatic disease, prior to morphologic degradation, is elusive in clinical practice. Certain quantitative MRI methods, including $T_{1\rho}$ and T_2 relaxation time mapping, are sensitive to biochemical changes in the ECM, and thus may be valuable for early diagnosis of intervertebral disc and cartilage degeneration.

The overall purpose of my dissertation is to develop a methodology for the quantification of $T_{1\rho}$ and T_2 magnetic resonance relaxation times in the intervertebral disc and knee cartilage, and characterize the spatial distribution of $T_{1\rho}$ and T_2 in the extracellular matrix in IVDD and OA.

The first portion of this dissertation focuses on the methodology for MR relaxation time mapping. This study evaluated the impact of signal to noise ratio and T_2 fitting algorithms on the T_2 quantification. Simulations were performed determine the minimum SNR that can be used to distinguish healthy cartilage from degenerative cartilage. In addition, various fitting algorithms (noise correction vs. no noise correction) were assessed to determine whether their impact on the accuracy of T_2 quantification.

The second dissertation study examined the relationship between structural changes of trabecular bone and cartilage in patients with varying degrees of OA over two years, using MR imaging. A positive relationship was established between cartilage changes and localized bone changes closest to the joint line, while a negative relationship was established between cartilage changes and global bone changes farthest from the joint line. This study demonstrated a longitudinal relationship between the changes in bone and cartilage structure in patients with varying degrees of OA.

The third dissertation study evaluated the mean and spatial distribution of cartilage T_2 in subjects with and without OA. The mean T_2 values, their standard deviation, and their entropy were greater in OA patients than in controls, indicating that the T_2 values in osteoarthritic cartilage are not only elevated, but also more heterogeneous than those in healthy cartilage. The longitudinal results demonstrate that changes in texture parameters of cartilage T_2 may precede morphological changes in thickness and volume in the progression of OA.

The fourth dissertation study focused on the longitudinal changes in the spatial distribution of cartilage T_2 values in subjects with OA. This study evaluated both the morphologic and biochemical changes in cartilage using MR imaging as well as clinical data

from the OAI. Entropy of cartilage T_2 at baseline (all compartments combined except the lateral tibia) was associated with an increase in WOMAC pain score over 2 years. This study demonstrated that the baseline heterogeneity of cartilage T_2 is associated with changes in clinical pain scores.

The fifth dissertation study assessed the feasibility of quantifying $T_{1\rho}$ relaxation time for the non-invasive detection of disc degeneration. The *in vivo* results indicated that the median $T_{1\rho}$ value of the nucleus is significantly greater than that of the annulus. The results of this study suggest that *in vivo* $T_{1\rho}$ quantification is feasible and may potentially be a clinical tool to identify early degenerative changes in the intervertebral disc.

The sixth dissertation study built upon the results from the fifth study by evaluating $T_{1\rho}$ and T_2 in subjects with varying degrees of disc degeneration. A positive relationship was evident between MR parameters and clinical questionnaire scores and a negative relationship was evident between degenerative grade and relaxation time. This study suggests that $T_{1\rho}$ relaxation time may be sensitive to early degenerative changes and clinical symptoms in intervertebral disc degeneration.

The results of this project suggest that quantifying the spatial distribution of MRI relaxation times improves the clinical assessment of IVDD and OA, by providing a non-invasive evaluation of biochemical composition in the intervertebral disc and cartilage tissues. $T_{1\rho}$ and T_2 relaxation times are not only sensitive to biochemical changes in OA and IVDD, they are also related to the clinical assessment of pain.

Table of Contents

Chapter 1: Introduction	1
1.1 Motivation	1
1.2 Thesis Aims	2
1.3 References	4
Chapter 2: Background [1]	5
2.1 Structure of the Knee Joint	5
2.2 Osteoarthritis	6
2.2.1 Prevalence and Risk Factors.....	6
2.2.2 Diagnosis of OA	7
2.2.3 Treatment of OA.....	7
2.2.4 Cartilage Degeneration in OA.....	8
2.2.5 Bone Changes in OA.....	11
2.2.5.1 OA Bone: Matrix Level.....	12
2.2.5.2 OA Bone: Matrix Level Mechanical Properties	12
2.2.5.3 OA Bone: Apparent Level.....	14
2.2.5.4 OA Bone: Apparent Level Mechanical Properties	17
2.3 Structure of the Intervertebral Disc	19
2.4 Degenerative Disc Disease	20
2.5 References	22
Chapter 3: Background [2]	27
3.1 Fundamentals of Magnetic Resonance Imaging	27
3.2 Overview of Magnetic Resonance Relaxation Time	29
3.3 Overview of Texture Analysis	31
3.4 Review of Literature: Imaging of Cartilage in OA	32
3.4.1 Radiography	32
3.4.2 Magnetic Resonance Imaging.....	33
3.4.3 Cartilage Volume and Thickness.....	33
3.4.4 Cartilage T_2 Relaxation Time.....	37
3.4.4.1 In Vitro Imaging	38
3.4.4.2 In Vivo Imaging	39
3.4.5 Cartilage $T_{1\rho}$ Relaxation Time	43
3.5 Review of Literature: Imaging of Degenerative Disc Disease	47
3.5.1 Current Clinical Imaging Techniques	47
3.5.2 Magnetic Resonance Relaxation Time Measurement.....	47
3.6 References	49
Chapter 4: Development of a Methodology for T_2 Relaxation Fitting for Cartilage Imaging at 3 Telsa	63
4.1 Introduction	63
4.2 Impact of Signal to Noise Ratio on T_2 Fitting	64
4.2.1 Simulations	64
4.2.2 Results.....	65
4.3 Fitting Techniques	70
4.3.1 Image Analysis.....	70
4.3.2 Impact of Fitting Routine on T_2 Calculation.....	71
4.3.3 Statistical Analysis	72
4.3.4 Results.....	72

4.4 Discussion and Conclusion.....	75
4.5 References	75
Chapter 5: A Pilot, Two-Year Longitudinal Study of the Interrelationship between Trabecular Bone and Articular Cartilage in the Osteoarthritic Knee.....	77
5.1 Introduction.....	77
5.2 Methods	78
5.2.1 Subjects.....	78
5.2.2 Magnetic Resonance Imaging.....	80
5.2.3 Image Analysis.....	81
5.2.4 Statistical Analysis	84
5.3 Results.....	86
5.3.1 Patient Characteristics	86
5.3.2 Cartilage and Bone Structure Parameters.....	86
5.3.3 Cartilage T ₂	89
5.3.4 Correlations Between Cartilage and Bone Structure	90
5.4 Discussion and Conclusion.....	92
5.5 References	96
Chapter 6: The Feasibility of Characterizing the Spatial Distribution of Cartilage T₂ using Texture Analysis	101
6.1 Introduction.....	101
6.2 Methods	102
6.2.1 Subjects.....	102
6.2.2 Magnetic Resonance Imaging.....	102
6.2.3 Image Analysis.....	103
6.2.4 Statistical Analysis:.....	105
6.3 Baseline Results.....	106
6.3.1 Baseline Patient Characteristics	106
6.3.2 Baseline T ₂ and Texture Analysis.....	106
6.3.3 Correlations Between Measurements	109
6.3.4 WOMBS Scoring	109
6.4 Longitudinal Results	110
6.4.1 Mean and standard deviation of cartilage T ₂	110
6.4.2 Cartilage Thickness and Volume.....	111
6.4.3 Texture Analysis	112
6.5 Discussion and Conclusion.....	113
6.6 References	118
Chapter 7: Longitudinal Changes in the Spatial Distribution of Cartilage MR T₂ in a Subset of Patients from the Osteoarthritis Initiative	121
7.1 Introduction.....	121
7.2 Methods	122
7.2.1 Subjects.....	122
7.2.2 Clinical Assessment.....	122
7.2.3 Magnetic Resonance Imaging.....	122
7.2.3 Image Analysis.....	122
7.2.4 Statistical Analysis	124
7.3 Results.....	124
7.3.1 Cartilage Thickness	124
7.3.2 Cartilage T ₂	125

7.3.3 Texture Analysis of Cartilage T_2	125
7.4 Discussion and Conclusion.....	126
7.5 References	126
Chapter 8: A Feasibility Study of In Vivo Magnetic Resonance $T_{1\rho}$ Imaging of the Intervertebral Disc.....	129
8.1 Introduction.....	129
8.2. Materials and Methods.....	132
8.2.1 Phantom Design.....	132
8.2.2 Human Subjects.....	132
8.2.3. Magnetic Resonance Imaging.....	132
8.2.4. Image Analysis.....	133
8.2.5. Reproducibility.....	134
8.2.6. Statistical Analysis.....	135
8.3. Results.....	136
8.3.1. Phantom.....	136
8.3.2. In Vivo.....	137
8.4 Discussion and Conclusion.....	139
8.5 References.....	142
Chapter 9: In Vivo 3.0 Tesla Magnetic Resonance $T_{1\rho}$ and T_2 Relaxation Mapping in Subjects with Intervertebral Disc Degeneration and Clinical Symptoms	146
9.1 Introduction.....	146
9.2 Methods.....	148
9.2.1 Subjects.....	148
9.2.2 Magnetic Resonance Imaging.....	149
9.2.3 Image Analysis.....	149
9.2.4 Statistical Analysis.....	151
9.3 Results.....	152
9.3.1 T_2 and $T_{1\rho}$ versus Pfirrmann Grade.....	152
9.3.2 MR Parameters Versus Clinical Findings.....	156
9.3.3 T_2 and $T_{1\rho}$ by Disc Level.....	157
9.4 Discussion and Conclusion.....	158
9.5 References:.....	163
Chapter 10: Summary and Conclusions	167
10.1 Summary.....	167
10.2 Conclusions.....	167
10.2.1 MR Relaxation Time Mapping Technique Development.....	167
10.2.2 MR T_2 Relaxation Time Mapping in Osteoarthritis.....	167
10.2.3 MR T_2 and $T_{1\rho}$ Relaxation Time Mapping in Degenerative Disc Disease.....	170
10.3 Future Directions.....	172

List of Figures

Figure 2.1: Anatomy of the knee joint	5
Figure 2.2: An Illustration of the cartilage extracellular matrix	9
Figure 2.3: An Illustration of the zonal pattern in cartilage.....	9
Figure 2.4: An MR image of healthy cartilage and disease cartilage	10
Figure 2.5: An illustration of a “normal” knee and a knee with OA.	11
Figure 2.6: The differences between bone on the matrix and apparent levels.....	12
Figure 2.7: An illustration of the structure of the intervertebral disc.	20
Figure 3.1: An illustration of the precession.....	28
Figure 3.2: An illustration of the net magnetization which is initially in the z axis (longitudinal plane) and then in the XY plane (transverse plane) following excitation.....	29
Figure 3.3: An example of femoral and tibial cartilage segmentation. This image was acquired at 1.5T with an in-plane resolution of $0.234 \times 0.234 \text{ mm}^2$ and a slice thickness of 2 mm.	34
Figure 3.4: An example of femoral cartilage thickness map demonstrating the variation in cartilage thickness throughout the femur.....	35
Figure 3.5: An example of T_2 calculation using four T_2 -weighted images acquired with different echo-times (TE). The graph shows signal (S) as a function of time. T_2 is calculated for each pixel in an image using the above equation, and is defined as the time at which the signal decays to 37% of the maximum signal.....	37
Figure 3.6: Representative Z-score maps a control, a mild OA subject, and a severe OA subject. The maps show an increase in area of regions of high in the OA subjects. The regional variations in femoral and tibial cartilage compared to control subjects are also evident.....	41
Figure 3.7: $T_{1\rho}$ maps (first row) and T_2 maps (second row) for a healthy control (a), a patient with mild OA (b), and a patient with severe OA (c). a) Control: The average $T_{1\rho}$ value was $40.1 \pm 11.4 \text{ ms}$ and T_2 values was $33.3 \pm 10.5 \text{ ms}$ in cartilage. (b) A patient with early OA (male, 66). The average $T_{1\rho}$ value was $45.5 \pm 14.5 \text{ ms}$ and T_2 values was $35.0 \pm 10.9 \text{ ms}$ in cartilage. (c) A patient with advanced OA (male, 46). The average $T_{1\rho}$ value was $55.4 \pm 26.0 \text{ ms}$ and T_2 values was $43.8 \pm 11.1 \text{ ms}$ in cartilage. The maps illustrate the differences between $T_{1\rho}$ and T_2 (arrows) and demonstrate differences in cartilage heterogeneity between OA severity and between T_2 and $T_{1\rho}$ maps.....	46
Figure 4.1: An illustration of the relationship between SNR of the first echo and calculated T_2 with TE = 10-70. The minimum SNR that can distinguish a healthy and degenerative cartilage pixel (accounting for error) is approximately 21.	66
Figure 4.2: An illustration of the relationship between SNR of the first echo and calculated T_2 with TE = 10-60. The minimum SNR that can distinguish a healthy from a degenerative cartilage pixel (accounting for error) is approximately 23.	67

Figure 4.3: An illustration of the relationship between SNR of the first echo and calculated T_2 with TE = 10-50. The minimum SNR that can distinguish a healthy from a degenerative cartilage pixel (accounting for error) is approximately 25. 68

Figure 4.4: An illustration of the relationship between SNR of the first echo and calculated T_2 with TE = 10-70, in an ROI. The ROI consists of 200 pixels. The minimum SNR that can be used to calculate accurate T_2 values and distinguish healthy cartilage from degenerative cartilage is about 15..... 69

Figure 4.5: The standard deviation of T_2 values calculated per pixel, and calculated per ROI that consists of 200 pixels. The standard deviation is much lower when evaluating T_2 values averaged over 200 pixels. 70

Figure 4.6: An illustration of the segmented cartilage regions..... 71

Figure 4.7: An illustration of the T_2 values in each patient calculated the two fitting routines (no noise correction, noise correction)..... 73

Figure 4.8: An illustration of the RMSE values in each patient calculated using the two fitting algorithms (no noise correction, noise correction). The graph demonstrates that the RMSE's are lower using the noise correction algorithm, demonstrating a greater goodness of fit..... 74

Figure 4.9: An illustration of the mean adjusted R^2 values in each patient calculated using the two fitting algorithms (no noise correction, noise correction). The graph demonstrates that most of the RMSE's are lower (12/13) using the T_2 fitting algorithm without noise correction. 74

Figure 5.1: A tree diagram of OA subject characteristics at baseline..... 80

Figure 5.2: A high-resolution, axial image acquired for assessing trabecular bone structure, using a 3-D fast gradient echo sequence (TE = 4.5 ms, TR = 30 ms, flip angle = 40°, resolution = .195 x .195 x 1 mm³, FOV = 10 cm, scan time = 18:26 minutes). The epicondylar distance is labeled. 81

Figure 5.3: A graphical representation of the segmented bone and cartilage regions. The femur (FM, blue), tibia (TB, yellow), medial condyle (MC, green), lateral condyle (LC, turquoise), medial tibia (MT, pink), lateral tibia, (LT, orange) and cartilage compartments (red) are shown. 82

Figure 5.4: A Comparison of OA1 and OA2 mean bone and cartilage parameters over two years. The graphs show (1) a decrease in mean apparent trabecular number (app. Tb.N) of the femur, (2) a decrease in mean app. Tb.N of the medial condyle, and (3) a decrease in medial and lateral tibial normalized cartilage volume over two years. 87

Figure 5.5: A comparison of mean T_2 values (\pm one standard deviation) across twelve patients in the knee cartilage compartments at baseline and follow-up. The T_2 was observed to significantly ($p < 0.05$) increase over time for all compartments except the lateral tibia. Mean T_2 values for three normal volunteers (standard deviations are listed in the table) are shown for qualitative comparison, and are lower in all cases except the baseline scan of the medial tibia..... 89

Figure 6.1: Representative T_2 colormaps overlaid on T_2 -weighted images of an advanced OA patient (cartilage WOMMS = 5) (left), a mild OA patient (cartilage WOMMS = 1) (center), and a control subject (right). The entropy and ASM of cartilage T_2 for the OA patients and control subject are listed in the table. The OA patients both have greater entropy and lower ASM than the control subject..... **107**

Figure 6.2: Entropy (top row) of cartilage T_2 is greater in OA patients than in controls in all compartments combined, and the lateral and medial tibia at 0 degrees (top left) and 90 degrees (top left). ASM (bottom row) of cartilage T_2 greater in controls than in OA patients in all compartments combined and the lateral and medial tibia at 0 degrees (bottom left) and 90 degrees (bottom right)..... **108**

Figure 6.3: Increased ($p < 0.10$) cartilage T_2 ASM was evident in OA patients from baseline to 9 months. Decreased ($p < 0.10$) cartilage T_2 entropy was evident in OA patients from baseline to 9 months..... **112**

Figure 6.4: Sagittal T_2 -weighted FSE images (top row) and cartilage T_2 maps overlaid on T_2 -weighted FSE images (bottom row) of an OA patient at baseline and 9 months. At baseline, the cartilage signal at the posterior lateral tibia (arrow) is inhomogeneous (a) and at 9 months, an extensive cartilage defect with a more homogeneous signal has developed in the same area (arrow in (b)). An extensive adjacent bone marrow edema pattern is also evident. Visually, there is a decrease in the heterogeneity of T_2 values from baseline to follow-up. **115**

Figure 7.1: A representative T_2 map overlaid on the first echo ($TE = 10$ ms) of the MSME sequence..... **123**

Figure 7.2: A model illustrating the effect of baseline entropy of cartilage T_2 on changes in WOMAC pain over time..... **125**

Figure 8.1:Diagram of $T_{1\rho}$ imaging sequence..... **133**

Figure 8.2: a, left) A histogram of the nucleus and annulus b, right) representation of the segmented nucleus (inner circle) and annulus (outer circle). **134**

Figure 8.3: Three phantoms with different agarose concentrations, scanned at three different positions along the coil. **135**

Figure 8.4: a, left) SNR in a phantom as a function of distance from the surface of the coil. The range of 60-100 mm represents the approximate position of the intervertebral disc. b, right) $T_{1\rho}$ in a phantom as a function of distance away from the coil. The shaded region represents the median $T_{1\rho} \pm$ standard deviation. The $T_{1\rho}$ values are within one standard deviation of the median $T_{1\rho}$ value of the phantom **136**

Figure 8.5. Axial $T_{1\rho}$ map and axial $T_{1\rho}$ color map of the intervertebral disc. **137**

Figure 8.6: $T_{1\rho}$ values of the nucleus and annulus ($n = 11, 33$ discs, 3 from each subject). **138**

Figure 9.1: An illustration of the $T_{1\rho}$ fitting and quantification procedure. First, sagittal images for $T_{1\rho}$ mapping were acquired, and $T_{1\rho}$ maps were created on a pixel-by-pixel basis. A representative $T_{1\rho}$ map is shown. Median $T_{1\rho}$ and T_2 values were calculated in 5-mm diameter regions of interest (ROI's) that were drawn manually in the center of the nucleus in discs L5/S1, L4/L5, L3/L4, L2/L3, and L1/L2 in each subject. A $T_{1\rho}$ colormap of the intervertebral discs in a healthy subject is shown. T_2 maps were created analogously. **151**

Figure 9.2: Representative $T_{1\rho}$ colormaps from 2A) a 24-year old subject with non-degenerated discs (Pfirrmann Grades L5/S1=1, L5/L4=1, L4/L3 = 1, L3/L2 =1; L2/L1 = 2) and an Oswestry Disability Index (O.D.I) score of 0; 2B) a 32-year old subject with mildly degenerated discs (Pfirrmann Grades L5/S1=3, L5/L4=3, L4/L3 = 2, L3/L2 =2; L2/L1 = 2) and an O.D.I score of 12; 2C) a 65-year old subject with mild and severely degenerated discs (Pfirrmann Grades L5/S1=5, L5/L4=4, L4/L3 = 3, L3/L2 =3; L2/L1 = 3) and an O.D.I score of 20. The $T_{1\rho}$ values in the healthy discs are greater than those in the degenerative discs. **153**

Figure 9.3: Median $T_{1\rho}$ values (\pm standard deviation) in each Pfirrmann grade are illustrated in the graph (16 patients, 77 discs). The plot is limited because it ignores differences between lumbar regions and is unable to properly account for the within- and between-subject structure of the data. However, the plot does provide a striking illustration of the behavior of $T_{1\rho}$ values with respect to Pfirrmann grade. Groups that are significantly different ($p < 0.05$) are categorized by different colors, as determined from the linear regression model. Note that the $T_{1\rho}$ values in the Pfirrmann grade 2 discs were significantly different from those in Pfirrmann grade 1, as evidenced by the mixed-effects regression model (which allows for subject-specific random effects), suggesting that $T_{1\rho}$ relaxation time may be sensitive to early degenerative changes. **154**

Figure 9.4: Median T_2 values (\pm standard deviation) in each Pfirrmann grade are illustrated ($n = 9$ patients, 44 discs) in the graph. The plot is limited because it ignores differences between lumbar regions and is unable to properly account for the within- and between-subject structure of the data. However, the plot does provide an illustration of the behavior of T_2 values with respect to Pfirrmann grade. Groups that are significantly different ($p < 0.05$) are categorized by different colors, as determined from the linear regression model. **155**

Figure 9.5: Decreasing trends in $T_{1\rho}$ and T_2 values were evident in discs L1/L2 to L5/S1. **158**

Figure 9.6: The correlation between $T_{1\rho}$ and T_2 values was $r = 0.76$ ($p < 0.01$). The figure shows a $T_{1\rho}$ and T_2 map in the same subject. The disparity between the $T_{1\rho}$ and T_2 values is evident by the differences in the spatial distribution and range of values in the discs. **160**

List of Tables

Table 2.1: A summary of the ECM components of cartilage and the intervertebral disc.....	20
Table 4.1: Inclusion criteria for the 3 subject-groups in the OAI.....	64
Table 5.1: OA subject characteristics at baseline.	79
Table 5.2: Least squares mean percentage change of cartilage parameters (standard error in parenthesis) for OA0 (n = 8), OA1 (n =13), and OA2 (n=17) subjects over two years. A decrease in cartilage thickness and volume in the femoral condyles was evident in both osteoarthritic groups. However, the relative difference in the least squares mean percentage change of only cartilage thickness between the osteoarthritic and control groups approached marginal significance (p = 0.083 for the lateral condyle and p = 0.068 for the medial condyle).....	88
Table 5.3: Significant (**0.00 < p <= 0.05; *0.05 < p <= 0.10) Spearman correlations between changes in cartilage thickness and between changes in T ₂ in different regions.	90
Table 5.4: Significant (p < 0.05) Spearman correlations between percentage changes in bone parameters (apparent bone volume fraction (app. BV/TV), apparent trabecular number (app. Tb.N), apparent trabecular thickness (app. Tb.Th), and apparent trabecular separation (app. Tb.Sp)) from baseline to follow-up 1. The table shows that a positive relationship was established between bone structure changes in the femur and tibia, the femur and the medial condyle, and the lateral and medial tibia. The highest correlations were established between bone structure of the medial and lateral tibia, suggesting a strong interdependence.....	91
Table 6.1: Correlations between texture parameters of cartilage T ₂ are shown in the table.	109
Table 6.2: Least square means (LSMeans) analysis (baseline and follow-up combined) of ASM and entropy of cartilage T ₂ , mean and standard deviation of cartilage T ₂ , and cartilage volume and thickness between OA patients and controls using data from baseline and 9 months are shown in the table.....	111
Table 6.3: The longitudinal changes in ASM and entropy of cartilage T ₂ , mean and standard deviation of cartilage T ₂ , and cartilage volume and thickness in OA patients are shown in the table. The standard deviation of T ₂ and entropy of T ₂ significantly decreased from baseline to 9 months. Control subjects did not show significant changes in these parameters.	113
Table 7.1: Annual percentage changes in cartilage thickness, calculated using data from baseline, 1-year and 2-year follow-up.	124
Table 8.1: The coefficient of variation for three phantoms with different agarose concentrations scanned twice at isocenter, twice at 3 cm superior to isocenter, and twice at 3 cm inferior to isocenter (illustrated in Figure 8.3).....	137
Table 8.2: Median T _{1ρ} values in the nucleus and annulus of different discs. The standard deviation is in parentheses.	138
Table 9.1: Spearman correlations (r) between MR parameters, clinical questionnaire scores, and subject age.....	156

Table 9.2: Relationship (R^2) between Clinical Questionnaire Scores (O.D.I. and SF-36 Physical Health) and MR parameters ($T_{1\rho}$, T_2 , and Pfirrmann Grade). The R^2 value, calculated using the JMP procedure for mixed effects models, accounts for both within- and between-subject variation. **157**

Chapter 1: Introduction

1.1 Motivation

The extracellular matrix (ECM) is a network of extracellular macromolecules that is present in both cartilage and intervertebral disc tissues. The ECM plays an integral role in cell function and provides structural support to cells. While both cartilage and intervertebral disc tissues are comprised of an ECM, their form and structure vary. Likewise, each tissue has unique characteristics during degeneration. This project will investigate the non-invasive detection of early degenerative changes of cartilage and disc tissues in osteoarthritis (OA) and intervertebral disc degeneration (IVDD) using novel magnetic resonance imaging methods.

OA is a debilitating disease causing pain, stiffness, and loss of mobility to approximately 14% of the adult population (1). The prevalence of knee OA is 20-40 percent in people 75 years and older (2). IVDD is the leading cause of pain and disability in adults in the United States (3). Despite the high prevalence of OA and IVDD worldwide, diagnosis in the early stages of symptomatic disease, prior to morphologic degradation, is elusive in clinical practice. Ideally, a method that detects the initial biochemical changes in OA and in IVDD would be essential for early diagnosis of each disease. Certain quantitative MRI methods, including $T_{1\rho}$ and T_2 relaxation time mapping, are sensitive to biochemical changes in the ECM, and thus may be valuable for early diagnosis of intervertebral disc and cartilage degeneration. While initial studies have exhibited promising results showing that $T_{1\rho}$ and T_2 relaxation time are sensitive to changes in the ECM, further studies are necessary to determine whether $T_{1\rho}$ and T_2 imaging can be used as markers for early degeneration in the IVDD and OA.

1.2 Thesis Aims

The overall purpose of my dissertation is to develop a methodology for the quantification of $T_{1\rho}$ and T_2 magnetic resonance relaxation time in knee cartilage and the intervertebral disc, and characterize the spatial distribution of $T_{1\rho}$ and T_2 in the extracellular matrix in OA and IVDD. The thesis is divided into three major parts: the background, the technical development, and the clinical application.

The primary contributions of this thesis include:

- 1) Development of a methodology for accurate quantification of the mean and spatial distribution of magnetic resonance T_2 relaxation times in cartilage and the intervertebral disc.
- 2) Evaluation of the longitudinal changes in quantitative MR cartilage and bone parameters in the progression of OA.
- 3) Assessment of the mean and spatial distribution of cartilage T_2 relaxation time in healthy subjects and those with OA.
- 4) Quantification of $T_{1\rho}$ and T_2 magnetic resonance relaxation time in subjects with different grades of IVDD.
- 5) Investigation of the relationship between magnetic resonance relaxation time and clinical symptoms in patients with OA and IVDD.

The background consists of:

Chapter 2, which provides introductory information on the clinical aspects of this project including cartilage, intervertebral disc, osteoarthritis, and degenerative disc disease; and

Chapter 3, which reviews fundamental magnetic resonance imaging and image processing techniques pertaining to this project.

The technical development component consists of:

Chapter 4, which describes the development of an MR relaxation time mapping methodology for evaluating the cartilage extracellular matrix.

The clinical application component consists of:

Chapter 5, which describes a study of quantitative MRI of cartilage and trabecular bone in OA; and

Chapter 6, which discusses the quantification of the spatial distribution of cartilage T_2 in osteoarthritis; and

Chapter 7, which characterizes the spatial distribution of cartilage T_2 in patients from the Osteoarthritis Initiative; and

Chapter 8, which characterizes the feasibility of *in vivo* $T_{1\rho}$ relaxation time mapping in the intervertebral disc; and

Chapter 9, which describes the quantification of *in vivo* $T_{1\rho}$ relaxation time in subjects with different grade of disc degeneration.

Lastly,

Chapter 10 summarizes the results and relevant clinical implications.

1.3 References

1. Forman M, Malamet R, Kaplan D. A survey of osteoarthritis of the knee in the elderly. *J Rheumatol* 1983;10:282-287.
2. Felson DT. Epidemiology of hip and knee osteoarthritis. *Epidemiol Rev* 1988;10:1-28.
3. Errico TJ. Lumbar disc arthroplasty. *Clin Orthop Relat Res* 2005(435):106-117.

Chapter 2: Background [1]

2.1 Structure of the Knee Joint

The knee joint is composed of three bones: the tibia, the femur, and the patella, and has two articulations: one between the femur and tibia and one between the femur and patella. Each bone in the knee joint has an articular surface, which is covered by cartilage. The bones in the joint are connected by ligaments: the collateral ligaments run along the medial and lateral sides of the knee, the anterior cruciate ligament connects the anterior tibia to the posterior femur, and the posterior cruciate ligament connects the posterior tibia and the anterior femur. The menisci, which are two crescent shaped fibro-cartilage pads, lie between the femur and tibia and provide cushioning between the joints. In addition, muscles in the anterior, posterior and medial sides of the joint support joint movement and function.

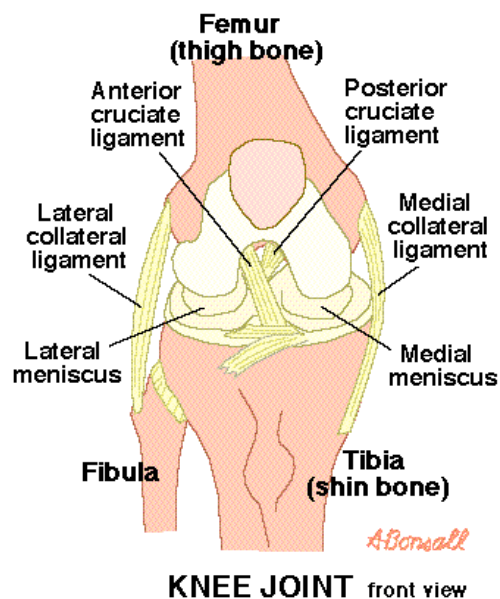


Figure 2.1: Anatomy of the knee joint. Image from the following website:
<http://www.emedicinehealth.com/script/main/art.asp?articlekey=8845>

2.2 Osteoarthritis

2.2.1 Prevalence and Risk Factors

Osteoarthritis (OA) is a heterogeneous and multi-factorial disease characterized by the progressive loss of hyaline articular cartilage and the development of altered joint congruency, subchondral sclerosis, intraosseous cysts, and osteophytes. It affects approximately 14% of the adult population (1) and is the second most common cause of permanent disability among people over the age of fifty (2). The initiation and pathogenesis of OA can be affected by many factors including altered mechanical loading and previous knee injury.

The relationships between knee OA and heavy mechanical work, obesity, and malalignment are well established (3,4). Previous studies have demonstrated that weight gain increases the risk of OA (5), while weight loss reduces the risk (6). Sharma et al. (7) have shown that varus alignment at baseline is associated with a 4-fold increase in the odds for medial OA progression, while valgus alignment at baseline is associated with a 3-fold increase in the odds for lateral OA progression. Cicuttini et al. have shown that malalignment at baseline is associated with cartilage loss over two years (8).

Post-traumatic OA, that follows injuries that deform the articular surface or alter joint geometry, tends to develop relatively soon (relative to other risk factors), after the index injury (e.g., two years (9)). In cases of post-traumatic OA, the onset of the disease is a result of a severe alteration in joint biomechanics. In a five-year follow-up of thirty-two patients who underwent surgery for an anterior cruciate ligament (ACL) tear, 72% complained of knee pain, 66% had knee swelling, and 37% reported impaired activities of daily living (9,10). Numerous articles have reported an increased incidence of knee OA following

meniscal surgery (11-13). In a three to ten year (average 3.8) follow-up of 196 patients with meniscal tears associated with ACL injury, Lynch et al. (11) observed radiographic changes consistent with degenerative joint disease (joint-space narrowing, osteophytes and articular surface flattening) in 88% of the 140 patients who underwent partial or complete meniscectomy. The studies suggest that traumatic injury and surgical intervention are risk factors for OA.

2.2.2 Diagnosis of OA

OA can be diagnosed using imaging techniques such as radiography and magnetic resonance imaging (MRI). Radiography can be used to measure joint space narrowing, which is an indicator of OA severity. The Kellgren Lawrence scoring system (14) can be used to assess the severity of OA. The scoring system ranges from 0 to 4; a score of 0 signifies having no signs of OA, while a score of 4 signifies having severe OA (osteophytes, substantially impaired joint space, sclerosis of subchondral bone).

Radiography examines cartilage indirectly, and therefore may not be optimal for diagnosis for OA. MRI, another imaging technique that can be used for the assessment of OA, is non-ionizing and provides direct visualization of cartilage and trabecular bone structure. MRI has been used to measure cartilage volume and thickness, as well as trabecular bone volume fraction.

2.2.3 Treatment of OA

Various treatment options have been proposed to relieve pain and symptoms of OA. Non-pharmacologic measures include exercise, weight loss, and physical therapy. Strengthening exercises can relieve short-term pain sensation, and aerobic exercise can improve long-term function. Pharmacologic measures include prescription of anti-

inflammatory drugs and nutritional supplements (i.e. glucosamine and chondroitin), and injection of intra-articular agents. However, anti-inflammatory drugs have side effects (gastrointestinal and renal toxicity), and the injection of intra-articular agents is an invasive procedure having limited long-term data on efficacy. Therefore, novel research studies on the development of therapeutic measures for OA are critical for the treatment of the disease.

2.2.4 Cartilage Degeneration in OA

Hyaline cartilage lines the articular surfaces of the femur, tibia, and patella. The primary function of cartilage is to minimize the contact stresses that occur during the joint loading (15), thus acting as a cushion in the joint. Cartilage is composed of an extracellular matrix (ECM), which contains chondrocytes, collagen, proteoglycan, and water molecules (Figure 2.2). Chondrocytes are cartilage cells that regulate the production and maintenance of the ECM. In healthy tissue, the water molecules constitute about 65-80% of the dry tissue weight. The collagen constitutes approximately 75% of the dry weight of tissue and is responsible for the tensile strength (15). Proteoglycan, are negatively charged macromolecules that constitute approximately 20-30% of the dry tissue weight. The strong negative charge is neutralized by positive ions in the surrounding fluid, therefore creating a swelling pressure. The proteoglycan is responsible for the compressive strength in the cartilage. It is made up of a protein core with glycosaminoglycan (GAG) side chains (chondroitin sulfate and keratin sulfate) (16,17).

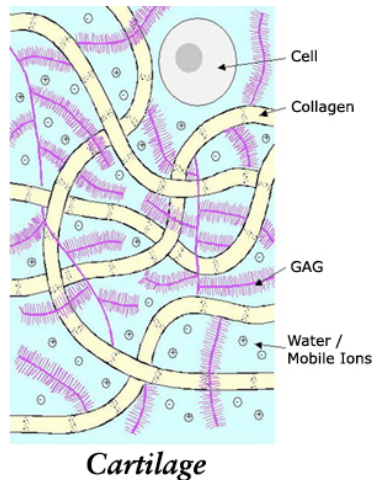


Figure 2.2: An Illustration of the cartilage extracellular matrix. Image from the following website: <http://www.bidmc.org/>

Cartilage is composed of four primary zones: Zone 1 is closest to the cartilage surface and contains collagen fibers that are oriented parallel to the surface. Zone 2 is the largest zone that is adjacent to Zone 1 and has collagen fibers that are randomly oriented. Zone 3 contains collagen fibers that are oriented perpendicular to the joint surface. Finally, Zone 4 is the calcified cartilage that is the junction between the cartilage and subchondral bone (Figure 2.3).

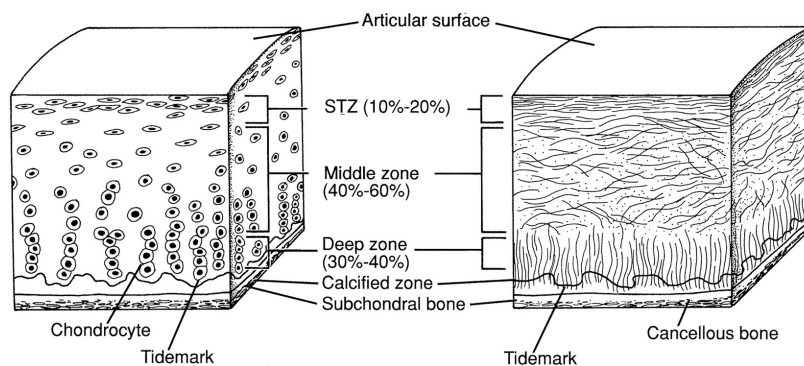


Figure 2.3: An Illustration of the zonal pattern in cartilage. Image from the following website: <http://ajs.sagepub.com/content/26/2/309/F2.large.jpg>

The initial stages of OA include proteoglycan loss, increased water content, and disorganization of the collagen network. With further degeneration, cartilage tissue becomes

ulcerated causing proteoglycans to diffuse into the synovial fluid, thus decreasing water content in cartilage. The intermediate stages of OA include cartilage thinning, fibrillation, and decreased proteoglycan and water content. In the late stages of OA, collagen, proteoglycan, and water content is further reduced, and the collagen network is severely disrupted (18). Figure 2.4 illustrates the difference in healthy knee cartilage and osteoarthritic knee cartilage.

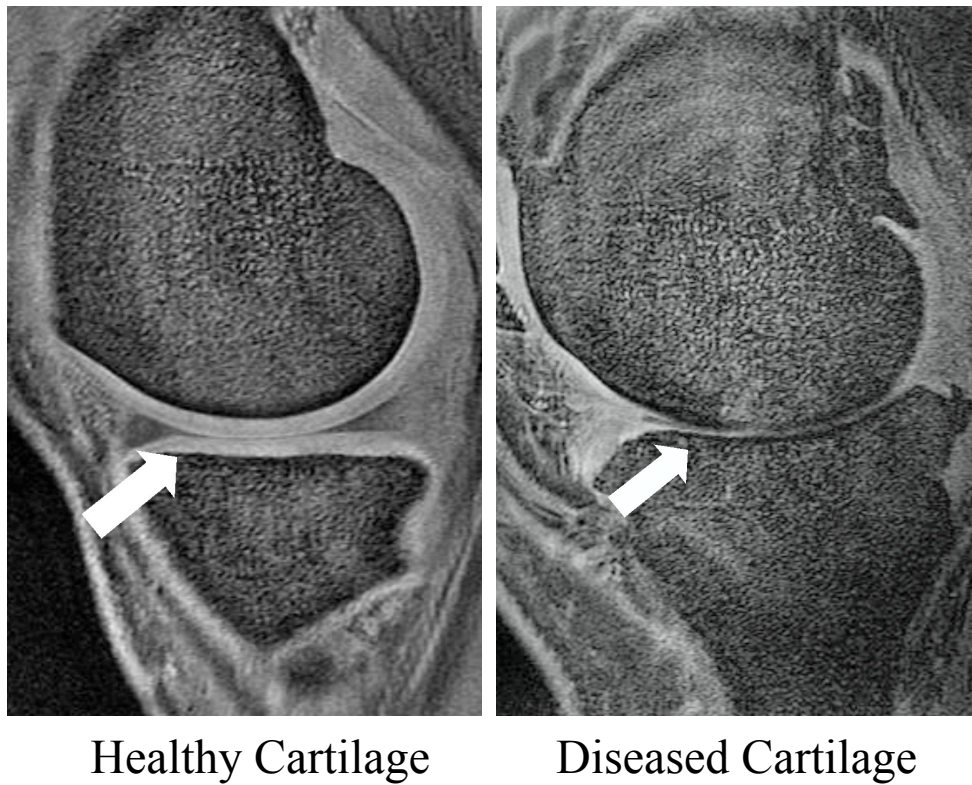


Figure 2.4: An MR image of healthy cartilage (left) and disease cartilage (right)

Although OA has been considered a disease primarily characterized by cartilage degeneration, the accompanying changes in the bone and surrounding tissues are critical in the pathogenesis of OA. Figure 2.5 demonstrates other joint tissues that degenerate as a result of the OA.

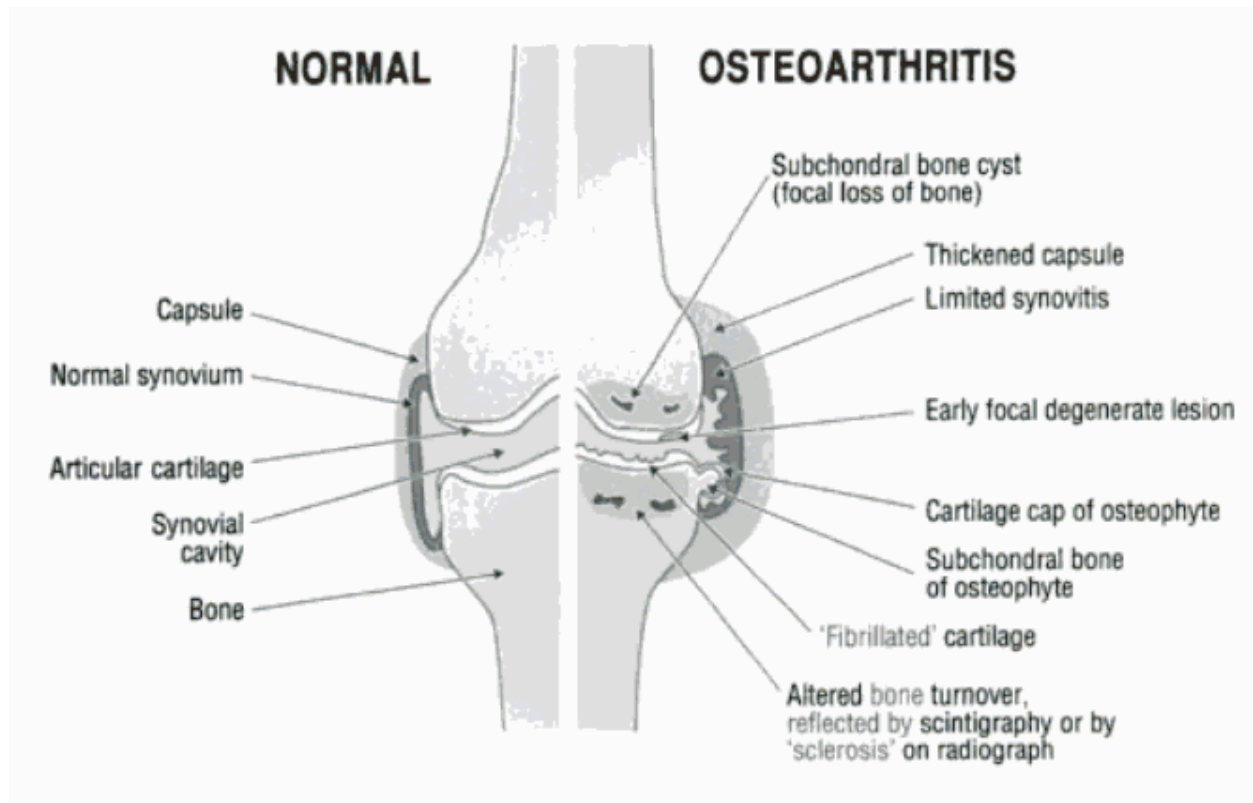


Figure 2.5: An illustration of a “normal” knee and a knee with OA. Image taken from Moskowitz et al. (19)

2.2.5 Bone Changes in OA

In OA, bone changes are evident on both the matrix and apparent levels. The “matrix level” refers to bone changes on the scale of 10 to 100’s of microns. In OA, bone changes on this level include changes to the bone tissue such as altered remodeling and mineralization. The “apparent level” refers to bone changes on a scale of millimeters to centimeters. The bone changes on the apparent level are larger scale and include changes such as altered trabecular architecture. The mechanical properties of the “apparent level” include the effects from the matrix level. Figure 2.6 illustrates the differences between the matrix and apparent levels in bone tissue (20). The pathogenesis of osteoarthritic bone includes changes on both the matrix and apparent levels, which are reviewed in detail below.

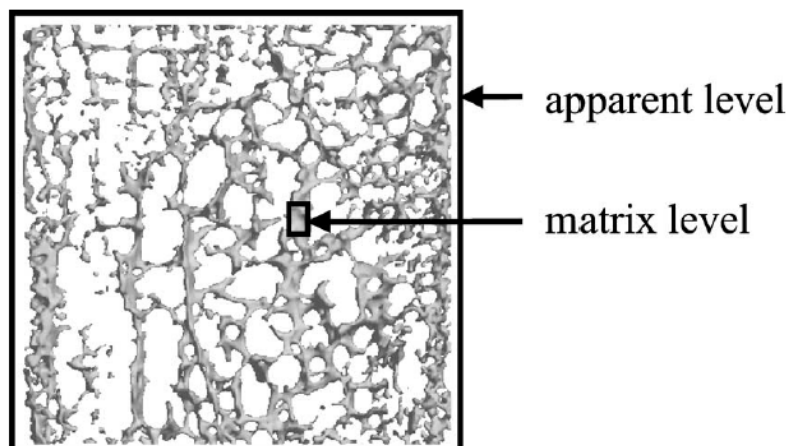


Figure 2.6: The differences between bone on the matrix and apparent levels (adapted from (20)).

2.2.5.1 OA Bone: Matrix Level

Many *in vitro* research studies have evaluated the changes in osteoarthritic bone tissue on the matrix level. Cellular changes, such as remodeling, are altered in osteoarthritic bone, thus modifying the mechanical properties of the joint. The remodeling activity is increased in osteoarthritic bone, demonstrating an abnormal behavior of osteoclasts and osteoblasts. Osteoblasts in osteoarthritic bone are more numerous and flatter than in healthy bone (21). One study has shown that subchondral bone remodeling is one of the initial stages of OA using a guinea pig OA model (22). This increased remodeling results in a lower mean level of mineralization, thus altering the quality of the bone matrix, and its responses to mechanical loading (20).

2.2.5.2 OA Bone: Matrix Level Mechanical Properties

The mechanical properties of osteoarthritic bone have been evaluated on the matrix level using *in vitro* mechanical testing and computer modeling. On the matrix level, osteoarthritic bone has a lower elastic modulus, or stiffness. This decreased stiffness affects

the ability of bone to sustain weight, and absorb energy from impact. Using a mechanical compression testing Li and Aspden (23) found a decrease in OA bone stiffness on the matrix level by 15% in specimens from patients having hip arthroplasty. Using compression testing and finite element modeling of human osteoarthritic proximal tibia specimens, Day et al. (24) found a decrease in bone stiffness on the matrix level by 45%. The relative differences in loss of stiffness could be due to factors such as location of specimen (e.g. tibia vs. femur), as well as differences in the patient population. Overall, these studies both demonstrate that the tissue stiffness in osteoarthritic bone is decreased on the matrix level.

The decrease in stiffness of osteoarthritic bone on the matrix level could be due to many factors such as altered mineralization and changes in the collagen of the bone matrix. In the bone matrix, the collagen provides tensile strength through cross linking. Changes in the nature of collagen cross-linking have been linked to osteoarthritic bone (25). One study found increases in bone collagen metabolism in OA femoral heads compared to normal controls, with the greatest increase occurring in the subchondral bone. However, the cross-linking was similar in OA and healthy bone. The authors hypothesize that the changes in collagen synthesis in the bone matrix produces altered mechanical properties, thus, exacerbating the degeneration of the other parts of the joint (26). The increased collagen synthesis may be affected by osteoblast phenotypic expression, chondrocyte apoptosis, matrix metalloproteinases, and growth factors (27). These factors need to be further investigated to determine their individual and combined effects on collagen synthesis on the evolution and progression of OA. Furthermore, since the above studies reported differences on the effects of cross-linking in OA, further studies with a greater sample size are warranted.

The changes in remodeling in OA may be associated with alterations in mechano-transduction. A recent study by Bakker et al. (28) found that the cellular response in bone cells is altered in response to mechanical stress. These results demonstrate the effects of mechanical properties on the bone matrix, and suggest that changes in mechano-transduction may play a role in the altered bone quality in OA.

2.2.5.3 OA Bone: Apparent Level

On the apparent level, changes in osteoarthritic bone involve alterations to subchondral cortical bone, trabecular bone, and the global mechanical properties of the joint. Subchondral bone sclerosis is a prominent feature of OA, which can result from increased rate of bone apposition and decreased rate of bone resorption. Since the pathogenesis of OA is often initiated by injury, such as a rupture of the ACL, many animal models have been used to study spontaneous OA. The spontaneous OA model allows researchers to study OA on an accelerated level, by inducing an injury (e.g. ACL transection) and evaluating the results osteoarthritic response. One such study, evaluating ACL transection in dogs, found loss of trabecular bone at three, eighteen, and fifty-four months, and found subchondral bone sclerosis at eighteen months and fifty-four months, but not at three months (29). These results demonstrate the response of subchondral cortical bone and subchondral trabecular bone may have different time courses. Since the trabecular bone has a greater surface area in contact with bone marrow, the remodeling response may be accelerated. Another longitudinal study on a guinea pig model of OA found similar results, which showed thickening of subchondral cortical bone at twenty-four weeks using histological and microfocal x-ray techniques (30). These studies demonstrate that that subchondral bone has altered microstructure in the evolution of OA.

Subchondral bone sclerosis is often evident *in vivo* on both radiographs and on magnetic resonance imaging scans. A study by Buckland-Wright et al. (31) has shown evidence of increased subchondral bone sclerosis in patients with OA, and well as changes in trabecular architecture in the subchondral trabecular bone.

Other features of OA pathology that can be non-invasively evaluated using imaging are joint space narrowing, osteophytes, and subchondral cysts. These are some of the fundamental characteristics that are used for the diagnosis of OA in the clinical setting. One of the main characteristics of OA is joint space narrowing, or the decrease in the space between two joints (e.g. proximal tibia and the distal femur). Joint space narrowing is directly related to the amount of cartilage: the less cartilage, the smaller the joint space width. Osteophytes, or bony growths, are also evident in OA bone, and are often seen in both radiographs and magnetic resonance imaging (MRI) scans. A bone cyst, another characteristic of OA bone, is often visible on MRI scans, and contains “fibrovascular tissue, linked to active new bone formation” (32). Using the Kellgren Lawrence scale, radiologists are able to classify different grades of OA using markers such as joint space width, osteophytes, and subchondral cysts. Since soft tissue such as cartilage or the meniscus cannot be seen on radiographs, features including joint space narrowing, subchondral sclerosis and osteophytes are used for the classification of OA.

Changes in trabecular bone architecture of osteoarthritic joints are evident in OA. Increased trabecular thickness, and decreased trabecular spacing is common in OA bone. One study found increased trabecular thickness in the principal compressive stress regions of the femoral head in from human femoral specimens (33). Ding et al. (34) examined OA bone from human tibial specimens using micro-computed tomography and found that OA

trabecular bone was thicker and more “plate-like” than normal, healthy bone. Another study using a guinea pig model for OA found similar results in that OA trabecular bone was thicker, changed from being rod-like to more plate-like and became more axially oriented (35).

Aside from examining the changes in trabecular structure using bone cores, it is also interesting to evaluate whether the trabecular structure differs depending on the location of the bone sample (e.g. medial or lateral side of the joint, or its proximity to the joint line), whether there are changes depending on the type of joint (e.g. proximal/distal femur, tibia, vertebra), and whether there are differences depending on the severity of OA. Studies have used MRI to quantify trabecular structure in different regions of the joint to determine whether there are differences in trabecular structure. MR Imaging can be used to quantify apparent bone volume fraction, apparent trabecular thickness, apparent trabecular spacing, and apparent trabecular number, using a spatial resolution on the order of the thickness of trabeculae. One study by Beuf et al. (36) demonstrated differences in trabecular structure between the femur and the tibia in osteoarthritic knees using MRI. It was interesting to note that they also found that the differences in trabecular structure became less pronounced in patients with more severe OA. This demonstrates that trabecular structure is constantly changing, and may become less heterogeneous as the disease progresses. Possibly, at the initial stages of OA, the femur and tibia behave differently, but as the disease progresses, the responses become less disparate. Thus, changes in trabecular microarchitecture should be evaluated separately in different regions of the joint, and in patients with different disease severity.

Other imaging studies have found that bone microstructure is dependent on location. Lindsey et al. (37) examined patients with OA of the knee using MRI. They found that as cartilage was lost on the medial side of the joint, there was an increase in bone on the medial side of the joint, and a loss of bone on the lateral side of the joint. These results demonstrated the response of bone to OA varies depending on location. The authors suggested that bone responses may be due to joint malalignment. OA can be affected by varus or valgus alignment, which distributes the forces during stance toward the medial and lateral sides of the joint, respectively. In the case of varus alignment, the cartilage and bone on the medial side of the joint experience more mechanical stress. Therefore, as the cartilage degenerates on the medial side of the joint, the bone may respond to the increased loading, by getting stronger. There may be an unloading effect on the lateral side of the joint, and the bone may respond by getting weaker. Another longitudinal study (38) found that cartilage degeneration was related to trabecular bone loss closer to the joint line, and trabecular bone gain farther from the joint line. The authors hypothesize that cartilage loss is related to subchondral plate sclerosis (greater absorption of local stresses and decreased load transmission). Thus, osteopenia occurs in the subarticular bone, and there is reactive bone formation farther from the joint line, compensating for the localized bone loss. Therefore, in OA, the trabecular structure has a varied response on the medial/lateral and proximal/distal areas of the joint, demonstrating the importance of location when examining trabecular bone structure in OA.

2.2.5.4 OA Bone: Apparent Level Mechanical Properties

The mechanical properties of OA bone on an apparent level are altered during the progression of the disease, and are influenced by changes in trabecular and cortical plate

architecture. One of the first theories on the initiating factors in OA was proposed by Radin et al. (39). They hypothesized that the initiating factor in the pathogenesis of OA is an increased stiffness in subchondral bone in OA. This increased stiffness adversely affects the bone's ability to absorb energy. Radin et al. (39) hypothesized that the bone becomes stiffer due to micro-fracture of the trabecular bone. The micro-fracture is followed by increased bone remodeling and localized stiffening of bone. Specifically, the healing of the micro-fractures (evident through callous formation) causes the bone to increase in stiffness. The changes in mechanical properties of the bone consequently increase the stress in the overlying cartilage. This is because the subchondral bone loses its mechanical ability to withstand loading (due to its decrease in energy absorbing capacity). Therefore, the onset of OA may be due to microfractures in bone.

The hardness properties of OA trabecular bone have been examined in using micro-indentation techniques. Material properties of subchondral bone from patients with osteoporosis or osteoarthritis by micro-indentation testing and electron probe microanalysis]. Lereim et al. (40) used the Brinell Hardness Test (with a 5 mm indentation) and reported a fifty percent reduction of hardness in subchondral plate of the tibial plateau OA bone. A study by Coats et al. (41) examined the hardness properties of trabecular structure, and similarly, found a reduction of hardness in OA trabecular bone. It was interesting to note that the trabecular bone closest to the joint line was 'harder' than bone farther from the joint line, demonstrating different responses to mechanical loading in different parts of the joint.

Studies have evaluated the differences in trabecular modulus, in trabecular bone specimens from patients with different severities of OA. A research study examining human trabecular specimens of the femoral condyle with mild OA found a forty percent increase in

apparent modulus (42). Another study (43) examined trabecular bone specimens from the femoral head of patients with severe OA also found increased apparent modulus of the bone. These studies demonstrate that trabecular bone modulus is increased in patients with both mild and severe OA. Similar results are seen for trabecular bone samples in the knee and the femur, illustrating similarities in the pathogenesis of OA in different affected areas.

2.3 Structure of the Intervertebral Disc

Intervertebral discs are fibrocartilaginous cushions, serving as the spine's shock absorbing system by protecting the vertebrae, brain, and other structures including the nerves. The intervertebral disc consists of two primary regions: the nucleus (the inner core of the disc) and a surrounding annulus. The annulus is composed of tightly woven collagen fibers, while the nucleus is composed of a hydrated gel. The endplate separates each intervertebral disc from the surrounding vertebral bodies. Figure 2.7 illustrates the anatomy of the intervertebral disc.

The intervertebral disc is composed of an extracellular matrix (ECM), which serves two primary functions: it provides biomechanical strength and regulates the nutrients absorbed. The disc cells, which are part of the ECM, occupy < 1% of tissue volume and function to synthesize and degrade ECM. Water is another component of the ECM: the nucleus of the disc contains about 80% water by volume, while the annulus contains about 65%. Water is expressed from the disc with normal loading and about 25% of water is lost and regained daily. Collagen and proteoglycans are also components of the ECM. The nucleus contains approximately 25% dry weight of collagen and the annulus contains about 70% (44). Proteoglycans are trapped within the collagen network. Having a fixed negative charge, they attract interstitial fluid with a positive charge such as Na^+ , thus imbibing water.

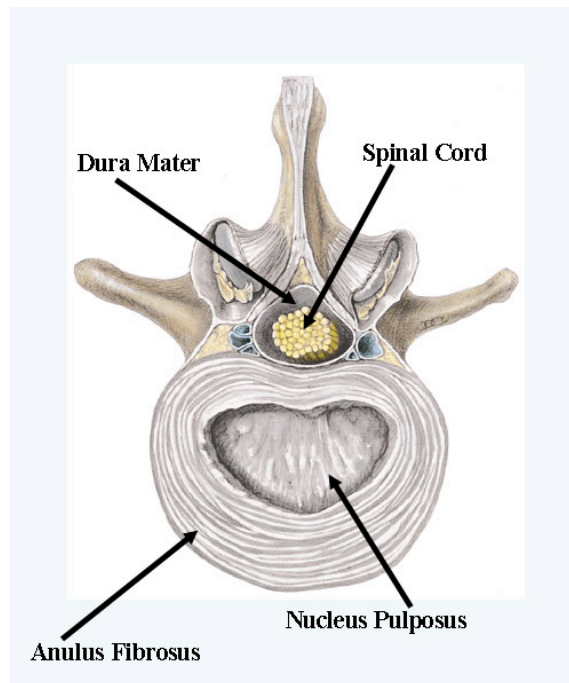


Figure 2.7: An illustration of the structure of the intervertebral disc. Image taken from <http://www.ithaca.edu/faculty/lahr/LE2000/Back/FinishedPics/JPEGs/CutDisc.jpg>

Table 2.1: A summary of the ECM components of cartilage and the intervertebral disc.

	<i>Type of Cartilage</i>	<i>Proteoglycan</i>	<i>Collagen</i>	<i>Cell</i>	<i>Water Content</i>
Cartilage	Hyaline Cartilage	20-30% of dry weight	75% of dry weight	1-2% tissue volume	65-80% dry weight
Intervertebral disc nucleus		50% of dry weight/	25% of dry weight/		80% water by volume/
/annulus	Fibrocartilage	<1% of dry weight	70% of dry weight	<1% tissue volume	65% water by volume

2.4 Degenerative Disc Disease

Intervertebral disc degeneration (IVDD), a significant cause of lower back pain, is characterized by biochemical and morphologic changes in the nucleus pulposus and annulus fibrosus. Intervertebral disc degeneration (IVDD) is the leading cause of pain and disability in adults in the United States (45). Despite the high prevalence of IVDD worldwide, diagnosis in the early stages of symptomatic disease is elusive in clinical practice. The traditional methods for imaging disc degeneration, including radiography, magnetic resonance imaging (MRI), and computed tomography (CT), are limited to depicting late-

stage, gross morphologic changes. Ideally, a method that detects the initial biochemical changes in disc degeneration would be valuable in preventing disease progression. Such a method would improve diagnostic capabilities and enable preventative measures to be taken at the early stages of the disease.

The process of disc degeneration is characterized by a loss of cellularity, degradation of the extracellular matrix, and as a result, morphological changes and alterations in biomechanical properties. The most consistent chemical change observed with aging is loss of proteoglycan and concomitant loss of water and disc pressure(46,47). During the course of IVDD, small-degraded fragments of molecules can seep from the tissue, resulting in a loss of osmotic pressure and hydration (47), and thus altering mechanical properties. Secondary changes due to redistribution of tissue stress include fibrocartilage production with disorganization of the annular architecture and increases in type II collagen(48). During disc degeneration, Type I collagen fibers replace the type II collagen fibers in the annulus (49), thus altering the tensile properties of the tissue. Other late-stage changes include loss of a distinct boundary between the nucleus and annulus. In the later stages of IVDD, morphologic changes including a loss of disc height, disc herniation, annular tears, and radial bulging are evident (49).

Together, degeneration-associated changes in the nucleus and annulus are fundamental to the development of specific spinal disorders. For instance, changes in proteoglycan content within the nucleus leads to reduced imbibition of water, depressurization, and flattening of the disc. The annulus may then bulge into the spinal canal and neural foramen (disc protrusion). Disc height loss also results in narrowing of the spinal canal and unfolding of the ligamentum flavum, contributing directly to the development of

spinal stenosis (constriction of spinal nerves or spinal cord). Herniation of the intervertebral disc can occur as a result of mechanical annular disruption and fissuring due to chronic non-physiologic stress secondary to nuclear dehydration. Thus, IVDD is a complex and multifaceted process whose biochemical and morphologic changes adversely affect the mechanical and functional integrity of the disc.

2.5 References

1. Forman M, Malamet R, Kaplan D. A survey of osteoarthritis of the knee in the elderly. *J Rheumatol* 1983;10:282-287.
2. Peyron JG. The epidemiology of osteoarthritis. In: Moskowitz R, editor. *Osteoarthritis Diagnosis and Management*: W. B. Saunders; 1984. p 9-27.
3. Kohatsu N, Schurman D. Risk factors for the development of osteoarthritis of the knee. *Clin Orthop* 1990;261:242-246.
4. Lindberg H, Montgomery F. Heavy labour and the occurrence of gonarthrosis. *Clin Orthop* 1987;214:235-236.
5. Ding C, Cicuttini F, Scott F, Cooley H, Jones G. Knee structural alteration and BMI: a cross-sectional study. *Obes Res* 2005;13(2):350-361.
6. Felson DT, Zhang Y, Anthony JM, Naimark A, Anderson JJ. Weight loss reduces the risk for symptomatic knee osteoarthritis in women. The Framingham Study. *Ann Intern Med* 1992;116(7):535-539.
7. Sharma L. Local factors in osteoarthritis. *Curr Opin Rheumatol* 2001;13(5):441-446.
8. Cicuttini F, Wluka A, Hankin J, Wang Y. Longitudinal study of the relationship between knee angle and tibiofemoral cartilage volume in subjects with knee osteoarthritis. *Rheumatology* 2004;43(3):321-324.
9. Wright V. Post-traumatic osteoarthritis - A medicolegal minefield. *Br J Rheum* 1990;29:474-478.
10. Feagin J. The syndrome of the torn anterior cruciate ligament. *Orthop Clin North Am* 1979;10:81-90.

11. Lynch M, Henning C, Glick K. Knee joint surface changes: long-term follow-up meniscus tear treatment in stable anterior cruciate ligament reconstructions. *Clin Orthop Rel Res* 1983;172:148-153.
12. Daniel D, Stone M, Dobson B, Fithian D, Rossman D, Kaufman K. Fate of the ACL-injured patient: a prospective outcome study. *Am J Sports Med* 1994;22:632-644.
13. Fairbank T. Knee joint changes after meniscectomy. *Bone Joint Surg* 1984;30:664-670.
14. Kellgren JH, Lawrence JS. Radiological assessment of osteo-arthritis. *Ann Rheum Dis* 1957;16(4):494-502.
15. Mow VC, Guo XE. Mechano-electrochemical properties of articular cartilage: Their Inhomogeneities and Anisotropies. *Annual Review of Biomedical Engineering* 2002;4(1):175-209.
16. Muir H. Proteoglycans as organizers of the intercellular matrix. *Biochemical Society Transactions* 1983;11(6):613.
17. Hardingham TE, Fosang AJ. Proteoglycans: many forms and many functions. *The FASEB Journal* 1992;6(3):861-870.
18. Dijkgraaf LC, de Bont LG, Boering G, Liem RS. The structure, biochemistry, and metabolism of osteoarthritic cartilage: a review of the literature. *J Oral Maxillofac Surg* 1995;53(10):1182-1192.
19. Moskowitz RW, Altman RD, Buckwalter JA, Goldberg VM, Hochberg MC. *Osteoarthritis: diagnosis and medical/surgical management*: Lippincott Williams & Wilkins; 2006.
20. Day JS, Van Der Linden JC, Bank RA, Ding M, Hvid I, Sumner DR, Weinans H. Adaptation of subchondral bone in osteoarthritis. *Biorheology* 2004;41(3-4):359-368.
21. Dequeker J, Mokassa L, Aerssens J, Boonen S. Bone density and local growth factors in generalized osteoarthritis. *Microsc Res Tech* 1997;37(4):358-371.
22. Layton MW, Goldstein SA, Goulet RW, Feldkamp LA, Kubinski DJ, Bole GG. Examination of subchondral bone architecture in experimental osteoarthritis by microscopic computed axial tomography. *Arthritis Rheum* 1988;31(11):1400-1405.

23. Li B, Aspden RM. Composition and mechanical properties of cancellous bone from the femoral head of patients with osteoporosis or osteoarthritis. *J Bone Miner Res* 1997;12(4):641-651.
24. Day JS, Ding M, van der Linden JC, Hvid I, Sumner DR, Weinans H. A decreased subchondral trabecular bone tissue elastic modulus is associated with pre-arthritis cartilage damage. *J Orthop Res* 2001;19(5):914-918.
25. Burr DB. Anatomy and physiology of the mineralized tissues: role in the pathogenesis of osteoarthritis. *Osteoarthritis Cartilage* 2004;12 Suppl A:S20-30.
26. Mansell JP, Bailey AJ. Abnormal cancellous bone collagen metabolism in osteoarthritis. *J Clin Invest* 1998;101(8):1596-1603.
27. Hunter DJ, Spector TD. The role of bone metabolism in osteoarthritis. *Curr Rheumatol Rep* 2003;5(1):15-19.
28. Bakker AD, Klein-Nulend J, Tanck E, Heyligers IC, Albers GH, Lips P, Burger EH. Different responsiveness to mechanical stress of bone cells from osteoporotic versus osteoarthritic donors. *Osteoporos Int* 2006;17(6):827-833.
29. Moskowitz RW. Bone remodeling in osteoarthritis: subchondral and osteophytic responses. *Osteoarthritis Cartilage* 1999;7(3):323-324.
30. Anderson-MacKenzie JM, Quasnicka HL, Starr RL, Lewis EJ, Billingham ME, Bailey AJ. Fundamental subchondral bone changes in spontaneous knee osteoarthritis. *Int J Biochem Cell Biol* 2005;37(1):224-236.
31. Buckland-Wright C. Subchondral bone changes in hand and knee osteoarthritis detected by radiography. *Osteoarthritis Cartilage* 2004;12 Suppl A:S10-19.
32. Dequeker J. The inverse relationship between osteoporosis and osteoarthritis. *Verh K Acad Geneesk Belg* 1987;49(4):273-309.
33. Fazzalari NL, Darracott J, Vernon-Roberts B. Histomorphometric changes in the trabecular structure of a selected stress region in the femur in patients with osteoarthritis and fracture of the femoral neck. *Bone* 1985;6(3):125-133.
34. Ding M, Odgaard A, Hvid I. Changes in the three-dimensional microstructure of human tibial cancellous bone in early osteoarthritis. *J Bone Joint Surg Br* 2003;85(6):906-912.

35. Ding M, Danielsen CC, Hvid I. Age-related three-dimensional microarchitectural adaptations of subchondral bone tissues in guinea pig primary osteoarthritis. *Calcif Tissue Int* 2006;78(2):113-122.
36. Beuf O, Ghosh S, Newitt DC, Link TM, Steinbach L, Ries M, Lane N, Majumdar S. Magnetic resonance imaging of normal and osteoarthritic trabecular bone structure in the human knee. *Arthritis Rheum* 2002;46(2):385-393.
37. Lindsey CT, Narasimhan A, Adolfo JM, Jin H, Steinbach LS, Link T, Ries M, Majumdar S. Magnetic resonance evaluation of the interrelationship between articular cartilage and trabecular bone of the osteoarthritic knee(1). *Osteoarthritis Cartilage* 2004;12(2):86-96.
38. Blumenkrantz G, Lindsey CT, Dunn TC, Jin H, Ries MD, Link TM, Steinbach LS, Majumdar S. A pilot, two-year longitudinal study of the interrelationship between trabecular bone and articular cartilage in the osteoarthritic knee. *Osteoarthritis Cartilage* 2004;12(12):997-1005.
39. Radin E, Rose R. Role of subchondral bone in the initiation and progression of cartilage damage. *Clinical orthopedics and Related research* 1986;213:34-40.
40. Lereim P, Goldie I, Dahlberg E. Hardness of the subchondral bone of the tibial condyles in the normal state and in osteoarthritis and rheumatoid arthritis. *Acta Orthop Scand* 1974;45(4):614-627.
41. Coats AM, Zioupos P, Aspden RM. Material properties of subchondral bone from patients with osteoporosis or osteoarthritis by microindentation testing and electron probe microanalysis. *Calcif Tissue Int* 2003;73(1):66-71.
42. Pugh JW, Radin EL, Rose RM. Quantitative studies of human subchondral cancellous bone. Its relationship to the state of its overlying cartilage. *J Bone Joint Surg Am* 1974;56(2):313-321.
43. Brown AN, McKinley TO, Bay BK. Trabecular bone strain changes associated with subchondral bone defects of the tibial plateau. *J Orthop Trauma* 2002;16(9):638-643.
44. Urban JPG, Winlove CP. Pathophysiology of the intervertebral disc and the challenges for MRI. *Journal of Magnetic Resonance Imaging* 2007;25(2):419-432.
45. Errico TJ. Lumbar disc arthroplasty. *Clin Orthop Relat Res* 2005(435):106-117.

46. Pearce RH, Grimmer BJ, Adams ME. Degeneration and the chemical composition of the human lumbar intervertebral disc. *J Orthop Res* 1987;5:198-205.
47. Raj PP. Intervertebral disc: anatomy-physiology-pathophysiology-treatment. *Pain Pract* 2008;8(1):18-44.
48. Rufai A, Benjamin M, Ralphs JR. The development of fibrocartilage in the rat intervertebral disc. *Anat Embryol (Berl)* 1995;192(1):53-62.
49. Adams MA, Roughley PJ. What is intervertebral disc degeneration, and what causes it? *Spine* 2006;31(18):2151-2161.

Chapter 3: Background [2]

3.1 Fundamentals of Magnetic Resonance Imaging

Nuclear magnetic resonance (NMR), a phenomenon primarily used for the study of chemical structure, was first discovered independently by Bloch et al.(1) and Purcell et al.(2) in 1946. In 1973, Paul Lauterbur acquired the first magnetic resonance (MR) image of a small test tube (3). Since then, MR imaging has become a rapidly growing modality that is widely used in research and clinical applications. The following section briefly describes the physical principals of MR imaging.

The fundamental principal of MR imaging is the interaction between an atom with a non-zero magnetic moment (μ) and an external magnetic field. Hydrogen (^1H), which is abundant in biological tissues and has a strong magnetic moment, is often imaged with MR. Additionally, other nuclei such as phosphorus (^{31}P) and sodium (^{23}Na) have also been used for imaging, but have a much lower relative physiologic concentration and thus lower sensitivity.

A potential energy (E), is generated when a nuclei with a magnetic moment (μ) experiences a magnetic field, which is described by

$$E = -\mu \cdot B \quad [3.1]$$

When a group of nuclei with magnetic moments are placed in a magnetic field, each can align to be in a state of low energy (aligned with the magnetic field) or high energy (aligned against the magnetic field). The proportion of nuclei in each energy state is based on Boltzmann statistics:

$$N_{upper} / N_{lower} = e^{-E/kT} \quad [3.2]$$

Where E is the energy difference between the spin states; k is Boltzmann's constant, 1.3805×10^{-23} J/Kelvin; and T is the temperature in Kelvin. In the presence of a magnetic field (B_0), the n_{lower} population outnumbers the n_{upper} population, and this difference, known as the *Zeeman Effect*, governs the basic principals of MR. The MR signal is proportional to this population difference.

When a proton with a magnetic moment is placed in a magnetic field (B_0), it experiences a torque and begins to precess (figure 3.1) with angular frequency ω_0 . The precession occurs around the axis of the magnetic field (z). The relationship between the magnetic field and the precession frequency is given by the Larmor equation:

$$\omega_0 = \gamma B_0 \quad [3.3]$$

where γ is the gyromagnetic ratio, which is unique to each element. The gyromagnetic ratio of ^1H is 42.58 MHz/Tesla.

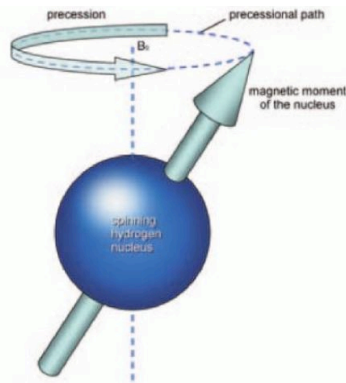


Figure 3.1: An illustration of the precession. Adapted from Westbrook et al. (4)

To perform an MR experiment, a radiofrequency (RF) pulse must displace the precessing nuclei from equilibrium to the higher energy state. This experiment is performed by tuning the RF pulse to match the precession frequency of the nuclei, a phenomenon called *resonance*. The application of an RF pulse to resonance conditions is called excitation. The

excitation causes net magnetization to tilt from the Z axis (longitudinal axis) to the XY plane (transverse plane) (Figure 3.2). After the spins are excited, their return to equilibrium results in an emission of free induction decay, a signal that can then be measured by a receiver coil. The receiver coil is tuned to the frequency of the nuclei in order to detect a signal induced by the moving magnetic field.

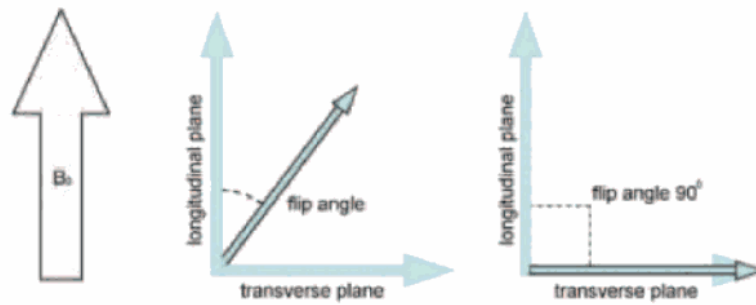


Figure 3.2: An illustration of the net magnetization which is initially in the z axis (longitudinal plane) and then in the XY plane (transverse plane) following excitation. Adapted from Westbrook et al. (4)

3.2 Overview of Magnetic Resonance Relaxation Time

Following the RF pulse, the magnetization vector relaxes to its original equilibrium state. The process of relaxation is governed by two independent processes: T_1 relaxation, which is the recovery of the Z component of the magnetization and T_2 relaxation, which is the recovery of the XY component of the magnetization. The T_1 relaxation is called spin lattice relaxation, while the T_2 relaxation is called spin-spin relaxation.

T_1 relaxation time occurs when nuclei exchange energy with their surrounding environment (the lattice). Following T_1 relaxation, the magnetization vector returns to its original equilibrium state which is parallel to the Z axis. The T_1 relaxation time is derived from the following Bloch equation:

$$\frac{dM_z}{dt} = -\frac{M_z - M_0}{T_1} \quad [3.4]$$

Where M_z is longitudinal magnetization, M_0 is the magnetization after excitation, t is time, and T_1 is the relaxation time constant for a particular tissue. For a 90 degree excitation, the longitudinal magnetization component is governed by equation 3.5

$$M_z = M_0(1 - e^{-t/T_1}) \quad [3.5]$$

The T_1 relaxation time constant is defined as the time it takes the magnetization to return to 63% of the longitudinal magnetization.

T_2 relaxation time is governed by the phase dispersion of the spins due to fluctuating local magnetic fields. T_2 relaxation time is derived from the following Bloch equation:

$$\frac{dM_{xy}}{dt} = -\frac{M_{xy}}{T_2} \quad [3.6]$$

Where M_{xy} is transverse magnetization, t is time, and T_1 is the relaxation time constant for a particular tissue. For a 90° excitation, the transverse magnetization component is governed by equation 3.7

$$M_{xy} = M_0 e^{-t/T_2} \quad [3.7]$$

The T_2 relaxation time constant is defined as the time at which the signal decays to 37% of the maximum signal.


$T_{1\rho}$ relaxation time describes the spin-lattice relaxation in the rotating frame (5). It probes the slow motion interactions between motion-restricted water molecules and their local macromolecular environment. $T_{1\rho}$ approximates T_1 at very low magnetic field strengths. and is governed by the following equation:

$$M_t = M_0 e^{-t/T_{1\rho}} \quad [3.8]$$

Where M_t is the detected magnetization, t is time, and $T_{1\rho}$ is the relaxation time constant for a particular tissue.

3.3 Overview of Texture Analysis

Texture analysis will be performed on a slice-by-slice basis on the cartilage T_2 maps. This method is based on the grey level co-occurrence matrix (GLCM) as described by Haralick et al.(6). The GLCM determines the frequency that neighboring grey-level values occur in an image. Analysis can be performed at a defined orientation (e.g. 0 degrees, 90 degrees) and a defined spacing (e.g. spacing = 1 for nearest-neighbor pixels). Texture parameters including angular second moment (ASM) and entropy are calculated from the co-occurrence matrix. ASM is a measure of order of an image, while entropy is a measure of disorder in an image. The equations for ASM and entropy are shown below (Equations 3.9 and 3.10). P represents the probability of the co-occurrence of pixel values i and j in an image. N represents the total number of pixel value co-occurrences in the image, and R is a normalizing constant.



[3.9]

[3.10]

In this project, texture analysis will be performed on the cartilage T_2 maps in the lateral femur, lateral tibia, medial femur, medial tibia, and trochlea. A grey level co-occurrence matrix will be defined for each cartilage region and used for texture analysis. Second order texture measures including entropy and ASM, will be calculated at 0°

(corresponding to the anterior-posterior axis) and at 90° (corresponding to the superior-inferior axis), with pixel offsets ranging from 1-3 pixels. The pixel offset range is chosen based on the fact that approximately 3 to 4 pixels span the cartilage thickness.

3.4 Review of Literature: Imaging of Cartilage in OA

3.4.1 Radiography

Radiographic images reflect the pathologic changes in cartilage and bone; however they may not correlate with the severity of pathologic joint destruction. Since the pathologic/radiographic findings of disease do not always reflect joint symptoms in cross-sectional studies, the pathologic aspect of the disease does not always parallel the clinical prevalence or natural history of OA. Dougados et al. (7) reported that although radiographic progression was rare by crude Kellgren and Lawrence (8) grading, some symptomatic improvement with current treatment was seen over one year of follow-up. Longer studies have shown that radiographic progression occurs in up to two-thirds of the patients and that improvement is rare (9,10). Radiographic progression was more prevalent in patients who had earlier evidence of structural changes, femoral or tibial sclerosis.

Primary evaluation of arthritis has principally relied on plain radiography, (11) which depicts only gross osseous changes that tend to occur late in the disease. Early changes in the cartilage and other articular tissues are not directly visible. Cartilage loss can only be indirectly inferred by the onset of joint-space narrowing, which can be highly unreliable even with careful attention to proper technique (12). False-positive rates as high as 20-40% have been reported for this parameter. In addition, plain radiographs are insensitive to focal cartilage loss, and widening of the joint space despite significant cartilage loss can occur in one compartment of the knee as a result of narrowing in the other compartment (13).

Furthermore, meniscal position and degeneration affect joint-space narrowing (14), demonstrating that joint-space narrowing is unspecific to global cartilage loss and can implicate various morphologic changes in the joint.

3.4.2 Magnetic Resonance Imaging

Magnetic resonance (MR) imaging is ideal for monitoring arthritis. MR offers multi-planar capabilities, high spatial resolution without ionizing radiation, and superior contrast between joint tissues; thus it has gained popularity as a modality for assessing OA. Using an in-plane resolution (469 microns x 938 microns) and relatively thin slices (1.5 mm) on a 1.5 T scanner, Recht, et al. (15) showed 96% sensitivity and 95% specificity for detecting cartilage abnormalities visible in cadaveric knees following pathological section. Several studies have recently been published that grade cartilage lesions in subjects with OA, and compare the severity of the lesions, with other findings such as meniscal defects, the presence of marrow lesions, as well as radiographic and clinical scores (16-18).

3.4.3 Cartilage Volume and Thickness

High-resolution MR imaging has been used to measure cartilage volume and thickness in OA. MR sequences that best delineate the cartilage from the surrounding tissues such as fat-suppressed spoiled gradient echo and fast double echo and steady state (DESS) with water-excitation, are used for segmentation. To date, a fully automated technique for cartilage segmentation has not been established due to the inherently low contrast between cartilage and surrounding tissues (19). The cartilage is segmented slice-by-slice using a semi-automatic technique such as region growing (20), edge detection (21), or shape modeling (22). An example of segmentation is illustrated in Figure 3.3, in which the femoral and tibial knee cartilage is segmented. Cartilage volume is calculated by summing the pixels

in the segmented regions, and cartilage thickness can be determined using methods such as the Euclidean Distance Transformation (23), or by calculating a vector perpendicular to the articular cartilage or bone surface (24,25). The inter-and intra-observer reproducibility of these techniques ranges from approximately 1-9% and has been elegantly summarized by Eckstein et al. (19)



Figure 3.3: An example of femoral and tibial cartilage segmentation. This image was acquired at 1.5T with an in-plane resolution of $0.234 \times 0.234 \text{ mm}^2$ and a slice thickness of 2 mm.

Average cartilage thickness measurements are useful for the quantification of global thickness; however they are relatively insensitive to the presence of focal cartilage defects. Cartilage thickness maps, which illustrate regional variations in thickness, are helpful for visualizing focal defects (Figure 3.4). Studies have used various sub-regional analysis schemes to quantify cartilage thickness and volume in the lateral or medial sides, or weight-bearing and non-weight-bearing regions of the joint (26). Since different areas of the joint experience different types of mechanical loading, sub-regional analysis may increase the sensitivity of cartilage thickness and volume measurements. While global thickness measurements have been used to differentiate OA patients from healthy subjects (27), the

quantification of cartilage lesions would provide additional information for the improved characterization of osteoarthritic cartilage. Lee et al. have implemented a gradient peak method to quantify focal cartilage lesion volume and area, demonstrating the feasibility of cartilage defect quantification using MRI (28). An image processing method that incorporates both global and focal thickness/volume quantification would be a powerful tool for the diagnosis of OA.

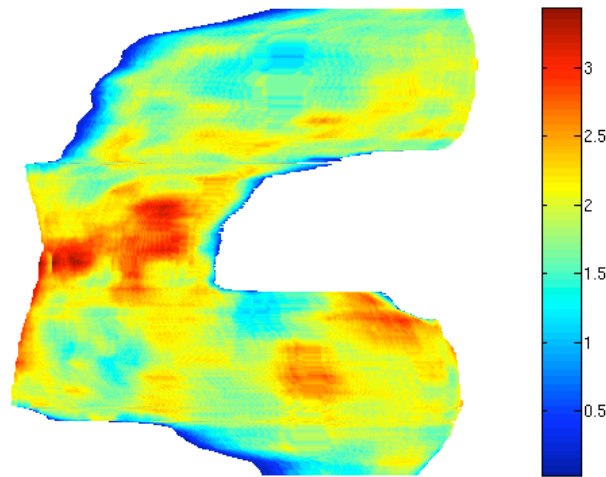


Figure 3.4: An example of femoral cartilage thickness map demonstrating the variation in cartilage thickness throughout the femur.

Longitudinal studies have been used to quantify cartilage changes in OA patients and have found a variety of results. Gandy et al. found no changes in cartilage thickness and volume in OA (29), while other studies (19) have reported an approximate loss of 4-6% of cartilage annually. It is interesting to note a large standard deviation in percentage of cartilage loss, which is indicative of the heterogeneity of the disease. Although the evolution of cartilage morphology in OA is heterogeneous, the quantification of cartilage

thickness and volume is reproducible (19), and may be a useful tool to monitor disease progression and the effect of therapeutic intervention.

MR imaging studies have evaluated the relationship between changes in cartilage and other knee joint tissues in OA. Lindsey et al. and Blumenkrantz et al. have found that cartilage loss on one side of the knee joint is related to trabecular bone loss on the opposite side of the knee joint (27,30). Cartilage degeneration is also associated with changes in subchondral bone architecture (31), as well as changes in trabecular bone proximal to the joint line (30). Other factors associated with cartilage loss include meniscal damage and bone marrow edema (32,33). A recent longitudinal study by Hunter et al. (34) has demonstrated that enlarging bone marrow lesions are associated with cartilage loss in OA. An inverse relationship between pain, as measured by the Western Ontario and McMaster Universities scoring system (WOMAC), and cartilage volume has been demonstrated (27,35-37). Therefore, the measurement of cartilage volume using MR imaging provides longitudinal quantification of cartilage loss in OA and links cartilage loss with degenerative changes in other tissues of the knee joint.

Although research studies have demonstrated a relationship between cartilage and bone morphology in OA, the question of whether cartilage changes precede bone structure changes in OA is remains unanswered. Radin and Rose postulated that subchondral bone sclerosis and stiffening results in cartilage degeneration (38). Carlson et al. reported that increases in subchondral bone thickness precede cartilage degeneration in an animal model of OA (39). Lindsey et al. and Blumenkrantz et al. have demonstrated changes in adjoining trabecular bone with changes in cartilage thickness, emphasizing the relationship between cartilage and bone in OA (27,30). The high-resolution extremity CT (40), has been used to

image trabecular structure in the radius and tibia with a nominal resolution (voxel size) of 82 microns. The high-resolution extremity CT is a useful tool for the *in vivo* evaluation of trabecular bone structure; however, due to imaging field-of-view limitations, it cannot accommodate the knee joint (which is commonly affected by OA). If this scanner could be modified to image the knee joint, it may be possible to determine OA changes in trabecular micro-architecture. The combination of quantitative MR imaging of soft tissue and high-resolution bone imaging shows promise for diagnosing early OA; however further studies are warranted to determine whether trabecular bone structure measurement can be a surrogate marker for cartilage degeneration.

3.4.4 Cartilage T_2 Relaxation Time

Cartilage T_2 maps are created using the following process: Typically, T_2 -weighted multi-echo, spin echo images with varying echo times (TE) and identical repetition times (TR) are acquired. Second, T_2 maps are computed (Figure 3.5) assuming exponential signal decay. T_2 is defined as the time at which the signal decays to 37% of the maximum signal.

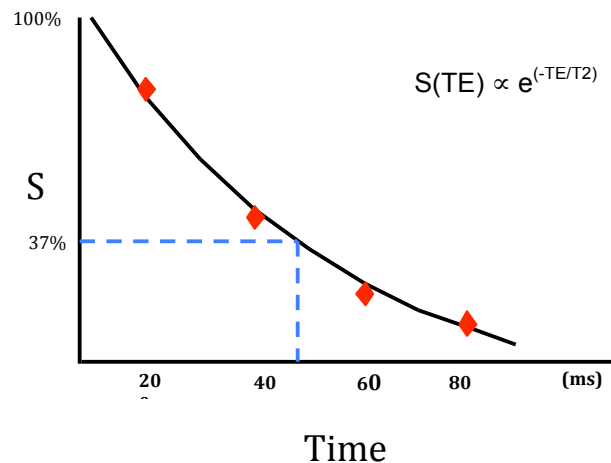


Figure 3.5: An example of T_2 calculation using four T_2 -weighted images acquired with different echo-times (TE). The graph shows signal (S) as a function of time. T_2 is calculated for each pixel in an image using the above equation, and is defined as the time at which the signal decays to 37% of the maximum signal.

Quantitative T_2 relaxation time is a non-invasive marker of cartilage degeneration because it is sensitive to tissue hydration and biochemical composition. Immobilization of water protons in cartilage by the collagen-proteoglycan matrix promotes T_2 decay and renders the cartilage low in signal intensity on long-TE (T_2 -weighted) images, while mobile water protons in synovial fluid retain their high signal. Loss of collagen and proteoglycan in degenerating cartilage increases the mobility of water, thus increasing its signal intensity on T_2 -weighted images (41). Signal intensity is further augmented in degenerative disease by the elevation of cartilage water content (i.e., proton density) that accompanies matrix loss (42). Consistent with this, foci of high signal intensity are often seen within the cartilage of knees with OA on T_2 -weighted images and have been shown to correspond to arthroscopically demonstrable abnormalities (43,44).

3.4.4.1 In Vitro Imaging

In vitro imaging studies have evaluated the relationship between biochemistry of cartilage and T_2 measurements. Cartilage T_2 is affected by hydration and the integrity of the collagen matrix; however, the relationship between T_2 and proteoglycan content remains controversial in literature. Proteoglycan loss in rat patellar cartilage induced by hyaluronidase degradation (which does not alter the collagen network) was associated with significantly increased global T_2 (45). However, other studies (46-48) found that the depletion of proteoglycan had minimal effects on T_2 . A positive relationship between water content and T_2 has been reported (49,50). These studies demonstrate that the biochemical changes associated with cartilage degeneration are related to elevated T_2 ; however the effects of proteoglycan concentration on T_2 must be further evaluated.

The relationship between T_2 relaxation time and the mechanical properties of cartilage is under investigation. A recent in vitro study (51) has shown that T_2 relaxation time in human patellar cartilage is significantly correlated to Young's Modulus, suggesting that T_2 quantification may predict the mechanical properties of cartilage.

The signal intensity of cartilage in an MR image is dependent on its orientation to the main magnetic field. An in vitro study using high-field (8.6T) microscopic MRI (μ MRI) has suggested that the angular dependency of T_2 with respect to the main magnetic field (B_0) can provide specific information about the collagen ultra-structure (52). However, the requirement for the specific orientation of cartilage to the main magnetic field and the required ultra-high resolution (at $13.7\mu\text{m}$) preclude it from in vivo applications with current techniques. Goodwin et al. (53) have described how T_2 will vary with depth from the articular surface due to collagen fibril orientation to B_0 . Imaging of the femoral condyles can be challenging due to the bulk curvature of the cartilage altering the depth-dependent fibril orientation. However, a comprehensive in vivo study has shown that the “magic-angle effect” may not be the major determinant of T_2 heterogeneity in high-curvature articular cartilage (54).

3.4.4.2 In Vivo Imaging

In vivo MR T_2 mapping has primarily been performed at 1.5 and 3.0 Tesla; however recent studies have demonstrated the feasibility of measuring relaxation properties in cartilage at 7.0 Tesla (55-57), thus providing increased SNR. The acquisition time for each sequence is an important consideration in study design – minimal acquisition time (while retaining accurate quantification of relaxation properties) is desirable, such that the chances of motion during scans are minimized and the number of scans per study is maximized.

Generally, the T_2 mapping acquisition time ranges from about 10-20 minutes (58), however various techniques have been recently developed to reduce acquisition time: Fast T_2 imaging using gradient and spin echo (GRASE) MR imaging has been recently developed and validated at 1.5 Tesla, yielding an acquisition time of 1 minute and 51 seconds (59). Parallel imaging sequences with an acceleration factor of 2 ($AF = 2$) have been developed at 3 Tesla for the measurement of cartilage relaxation times ($T_{1\rho}$, T_2) and morphologic measures (volume and thickness), demonstrating comparable results to the conventional method (60). These studies highlight technical MR imaging advancements with increasing field strength and decreasing acquisition time.

In vivo imaging studies have measured T_2 relaxation time to evaluate the effects of gender (61), age (62,63), disease (30,62,64-66), activity level (67-69), and treatment (e.g. chondrocyte transplantation (70)). Studies have demonstrated that cartilage T_2 values are related to age, and vary from the subchondral bone to the cartilage surface (62,71). Dunn et al. have shown that the cartilage T_2 values are associated with the severity of OA, and variations exist between tibial and femoral cartilage T_2 (72). The precision errors of T_2 measurements in patellar cartilage have been evaluated (73,74). The precision errors of T_2 were markedly smaller than the differences in T_2 between healthy and diseased cartilage, suggesting that T_2 may be discriminatory biomarker for disease. Dunn et al. used Z-score maps to compare cartilage T_2 values of OA subjects to those in control subjects(72). Voxel based Z-scores were generated in each compartment of the articular cartilage for the T_2 images. A voxel in a Z-image was calculated by $(Voxel_I - Mean_{normal,compartment})/SD_{normal,compartment}$, where $Voxel_I$ is the T_2 in the voxel of interest, $Mean_{normal,compartment}$ is the mean T_2 for all voxels of the normal knees in that compartment, and the $SD_{normal,compartment}$ is

the standard deviation of the same normal T_2 distribution. The Z-score maps normalize the T_2 results for each subject to the mean value of the control subjects. Figure 3.6 illustrates Z-score maps of a control, a mild OA subject, and a severe OA subject, respectively. These maps demonstrate the heterogeneity of cartilage T_2 values. Studies have evaluated the spatial distribution of cartilage T_2 : Dray et al. (75) found no difference between mean T_2 values in OA cartilage; however, they showed visual differences in the spatial distribution of the T_2 values. These results demonstrate the necessity to characterize and quantify the spatial distribution of cartilage T_2 values.

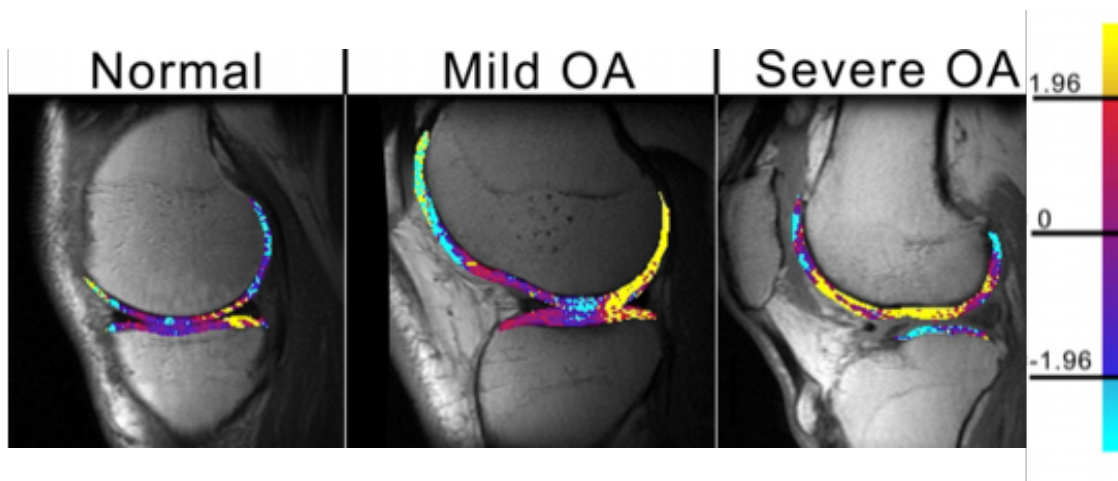


Figure 3.6: Representative Z-score maps a control, a mild OA subject, and a severe OA subject. The maps show an increase in area of regions of high in the OA subjects. The regional variations in femoral and tibial cartilage compared to control subjects are also evident. Adapted from Dunn et al (72).

A recent study employed grey level co-occurrence matrix (GLCM) texture analysis to quantify the differences in spatial distribution of cartilage T_2 values in OA patients and controls. The mean, standard deviation, and GLCM entropy of cartilage T_2 was significantly greater in OA patients than in controls (76), demonstrating that T_2 values in osteoarthritic cartilage are not only elevated, but also more heterogeneous than those in healthy cartilage.

Moreover, Carballido-Gamio et al. have demonstrated the feasibility of flattening cartilage for texture analysis, thus obtaining measurements both parallel and perpendicular to the natural cartilage layers (77). By non-invasively evaluating cartilage integrity, T_2 relaxation time may provide insight on both global (mean T_2) and focal (texture analysis of T_2) changes in cartilage degeneration in OA.

The evaluation of cartilage repair tissue using quantitative MRI is an emerging avenue of research. In addition to morphologic imaging techniques, T_2 relaxation time has been used to quantitatively assess the biochemical composition of cartilage repair tissue, thus providing insight on the tissue integrity. Previous studies have measured T_2 relaxation time to assess cartilage following cartilage repair techniques including chondrocyte transplantation(70,78-82)and microfracture (79,81,83). A recent longitudinal study by Welsch et al. performed MRI examinations on patients one year after they had undergone matrix-associated autologous chondrocyte transplantation(78). While there were no significant changes to cartilage morphology at one-year follow-up, changes to zonal T_2 values were evident. This study demonstrates the T_2 mapping may be an emerging tool to non-invasively and assess the longitudinal outcome of cartilage repair, and may supplement standard morphological cartilage assessment.

T_2 relaxation time has primarily been evaluated in cartilage in both healthy subjects and those with OA, however recent studies have measured T_2 in the meniscus (84). Rauscher et al. demonstrated differences in T_2 between OA patients and controls, as well as correlations with clinical findings (84). This study highlights that relaxation times measurements in both the cartilage and meniscus may be sensitive to degenerative changes in OA.

The relationship between T_2 and cartilage morphology has been evaluated cross-sectionally and longitudinally. Studies have shown an inverse relationship between cartilage T_2 and cartilage thickness (30,72). Another study has shown that higher medial cartilage T_2 results in greater loss of medial cartilage volume at twelve months, demonstrating a relationship between cartilage T_2 and cartilage volume (85). The relationship between cartilage T_2 and the underlying bone structure has been investigated (86,87). Bolbos et al. reported a negative relationship between T_2 relaxation time, and bone structural parameters including bone volume fraction (BV/TV), and trabecular number (Tb.N)) (86), highlighting the interplay between cartilage and bone structure.

3.4.5 Cartilage $T_{1\rho}$ Relaxation Time

A $T_{1\rho}$ sequence, consisting of a three-pulse cluster and gradient crushers, prepares the $T_{1\rho}$ -weighted magnetization. Briefly, first, a $\pi/2$ pulse applied along the x-axis flips the longitudinal magnetization into the transverse plane along the y-axis. Then, a long, low power pulse is applied along the y-axis to spin-lock the magnetization. The second $\pi/2$ pulse flips this spin-locked magnetization back to the z-axis. Residual transverse magnetization is then dephased by a crusher gradient. Magnetization stored along the z-axis is then read out by a fast spin echo (FSE) sequence or a gradient echo sequence. $T_{1\rho}$ can be calculated by fitting the signal (S) intensity obtained for different spin-locking times (TSL) using the equation 1. Quantitative $T_{1\rho}$ imaging methods are well-suited for probing macromolecular slow motions at high static fields in cartilage.

In cartilage, the proteoglycan (PG) largely responsible for the high elasticity and resilience of tissue, consists of a central protein core to which a large number of negatively charged glycosaminoglycan (GAG) sidechains are covalently attached. The PG content of

cartilage can be probed using spin lattice relaxation in the rotating frame ($T_{1\rho}$ -weighted imaging) (88-90).

In vitro studies have evaluated the relationship between $T_{1\rho}$ relaxation time and the biochemical composition of cartilage. Akella et al. have demonstrated that over 50% depletion of PG from bovine articular cartilage resulted in average $T_{1\rho}$ increases from 110–170 ms (90). Regression analysis of the data showed a strong correlation ($r^2=0.987$) between changes in PG and $T_{1\rho}$. Similar to T_2 , in vitro studies have demonstrated regional variations of cartilage $T_{1\rho}$. $T_{1\rho}$ values were highest at the superficial zone, decreased gradually in the middle zone, and increased in the region near the subchondral bone (90). Wheaton et al. found correlations between $T_{1\rho}$ relaxation time, proteoglycan, and mechanical properties of bovine cartilage explants including aggregate modulus and hydraulic permeability (91).

In vivo studies have quantified $T_{1\rho}$ relaxation time in knee cartilage and have documented its reproducibility. Pakin et al. reported an *in vivo* reproducibility (coefficient of variation) for patellar cartilage of 5% (92); Li et al. reported a coefficient of variation (in femoral and patellar cartilage) of 4.8% (93); Regatte et al. reported an intrasubject variability of < 6% (89). *In vivo* studies have demonstrated increased cartilage $T_{1\rho}$ values in OA subjects compared to controls: Li et al. showed average $T_{1\rho}$ relaxation times of 45.09 ± 2.59 ms and 53.06 ± 4.60 ms in healthy subjects and OA patients, respectively (93). In a more recent study, Li et al. also found elevated $T_{1\rho}$ relaxation time in OA patients (52.04 ± 2.97 ms) compared to healthy subjects (45.53 ± 3.28 ms) (94). Regatte et al. reported a larger range of $T_{1\rho}$ values in OA subjects (63 ± 4 ms to 95 ± 12 ms, depending on the degree of cartilage degeneration) compared to healthy subjects (44 to 55 ms) (95), and demonstrated a 25% to 30% elevation in $T_{1\rho}$ values in OA patients compared to healthy subjects. Studies

have used $T_{1\rho}$ imaging to evaluate cartilage overlying bone marrow edema (BME) caused by trauma. Average $T_{1\rho}$ values in cartilage overlying BME were significantly higher than that in surrounding cartilage (51.8 ± 10.8 ms vs. 43.0 ± 8.3 ms, $p = 0.032$), demonstrating that macromolecular changes in cartilage may be related to BME (96).

The differences between T_2 and $T_{1\rho}$ in cartilage have been explored. Mlyranik et al. (47) showed that the $T_{1\rho}$ relaxation times obtained were slightly longer than the corresponding T_2 values, but both parameters showed almost identical spatial distributions. Menezes et. al. (97) have recently shown that $T_{1\rho}$ and T_2 changes in articular cartilage do not necessarily coincide, and might provide complimentary information. These investigators showed that $T_{1\rho}$ and T_2 reflect changes that may be associated with proteoglycan, collagen content and hydration and the true mechanism of $T_{1\rho}$ may arise from a weighted-average of multiple biochemical changes occurring in cartilage in OA. Using this premise, it is possible that $T_{1\rho}$ may have a dependence on the angular orientation of the collagen fibers.

$T_{1\rho}$ has a larger dynamic range than T_2 (98), indicating that it may be more sensitive to degenerative changes occurring in cartilage OA. A recent study by Majumdar et al. investigated the differences in T_2 and $T_{1\rho}$ values between OA patients and controls. A significant correlation was found between average $T_{1\rho}$ and T_2 values within the cartilage, with a correlation coefficient $r^2=0.69$ and $p=0.017$. The average $T_{1\rho}$ in OA patients (52.28 ms) was 19.1% greater than that of controls (43.90 ms). The average T_2 (38.31 ms) in OA patients was only 9.6% greater than that of controls (34.94 ms). OA patients had a significantly ($p = 0.003$) increased cartilage $T_{1\rho}$ compared to controls, while the increase in T_2 was insignificant ($p = 0.202$) (96), demonstrating that patients with similar average T_2 may have different $T_{1\rho}$, or vice versa. These studies suggest that average $T_{1\rho}$ may be used to

distinguish OA cartilage from healthy cartilage, while T_2 may not be able to. Figure 3.7 shows $T_{1\rho}$ and T_2 maps from a control subject, a subject with mild OA, and a subject with severe OA. The differences between the $T_{1\rho}$ and T_2 maps are evident. These studies reflect the potential of $T_{1\rho}$ imaging for the non-invasive evaluation of diseased cartilage. However, further studies with larger symptomatic populations are necessary to examine whether $T_{1\rho}$ quantification can be used as a diagnostic tool for early OA.

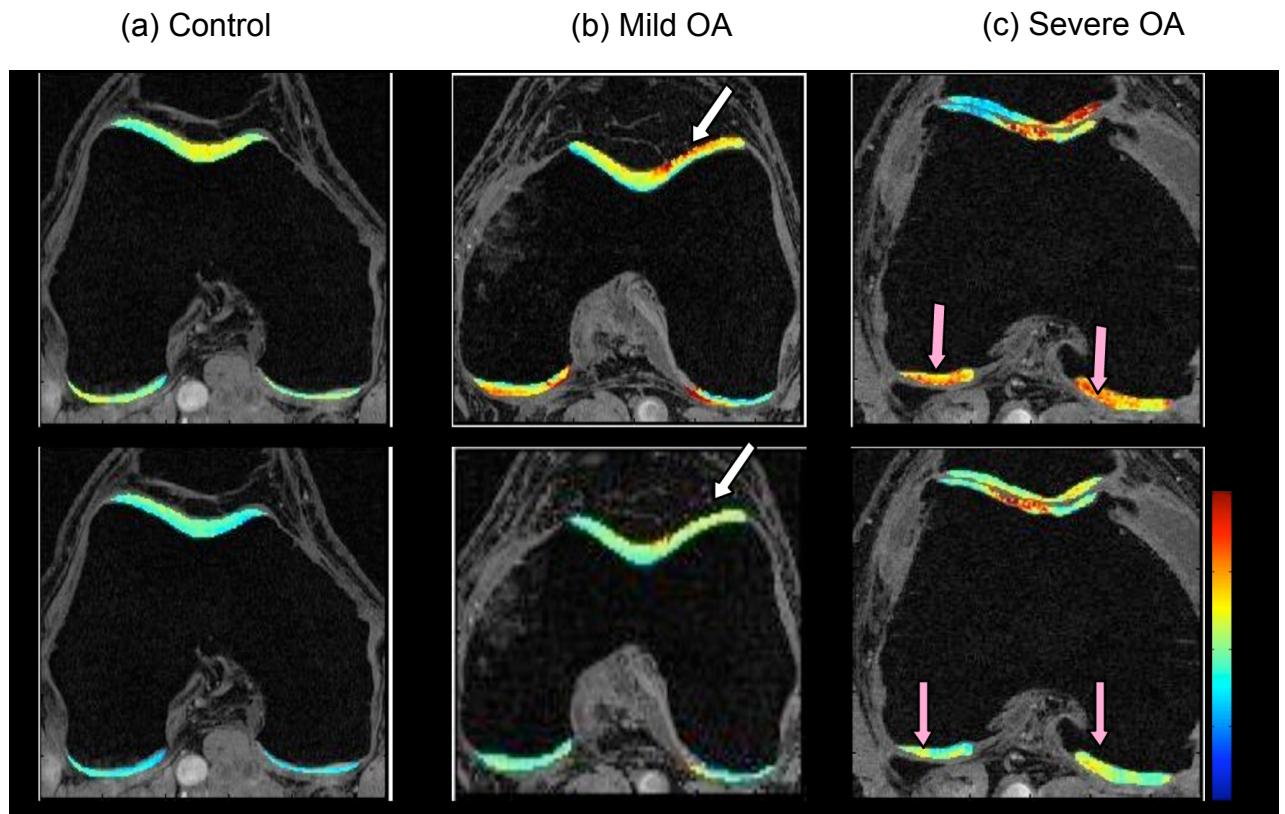


Figure 3.7: $T_{1\rho}$ maps (first row) and T_2 maps (second row) for a healthy control (a), a patient with mild OA (b), and a patient with severe OA (c). a) Control: The average $T_{1\rho}$ value was 40.1 ± 11.4 ms and T_2 values was 33.3 ± 10.5 ms in cartilage. (b) A patient with early OA (male, 66). The average $T_{1\rho}$ value was 45.5 ± 14.5 ms and T_2 values was 35.0 ± 10.9 ms in cartilage. (c) A patient with advanced OA (male, 46). The average $T_{1\rho}$ value was 55.4 ± 26.0 ms and T_2 values was 43.8 ± 11.1 ms in cartilage. The maps illustrate the differences between $T_{1\rho}$ and T_2 (arrows) and demonstrate differences in cartilage heterogeneity between OA severity and between T_2 and $T_{1\rho}$ maps.

3.5 Review of Literature: Imaging of Degenerative Disc Disease

3.5.1 Current Clinical Imaging Techniques

Various techniques have been proposed to assess the competence of the disc *in vivo* with particular emphasis on developing objective surgical indications. Radiographic imaging of the disc in the anteroposterior and lateral views can be used to assess disc height; however it is not well suited to evaluate soft tissue structure and disc herniation. Computed tomography (CT) scanning is the first line of investigation in vertebral spine trauma and but is of limited value in assessing suspected lumbar prolapsed intervertebral disc disease. CT can be used to identify gross morphologic changes including annular disc bulges and loss of disc height (using sagittal reformations). However, early degenerative changes are not well depicted. Both radiographs and CT imaging are sources of ionizing radiation, which may be harmful with repetitive exposure. While pain provocation using discography/CT discography(99-101) has been shown to improve the odds of a positive surgical outcome, there has been a reported high incidence of false positives(102) and there remains a significant number of severely degenerated discs that have been found to be symptomatic(103).

3.5.2 Magnetic Resonance Relaxation Time Measurement

Magnetic resonance imaging (MRI) has been used as a non-invasive measure of disc degeneration representing early and more advanced changes. The advantages of MR imaging are that 1) non-ionizing radiation is generated 2) excellent soft tissue contrast is achieved (allowing the delineation of the annulus from the nucleus) 3) multi-planar image acquisition is feasible and 4) and high spatial resolution can be achieved. Modic and Weinstein(104) reported that disc degeneration can be demonstrated by using the standard spin echo

sequence. With T₂-weighted, spine echo imaging sequences, normal intervertebral discs show a bright signal from the nucleus pulposus, and there is low signal from the annulus fibrosus. Disc degeneration is demonstrated by a change in the signal of the nucleus pulposus to give an irregular outline and a reduction in signal intensity. This technique has been shown to be as good or often a more accurate measure of degeneration than discography(105-107). However, patient symptoms in painful degenerated disc disease do not correlate with these standard MR imaging findings. In the intervertebral disc, the uptake of Gd DTPA enhancement has been observed clinically often in normal appearing discs(108) and there is a high prevalence of disc degeneration in asymptomatic populations(109). Stabler et al.(110) have shown that a band like contrast enhancement of the disc correlated with vascularization, often seen as a consequence of annular tears, and corresponded to pain, even in the absence of stenosis.

In an effort to improve the capability of MR techniques to quantitatively assess disc degeneration, surrogate MR measures of tissue hydration and biochemical composition, such as relaxation times (T₁ and T₂) and water diffusivity are being studied. Investigators have demonstrated correlations between 1/T₁, 1/T₂ water content and collagen content for disc tissue samples(111,112). In another study, Boos et al.(113) using age and gender matched symptomatic and asymptomatic disc herniations, showed that symptomatic disc herniations showed significantly shorter T₁ (p<0.04, -15%) and T₂ (p<0.003, -21%). Molecular diffusion shortens the spin-echo signal and has been used to study disc degeneration *in vitro*. In the spine, the addition of diffusion-weighted imaging (DWI) has been shown in multiple applications(114-118) to provide additional diagnostic information. Line Scan Diffusion Imaging (LSDI) (119), which is considerably more robust than other common sequences in

the presence of global motion and susceptibility differences(120), gives high quality diffusion weighted images and apparent diffusion coefficient (ADC) and anisotropy maps in the human spine.

Quantitative $T_{1\rho}$ imaging probes the interaction between motionally restricted water molecules and their macro-molecular environment, thus the extracellular matrix (ECM) in the intervertebral disc may potentially be investigated using these techniques. Previous studies have explored the relationship between $T_{1\rho}$ relaxation rate and biochemical analysis in cartilage and in the intervertebral disc. Regatte et al. have shown that $T_{1\rho}$ relaxation rate is correlated to proteoglycan content ($R^2 = 0.85$, $P < 0.0001$) in bovine patellar cartilage(121), and Johannessen et al.(122) have shown a strong correlation between $T_{1\rho}$ and s-GAG content ($r = 0.7$, $p < 0.01$) in intervertebral disc specimens. *In vivo* studies have reported significantly elevated $T_{1\rho}$ relaxation time in osteoarthritic subjects (95,123), demonstrating that $T_{1\rho}$ can be used to identify cartilage degeneration. Based on these data, we hypothesize that $T_{1\rho}$ can be used as a marker for early biochemical changes in the disc, and may complement measurements of T_2 relaxation time.

3.6 References

1. Bloch F, Hansen WW, Packard M. Nuclear induction. *Physical Review* 1946;70(7-8):460-474.
2. Purcell EM, Torrey HC, Pound RV. Resonance absorption by nuclear magnetic moments in a solid. *Physical Review* 1946;69(1-2):37-38.
3. Lauterbur PC. Image formation by induced local interactions: examples employing nuclear magnetic resonance. *Nature* 1973;242(5394):190-191.
4. Westbrook C, Kaut-Roth C, Talbot J. *MRI in Practice*: Wiley-Blackwell; 2005.

5. Sepponen R. Rotating Frame and Magnetization Transfer. In: Stark DD, Bradley WGJ, editors. Magnetic Resonance Imaging. Volume 1. St. Louis: Mosby-Year Book; 1992. p 204-218.
6. Haralick RM, Shanmugam K, Dinstein I. Textural Features for Image Classification. IEEE Transactions on Systems, Man, and Cybernetics 1973;SMC-3(6):610-618.
7. Dougados M, Gueguen A, Nguyen M, al. e. Longitudinal radiologic evaluation of osteoarthritis of the knee. J Rheumatology 1992;19:378 - 383.
8. Kellgren J, Lawrence J. Radiologic assessment of osteoarthritis. Ann Rheum Dis 1957;16:494-502.
9. Schouten J, van den Ouweland F, Valkenberg H. A 12 year follow up of osteoarthritis of the knee in the general population on prognostic factors of cartilage loss in osteoarthritis of the knee. Ann Rheum Dis 1992;51:932-937.
10. Spector T, Dacre J, Harris P, al. e. Radiological progression of osteoarthritis: an 11 year follow up study of the knee. Ann of Rheum Dis 1992;51:1107-1110.
11. Altman R, Fries J, Bloch D. Radiographic assessment of progression in osteoarthritis. Arthritis Rheum 1987;30:11.
12. Rogers J, Watt, Dieppe P. A comparison of the visual and radiographic detection of bony changes at the knee joint. BMJ 1990;300:367-368.
13. Chan W, Stevens M, Lang P, Sack K, Majumdar S, Stoller D, Genant H. Structural changes of osteoarthritis of the knee: radiography, CT, and MR imaging correlation. Radiology 1990;177 (P):183.
14. Hunter DJ, Zhang Y, X. T, M L, Niu J, Amin S, Guermazi A, Genant H, Gale D, Felson DT. Change in Joint Space Width: Hylaine Articular Cartilage Loss or Alteration in Meniscus. Arthritis Rheum 2006;54(8):2488-2495.
15. Recht M, Kramer J, Marcelis S, Pathria M, Trudell D, Haghghi P, Battens D, Resnick D. Abnormalities of articular cartilage in the knee: analysis of available MR techniques. Radiology 1993;187:473-478.

16. Link TM, Steinbach LS, Ghosh S, Ries M, Lu Y, Lane N, Majumdar S. Osteoarthritis: MR imaging findings in different stages of disease and correlation with clinical findings. *Radiology* 2003;226(2):373-381.
17. Felson DT, McLaughlin S, Goggins J, LaValley MP, Gale ME, Totterman S, Li W, Hill C, Gale D. Bone marrow edema and its relation to progression of knee osteoarthritis. *Ann Intern Med* 2003;139(5 Pt 1):330-336.
18. Felson DT, Chaisson CE, Hill CL, Totterman SM, Gale ME, Skinner KM, Kazis L, Gale DR. The association of bone marrow lesions with pain in knee osteoarthritis. *Ann Intern Med* 2001;134(7):541-549.
19. Eckstein F, Cicuttini F, Raynauld JP, Waterton JC, Peterfy C. Magnetic resonance imaging (MRI) of articular cartilage in knee osteoarthritis (OA): morphological assessment. *Osteoarthritis Cartilage* 2006;14 Suppl A:A46-75.
20. Peterfy CG, van Dijke CF, Janzen DL, Gluer CC, Namba R, Majumdar S, Lang P, Genant HK. Quantification of articular cartilage in the knee with pulsed saturation transfer subtraction and fat-suppressed MR imaging: optimization and validation. *Radiology* 1994;192(2):485-491.
21. Kshirsagar AA, Watson PJ, Tyler JA, Hall LD. Measurement of localized cartilage volume and thickness of human knee joints by computer analysis of three-dimensional magnetic resonance images. *Invest Radiol* 1998;33(5):289-299.
22. Solloway S, Hutchinson CE, Waterton JC, Taylor CJ. The use of active shape models for making thickness measurements of articular cartilage from MR images. *Magn Reson Med* 1997;37(6):943-952.
23. Stammberger T, Eckstein F, Englmeier KH, Reiser M. Determination of 3D cartilage thickness data from MR imaging: computational method and reproducibility in the living. *Magn Reson Med* 1999;41(3):529-536.
24. Losch A, Eckstein F, Haubner M, Englmeier KH. A non-invasive technique for 3-dimensional assessment of articular cartilage thickness based on MRI. Part 1: Development of a computational method. *Magn Reson Imaging* 1997;15(7):795-804.

25. Cohen ZA, McCarthy DM, Kwak SD, Legrand P, Fogarasi F, Ciaccio EJ, Ateshian GA. Knee cartilage topography, thickness, and contact areas from MRI: in-vitro calibration and in-vivo measurements. *Osteoarthritis Cartilage* 1999;7(1):95-109.
26. Stahl R, Blumenkrantz G, Carballido-Gamio J, Zhao S, Munoz T, Hellio Le Graverand-Gastineau M-P, Li X, Majumdar S, Link TM. MRI-derived T2 relaxation times and cartilage morphometry of the tibio-femoral joint in subjects with and without osteoarthritis during a one-year follow-up. *Osteoarthritis Cartilage* 2007;in press.
27. Lindsey CT, Narasimhan A, Adolfo JM, Jin H, Steinbach LS, Link T, Ries M, Majumdar S. Magnetic resonance evaluation of the interrelationship between articular cartilage and trabecular bone of the osteoarthritic knee(1). *Osteoarthritis Cartilage* 2004;12(2):86-96.
28. Lee KY, Dunn TC, Steinbach LS, Ozhinsky E, Ries MD, Majumdar S. Computer-aided quantification of focal cartilage lesions of osteoarthritic knee using MRI. *Magn Reson Imaging* 2004;22(8):1105-1115.
29. Gandy SJ, Dieppe PA, Keen MC, Maciewicz RA, Watt I, Waterton JC. No loss of cartilage volume over three years in patients with knee osteoarthritis as assessed by magnetic resonance imaging. *Osteoarthritis Cartilage* 2002;10(12):929-937.
30. Blumenkrantz G, Lindsey CT, Dunn TC, Jin H, Ries MD, Link TM, Steinbach LS, Majumdar S. A pilot, two-year longitudinal study of the interrelationship between trabecular bone and articular cartilage in the osteoarthritic knee. *Osteoarthritis Cartilage* 2004;12(12):997-1005.
31. Bobinac D, Spanjol J, Zoricic S, Maric I. Changes in articular cartilage and subchondral bone histomorphometry in osteoarthritic knee joints in humans. *Bone* 2003;32(3):284-290.
32. Raynauld JP, Martel-Pelletier J, Berthiaume MJ, Beaudoin G, Choquette D, Haraoui B, Tannenbaum H, Meyer JM, Beary JF, Cline GA, Pelletier JP. Long term evaluation of disease progression through the quantitative magnetic resonance imaging of symptomatic knee osteoarthritis patients: correlation with clinical symptoms and radiographic changes. *Arthritis Res Ther* 2006;8(1):R21.

33. Torres L, Dunlop DD, Peterfy C, Guermazi A, Prasad P, Hayes KW, Song J, Cahue S, Chang A, Marshall M, Sharma L. The relationship between specific tissue lesions and pain severity in persons with knee osteoarthritis. *Osteoarthritis Cartilage* 2006;14(10):1033-1040.
34. Hunter DJ, Zhang Y, Niu J, Goggins J, Amin S, LaValley MP, Guermazi A, Genant H, Gale D, Felson DT. Increase in bone marrow lesions associated with cartilage loss: a longitudinal magnetic resonance imaging study of knee osteoarthritis. *Arthritis Rheum* 2006;54(5):1529-1535.
35. Hunter DJ, March L, Sambrook PN. The association of cartilage volume with knee pain. *Osteoarthritis Cartilage* 2003;11(10):725-729.
36. Wluka AE, Wolfe R, Stuckey S, Cicuttini FM. How does tibial cartilage volume relate to symptoms in subjects with knee osteoarthritis? *Ann Rheum Dis* 2004;63(3):264-268.
37. Cicuttini F, Wluka A, Wang Y, Stuckey S. The determinants of change in patella cartilage volume in osteoarthritic knees. *J Rheumatol* 2002;29(12):2615-2619.
38. Radin E, Rose R. Role of subchondral bone in the initiation and progression of cartilage damage. *Clinical orthopedics and Related research* 1986;213:34-40.
39. Carlson CS, Loeser RF, Purser CB, Gardin JF, Jerome CP. Osteoarthritis in cynomolgus macaques. III: Effects of age, gender, and subchondral bone thickness on the severity of disease. *J Bone Miner Res* 1996;11(9):1209-1217.
40. Boutroy S, Bouxsein ML, Munoz F, Delmas PD. In vivo assessment of trabecular bone microarchitecture by high-resolution peripheral quantitative computed tomography. *J Clin Endocrinol Metab* 2005;90(12):6508-6515.
41. Konig H, Sauter R, Delmling M, Vogt M. Cartilage disorders: a comparison of spin-echo, CHES, and FLASH sequence MR images. *Radiology* 1987;164:753-758.
42. Lehner K, Rechl H, Gmeinwieser J, Heuck A, Lukas H, Kohl H. Structure, function, degeneration of bovine hyaline cartilage: assessment with MR imaging in vitro. *Radiology* 1989;170:495-499.

43. Broderick L, Turner D, Renfrew D, Schnitzer T, Huff J, Harris C. Severity of articular cartilage abnormality in patients with osteoarthritis: evaluation with fast spin-echo MR vs arthroscopy. *AJR* 1994;162:99-103.
44. Peterfy CG. Imaging of the disease process. *Curr Opin Rheumatol* 2002;14(5):590-596.
45. Watrin-Pinzano A, Ruaud JP, Olivier P, Grossin L, Gonord P, Blum A, Netter P, Guillot G, Gillet P, Loeuille D. Effect of proteoglycan depletion on T2 mapping in rat patellar cartilage. *Radiology* 2005;234(1):162-170.
46. Borthakur A, Shapiro EM, Beers J, Kudchodkar S, Kneeland JB, Reddy R. Sensitivity of MRI to proteoglycan depletion in cartilage: comparison of sodium and proton MRI. *Osteoarthritis Cartilage* 2000;8(4):288-293.
47. Mlynarik V, Trattnig S, Huber M, Zembsch A, Imhof H. The role of relaxation times in monitoring proteoglycan depletion in articular cartilage. *J Magn Reson Imaging* 1999;10(4):497-502.
48. Toffanin R, Mlynarik V, Russo S, Szomolanyi P, Piras A, Vittur F. Proteoglycan depletion and magnetic resonance parameters of articular cartilage. *Arch Biochem Biophys* 2001;390(2):235-242.
49. Lusse S, Claassen H, Gehrke T, Hassenpflug J, Schunke M, Heller M, Gluer CC. Evaluation of water content by spatially resolved transverse relaxation times of human articular cartilage. *Magn Reson Imaging* 2000;18(4):423-430.
50. Chou MC, Tsai PH, Huang GS, Lee HS, Lee CH, Lin MH, Lin CY, Chung HW. Correlation between the MR T2 value at 4.7 T and relative water content in articular cartilage in experimental osteoarthritis induced by ACL transection. *Osteoarthritis Cartilage* 2008.
51. Lammentausta E, Kiviranta P, Nissi MJ, Laasanen MS, Kiviranta I, Nieminen MT, Jurvelin JS. T2 relaxation time and delayed gadolinium-enhanced MRI of cartilage (dGEMRIC) of human patellar cartilage at 1.5 T and 9.4 T: Relationships with tissue mechanical properties. *J Orthop Res* 2006;24(3):366-374.
52. Xia Y. Relaxation anisotropy in cartilage by NMR microscopy (μ MRI) at 14-microm resolution. *Magn Reson Med* 1998;39(6):941-949.

53. Goodwin DW, Wadghiri YZ, Dunn JF. Micro-imaging of articular cartilage: T2, proton density, and the magic angle effect. *Acad Radiol* 1998;5(11):790-798.
54. Mosher TJ, Smith H, Dardzinski BJ, Schmithorst VJ, Smith MB. MR imaging and T2 mapping of femoral cartilage: in vivo determination of the magic angle effect. *AJR Am J Roentgenol* 2001;177(3):665-669.
55. Welsch GH, Mamisch TC, Hughes T, Zilkens C, Quirbach S, Scheffler K, Kraff O, Schweitzer ME, Szomolanyi P, Trattnig S. In vivo biochemical 7.0 Tesla magnetic resonance: preliminary results of dGEMRIC, zonal T2, and T2* mapping of articular cartilage. *Invest Radiol* 2008;43(9):619-626.
56. Krug R, Carballido-Gamio J, Banerjee S, Stahl R, Carvajal L, Xu D, Vigneron D, Kelley DA, Link TM, Majumdar S. In vivo bone and cartilage MRI using fully-balanced steady-state free-precession at 7 tesla. *Magn Reson Med* 2007;58(6):1294-1298.
57. Pakin SK, Cavalcanti C, La Rocca R, Schweitzer ME, Regatte RR. Ultra-high-field MRI of knee joint at 7.0T: preliminary experience. *Acad Radiol* 2006;13(9):1135-1142.
58. Regatte RR, Schweitzer ME. Novel contrast mechanisms at 3 Tesla and 7 Tesla. *Semin Musculoskelet Radiol* 2008;12(3):266-280.
59. Quaia E, Toffanin R, Guglielmi G, Ukmar M, Rossi A, Martinelli B, Cova MA. Fast T2 mapping of the patellar articular cartilage with gradient and spin-echo magnetic resonance imaging at 1.5 T: validation and initial clinical experience in patients with osteoarthritis. *Skeletal Radiol* 2008;37(6):511-517.
60. Zuo J, Li X, Banerjee S, Han E, Majumdar S. Parallel imaging of knee cartilage at 3 Tesla. *J Magn Reson Imaging* 2007;26(4):1001-1009.
61. Mosher TJ, Collins CM, Smith HE, Moser LE, Sivarajah RT, Dardzinski BJ, Smith MB. Effect of gender on in vivo cartilage magnetic resonance imaging T2 mapping. *J Magn Reson Imaging* 2004;19(3):323-328.
62. Mosher TJ, Dardzinski BJ, Smith MB. Human articular cartilage: influence of aging and early symptomatic degeneration on the spatial variation of T2--preliminary findings at 3 T. *Radiology* 2000;214(1):259-266.

63. Mosher TJ, Liu Y, Yang QX, Yao J, Smith R, Dardzinski BJ, Smith MB. Age dependency of cartilage magnetic resonance imaging T2 relaxation times in asymptomatic women. *Arthritis Rheum* 2004;50(9):2820-2828.
64. Li X, Benjamin Ma C, Link TM, Castillo DD, Blumenkrantz G, Lozano J, Carballido-Gamio J, Ries M, Majumdar S. In vivo T(1rho) and T(2) mapping of articular cartilage in osteoarthritis of the knee using 3 T MRI. *Osteoarthritis Cartilage* 2007;15(7):789-797.
65. Stahl R, Blumenkrantz G, Carballido-Gamio J, Zhao S, Munoz T, Hellio Le Graverand-Gastineau MP, Li X, Majumdar S, Link TM. MRI-derived T2 relaxation times and cartilage morphometry of the tibio-femoral joint in subjects with and without osteoarthritis during a 1-year follow-up. *Osteoarthritis Cartilage* 2007;15(11):1225-1234.
66. Koff MF, Amrami KK, Kaufman KR. Clinical evaluation of T2 values of patellar cartilage in patients with osteoarthritis. *Osteoarthritis Cartilage* 2007;15(2):198-204.
67. Mosher TJ, Smith HE, Collins C, Liu Y, Hancy J, Dardzinski BJ, Smith MB. Change in knee cartilage T2 at MR imaging after running: a feasibility study. *Radiology* 2005;234(1):245-249.
68. Stahl R, Luke A, Li X, Carballido-Gamio J, Ma CB, Majumdar S, Link TM. T1rho, T(2) and focal knee cartilage abnormalities in physically active and sedentary healthy subjects versus early OA patients-a 3.0-Tesla MRI study. *Eur Radiol* 2008.
69. Liess C, Lusse S, Karger N, Heller M, Gluer CC. Detection of changes in cartilage water content using MRI T2-mapping in vivo. *Osteoarthritis Cartilage* 2002;10(12):907-913.
70. Kurkijarvi JE, Mattila L, Ojala RO, Vasara AI, Jurvelin JS, Kiviranta I, Nieminen MT. Evaluation of cartilage repair in the distal femur after autologous chondrocyte transplantation using T2 relaxation time and dGEMRIC. *Osteoarthritis Cartilage* 2007;15(4):372-378.
71. Dardzinski BJ, Laor T, Schmithorst VJ, Klosterman L, Graham TB. Mapping T2 relaxation time in the pediatric knee: feasibility with a clinical 1.5-T MR imaging system. *Radiology* 2002;225(1):233-239.

72. Dunn TC, Lu Y, Jin H, Ries MD, Majumdar S. T2 Relaxation Time of Cartilage at MR Imaging: Comparison with Severity of Knee Osteoarthritis. *Radiology* 2004;232(2):592-598.
73. Glaser C, Mendlik T, Dinges J, Weber J, Stahl R, Trumm C, Reiser M. Global and regional reproducibility of T2 relaxation time measurements in human patellar cartilage. *Magn Reson Med* 2006;56(3):527-534.
74. Welsch GH, Mamisch TC, Weber M, Horger W, Bohndorf K, Trattnig S. High-resolution morphological and biochemical imaging of articular cartilage of the ankle joint at 3.0 T using a new dedicated phased array coil: in vivo reproducibility study. *Skeletal Radiol* 2008;37(6):519-526.
75. Dray N, Williams A, Prasad PV, Sharma L, Burstein D. T2 in an OA population: Metrics for reporting data? ; 2005; Miami, FL. p 1995.
76. Blumenkrantz G, Stahl R, Carballido-Gamio J, Zhao S, Lu Y, Munoz T, Hellio Le Graverand-Gastineau MP, Jain SK, Link TM, Majumdar S. The feasibility of characterizing the spatial distribution of cartilage T(2) using texture analysis. *Osteoarthritis Cartilage* 2008;16(5):584-590.
77. Carballido-Gamio J, Link TM, Majumdar S. New techniques for cartilage magnetic resonance imaging relaxation time analysis: texture analysis of flattened cartilage and localized intra- and inter-subject comparisons. *Magn Reson Med* 2008;59(6):1472-1477.
78. Welsch GH, Mamisch TC, Marlovits S, Glaser C, Friedrich K, Hennig FF, Salomonowitz E, Trattnig S. Quantitative T2 mapping during follow-up after matrix-associated autologous chondrocyte transplantation (MACT): Full-thickness and zonal evaluation to visualize the maturation of cartilage repair tissue. *J Orthop Res* 2009.
79. Welsch GH, Trattnig S, Scheffler K, Szomonanyi P, Quirbach S, Marlovits S, Domayer S, Bieri O, Mamisch TC. Magnetization transfer contrast and T2 mapping in the evaluation of cartilage repair tissue with 3T MRI. *J Magn Reson Imaging* 2008;28(4):979-986.

80. Welsch GH, Mamisch TC, Quirbach S, Zak L, Marlovits S, Trattnig S. Evaluation and comparison of cartilage repair tissue of the patella and medial femoral condyle by using morphological MRI and biochemical zonal T2 mapping. *Eur Radiol* 2008.
81. Welsch GH, Mamisch TC, Domayer SE, Dorotka R, Kutscha-Lissberg F, Marlovits S, White LM, Trattnig S. Cartilage T2 assessment at 3-T MR imaging: in vivo differentiation of normal hyaline cartilage from reparative tissue after two cartilage repair procedures--initial experience. *Radiology* 2008;247(1):154-161.
82. Trattnig S, Mamisch TC, Welsch GH, Glaser C, Szomolanyi P, Gebetsroither S, Stastny O, Horger W, Millington S, Marlovits S. Quantitative T2 mapping of matrix-associated autologous chondrocyte transplantation at 3 Tesla: an in vivo cross-sectional study. *Invest Radiol* 2007;42(6):442-448.
83. Domayer SE, Kutscha-Lissberg F, Welsch G, Dorotka R, Nehrer S, Gabler C, Mamisch TC, Trattnig S. T2 mapping in the knee after microfracture at 3.0 T: correlation of global T2 values and clinical outcome - preliminary results. *Osteoarthritis Cartilage* 2008;16(8):903-908.
84. Rauscher I, Stahl R, Cheng J, Li X, Huber MB, Luke A, Majumdar S, Link TM. Meniscal measurements of T1rho and T2 at MR imaging in healthy subjects and patients with osteoarthritis. *Radiology* 2008;249(2):591-600.
85. Blumenkrantz G, Dunn TC, Lindsey C, Ries MD, Link TM, Steinbach LS, Newitt DC, Majumdar S. Cartilage T2 as a Marker of Progression of Osteoarthritis. 2004; San Antonio, TX. p 234.
86. Bolbos RI, Zuo J, Banerjee S, Link TM, Ma CB, Li X, Majumdar S. Relationship between trabecular bone structure and articular cartilage morphology and relaxation times in early OA of the knee joint using parallel MRI at 3 T. *Osteoarthritis Cartilage* 2008;16(10):1150-1159.
87. Lammentausta E, Kiviranta P, Toyras J, Hyttinen MM, Kiviranta I, Nieminen MT, Jurvelin JS. Quantitative MRI of parallel changes of articular cartilage and underlying trabecular bone in degeneration. *Osteoarthritis Cartilage* 2007;15(10):1149-1157.

88. Duvvuri U, Reddy R, Patel SD, Kaufman JH, Kneeland JB, Leigh JS. T1rho-relaxation in articular cartilage: effects of enzymatic degradation. *Magn Reson Med* 1997;38(6):863-867.
89. Regatte RR, Akella SV, Borthakur A, Kneeland JB, Reddy R. In vivo proton MR three-dimensional T1rho mapping of human articular cartilage: initial experience. *Radiology* 2003;229(1):269-274.
90. Akella SV, Regatte RR, Gougoutas AJ, Borthakur A, Shapiro EM, Kneeland JB, Leigh JS, Reddy R. Proteoglycan-induced changes in T1rho-relaxation of articular cartilage at 4T. *Magn Reson Med* 2001;46(3):419-423.
91. Wheaton AJ, Dodge GR, Elliott DM, Nicoll SB, Reddy R. Quantification of cartilage biomechanical and biochemical properties via T1rho magnetic resonance imaging. *Magn Reson Med* 2005;54(5):1087-1093.
92. Pakin SK, Schweitzer ME, Regatte RR. 3D-T1rho quantitation of patellar cartilage at 3.0T. *J Magn Reson Imaging* 2006;24(6):1357-1363.
93. Li X, Han ET, Ma CB, Link TM, Newitt DC, Majumdar S. *In Vivo* 3T Spiral Imaging Based Multi-slice $T_{1\rho}$ Mapping of Knee Cartilage in Osteoarthritis. *Mag Res Med* 2005;54(4):929-936.
94. Li X, Benjamin Ma C, Link TM, Castillo DD, Blumenkrantz G, Lozano J, Carballido-Gamio J, Ries M, Majumdar S. In vivo T(1rho) and T(2) mapping of articular cartilage in osteoarthritis of the knee using 3T MRI. *Osteoarthritis Cartilage* 2007.
95. Regatte RR, Akella SV, Wheaton AJ, Lech G, Borthakur A, Kneeland JB, Reddy R. 3D-T1rho-relaxation mapping of articular cartilage: in vivo assessment of early degenerative changes in symptomatic osteoarthritic subjects. *Acad Radiol* 2004;11(7):741-749.
96. Majumdar S, X. L, Blumenkrantz G, K. S, B. M, H. K, J. L, Link TM. MR Imaging and Early Cartilage Degeneration and Strategies for Monitoring Regeneration. *Journal of Musculoskeletal and Neuronal Interactions* 2006.
97. Menezes NM, Gray ML, Hartke JR, Burstein D. T2 and T1rho MRI in articular cartilage systems. *Magn Reson Med* 2004;51(3):503-509.

98. Regatte RR, Akella SV, Lonner JH, Kneeland JB, Reddy R. T1rho relaxation mapping in human osteoarthritis (OA) cartilage: comparison of T1rho with T2. *J Magn Reson Imaging* 2006;23(4):547-553.
99. Simmons EH, Segil CM. An evaluation of discography in the localization of symptomatic levels in discogenic disease of the spine. *Clin Orthop Relat Res* 1975(108):57-69.
100. Colhoun E, McCall IW, Williams L, Cassar Pullicino VN. Provocation discography as a guide to planning operations on the spine. *J Bone Joint Surg Br* 1988;70(2):267-271.
101. Patrick BS. Lumbar discography: a five year study. *Surg Neurol* 1973;1(5):267-273.
102. Walsh TR, Weinstein JN, Spratt KF, Lehmann TR, Aprill C, Sayre H. Lumbar discography in normal subjects. A controlled, prospective study. *J Bone Joint Surg Am* 1990;72(7):1081-1088.
103. Wiesel SW, Tsourmas N, Feffer HL, Citrin CM, Patronas N. A study of computer-assisted tomography. I. The incidence of positive CAT scans in an asymptomatic group of patients. *Spine* 1984;9(6):549-551.
104. Modic MT, Pavlicek W, Weinstein MA, Boumpfrey F, Ngo F, Hardy R, Duchesneau PM. Magnetic resonance imaging of intervertebral disc disease: Clinical and pulse sequence considerations. *Radiology* 1984;152:103-111.
105. Gibson MJ, Buckley J, Mawhinney R, Mulholland RC, Worthington BS. Magnetic resonance imaging and discography in the diagnosis of disc degeneration. A comparative study of 50 discs. *J Bone Joint Surg Br* 1986;68(3):369-373.
106. Schneiderman G, Flannigan B, Kingston S, Thomas J, Dillin WH, Watkins RG. Magnetic resonance imaging in the diagnosis of disc degeneration: correlation with discography. *Spine* 1987;12(3):276-281.
107. Pfirrmann CW, Metzdorf A, Zanetti M, Hodler J, Boos N. Magnetic resonance classification of lumbar intervertebral disc degeneration. *Spine* 2001;26(17):1873-1878.

108. Hwang GJ, Suh JS, Na JB, Lee HM, Kim NH. Contrast enhancement pattern and frequency of previously unoperated lumbar discs on MRI. *Jour Magn Res Imag* 1997;7:575-578.
109. Jensen MC, Brant-Zawadzki MN, Obuchowski N, Modic MT, Malkasian D, Ross JS. Magnetic resonance imaging of the lumbar spine in people without back pain [see comments]. *N Engl J Med* 1994;331(2):69-73.
110. Stabler A, Weiss M, Scheidler J, Krodel A, Seiderer M, Reiser M. Degenerative disk vascularization on MRI: correlation with clinical and histopathologic findings. *Skeletal Radiol* 1996;25(2):119-126.
111. Weidenbaum M, Foster RJ, Best BA, Saed-Nejad F, Nickoloff E, Newhouse J, Ratcliffe A, Mow VC. Correlating magnetic resonance imaging with the biochemical content of the normal human intervertebral disc. *J Orthop Res* 1992;10:552-561.
112. Chiu EJ, Newitt DC, Hu SS, Lotz JC, Majumdar S. MRI measurement of water diffusion in the human intervertebral disc with compression. 1997; San Francisco, CA. Orthopaedic Research Society. p 123.
113. Boos N, Dreier D, Hilfiker E, Schade V, Kreis R, Hora J, Aebi M, Boesch C. Tissue characterization of symptomatic and asymptomatic disc herniations by quantitative magnetic resonance imaging. *J Orthop Res* 1997;15(1):141-149.
114. Robertson R, Maier S, Mulkern R, Vajapayam S, Robson C, Barnes P. MR Line-scan Diffusion Imaging of the Spinal Cord in Children. *AJNR Am J Neuroradiol* 2000;21:1344-1348.
115. Murphy BP, Zientara GP, Huppi PS, Maier SE, Barnes PD, Jolesz FA, Volpe JJ. Line scan diffusion tensor MRI of the cervical spinal cord in preterm infants. *J Magn Reson Imaging* 2001;13(6):949-953.
116. Baur A, Huber A, Ertl-Wagner B, Durr R, Zysk S, Arbogast S, Deimling M, Reiser M. Diagnostic value of increased diffusion weighting of a steady-state free precession sequence for differentiating acute benign osteoporotic fractures from pathologic vertebral compression fractures. *AJNR Am J Neuroradiol* 2001;22(2):366-372.

117. Spuentrup R, Buecker A, Adam G, Vaals JJ, Guenther RW. Diffusion-weighted MR Imaging for Differentiation of Benign Fracture Edema and Tumor Infiltration of the Vertebral Body. *AJR Am J Roentgenol* 2001;176:351-358.
118. Kerttula L, Kurunlahti M, Jauhiainen J, Koivula A, Oikarinen J, Tervonen O. Apparent Diffusion Coefficient and T2 Relaxation Time Measurements To Evaluate Disc Degeneration. *Acta Riologica* 2001;42:585-591.
119. Gudbjartsson H, Maier SE, Mulkern RV, Morocz IA, Patz S, Jolesz FA. Line Scan Diffusion Imaging. *MRM* 1996;36:509-519.
120. Bammer R, Augustin M, Prokesch RW, Stollberger R, Fazekas F. Diffusion-weighted imaging of the spinal cord: interleaved echo-planar imaging is superior to fast spin-echo. *J Magn Reson Imaging* 2002;15(4):364-373.
121. Regatte RR, Akella SV, Borthakur A, Kneeland JB, Reddy R. Proteoglycan depletion-induced changes in transverse relaxation maps of cartilage: comparison of T2 and T1rho. *Acad Radiol* 2002;9(12):1388-1394.
122. Johannessen W, Auerbach JD, Wheaton AJ, Kurji A, Reddy R, Borthakur A, Elliott DM. Non-Invasive Determination of Nucleus Pulposus Proteoglycan Content Using T1rho MRI. 2005; Switzerland.
123. Li X, Han ET, Ma CB, Link TM, Newitt DC, Majumdar S. *In Vivo* 3T Spiral Imaging Based Multi-slice T_{1ρ} Mapping of Knee Cartilage in Osteoarthritis. *Mag Res Med* 2005; 54(4):929

Chapter 4: Development of a Methodology for T₂ Relaxation Fitting for Cartilage Imaging at 3 Tesla

4.1 Introduction

Magnetic resonance (MR) T₂ relaxation time is sensitive to biochemical changes that occur during cartilage degeneration, including alterations in hydration, collagen content, and tissue anisotropy (1). Accurate quantification of T₂ relaxation time is dependent on various scanning parameters including echo times in the T₂ sequence, the signal to noise ratio (SNR) in the cartilage, and the T₂ fitting algorithm (2). This chapter will investigate the impact of various SNR's and T₂ fitting algorithms on the T₂ quantification, using data from the Osteoarthritis Initiative (OAI).

The Osteoarthritis Initiative (OAI; <http://www.oai.ucsf.edu/>) is a multi-center, longitudinal study aimed at assessing biomarkers in osteoarthritis (OA) including those derived from magnetic resonance (MR) imaging. The OAI is a cross-sectional and longitudinal dataset that includes both MRI and radiographic images of subjects scanned annually over 5 years. MR images that can be used to assess cartilage morphology and T₂ are available. Three subject groups (ages 45-79 years) will participate in the study: 1) the progression cohort: those with symptomatic knee OA at baseline 2) the incidence cohort: those with an elevated risk of developing symptomatic OA during the course of the study and 3) a control cohort. The inclusion criteria for each group are in the table 4.1.

Table 4.1: Inclusion criteria for the 3 subject-groups in the OAI.

Progression cohort	Incidence cohort	Control cohort
Those who have frequent knee symptoms defined as “pain aching or stiffness in or around the knee on most days” for at least on month during the past 12 months and radiographic finding relating to the presence of OA corresponding to Kellgren-Lawrence grade ≥ 2	Those who have characteristics that place them at increased risk for developing OA during the course of the study. These include being overweight, having previous knee injury, having previous knee surgery, having family history, and/or repetitive knee bending occupations	Those who have no pain aching or stiffness in either knee in the past year, no radiographic findings of OA (Kellgren-Lawrence grade = 0), and no eligibility risk factors from the incidence cohort

This database provides a means to study and longitudinally evaluate MRI biomarkers including T_2 relaxation time, in the development and progression of OA, thus providing a wealth of information on OA development progression.

4.2 Impact of Signal to Noise Ratio on T_2 Fitting

4.2.1 Simulations

The signal to noise ratio (SNR) in an image has an impact on the accuracy of T_2 quantification. Therefore, images with low SNR may yield inaccurate T_2 values. This study investigates the effects of SNR on the accuracy of T_2 quantification by simulating T_2 decay in cartilage images from the Osteoarthritis Initiative.

The T_2 decay curve in the absence of noise can be modeled using the following equation:

$$S = S_0 e^{-\frac{TE}{T_2}} \quad [4.1]$$

where S represents the signal amplitude measured at time intervals TE. S_0 represents the initial amplitude of the signal.

Simulations of T_2 decay with various magnitudes of noise were used to determine how noise affects T_2 quantification.

Simulated T_2 decay data were generated from

$$S_n = \sqrt{(\varepsilon_{real}(0,\sigma) + S_0 e^{-(TE_n/T_2)})^2 + \varepsilon_{imaginary}(0,\sigma)^2} \quad [4.2]$$

where S_n represents the signal amplitude measured at time intervals TE with $n = 1, 2, 3 \dots 7$. S_0 represents the initial amplitude of the signal, arbitrarily set to 100. The echo times from the OAI range from TE = 10, 20, 30 ... 70 ms. The term $\varepsilon(0,\sigma)$ indicates the addition of zero-mean, Gaussian noise with standard deviation of σ . Random noise was simulated independently from the real and imaginary channels. A broad range of SNR values (of the first echo) were simulated and defined as the (signal from the 1st echo/ σ). The simulated SNR values ranged from SNR = 3 to SNR = 41. 1000 trials were performed to determine the average \pm standard deviation of T_2 relaxation time for each SNR value.

4.2.2 Results

The results of the simulation showed that the T_2 value of the model strongly depends on the SNR. Simulations (Figure 4.1) were performed to determine the minimum SNR in a pixel and in ROI that can distinguish healthy cartilage T_2 ($T_2 = 40$ ms) and a degenerative cartilage T_2 ($T_2 = 44$ ms). In our experiments, the T_2 is calculated on a pixel-by-pixel basis and then averaged for each ROI. The ROI can contain a large number of pixels ranging from about 200-500 depending on the size of the cartilage. Figures 4.1-4.3 illustrate the SNR on a per-pixel basis, while figure 4.4 illustrates T_2 as a function of SNR calculated on a pixel-by-pixel basis and then averaged over an ROI.

Figure 4.1 illustrates the relationship between SNR and calculated T_2 in one pixel (1000 trials). The minimum SNR of the first echo must be at least 21 in order to be able to distinguish healthy and degenerative T_2 in one pixel, while accounting for error.

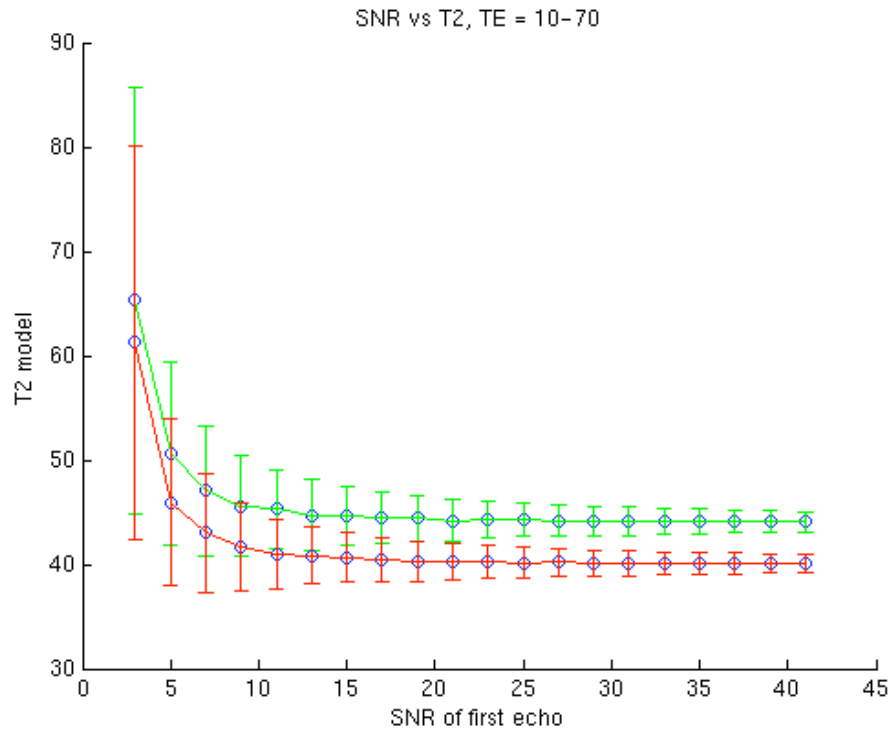


Figure 4.1: An illustration of the relationship between SNR of the first echo and calculated T_2 with TE = 10-70. The minimum SNR that can distinguish a healthy and degenerative cartilage pixel (accounting for error) is approximately 21.

Additionally, a simulation was performed to determine whether omitting the last echo time (TE = 70) yields more accurate T_2 values. The second simulation demonstrates the relationship between SNR of the first echo and calculated T_2 in one pixel using TE = 10-60 ms (Figure 4.2). The comparison of Figures 4.1 and 4.2 demonstrates that using all the data from echoes TE=10 - TE=70 provides a highest probability of distinguishing a healthy and degenerative cartilage pixel.

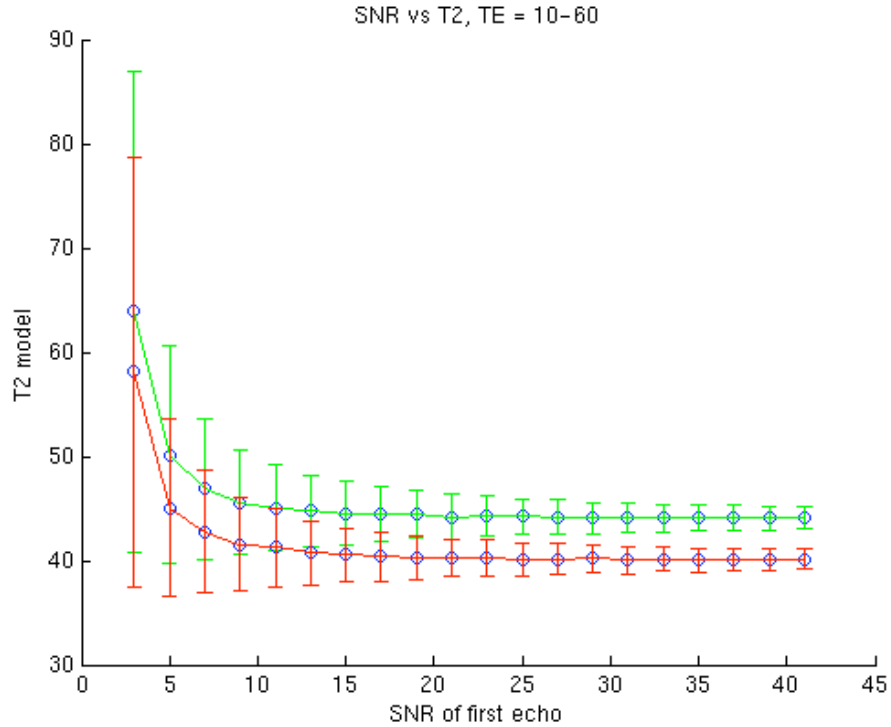


Figure 4.2: An illustration of the relationship between SNR of the first echo and calculated T₂ with TE = 10-60. The minimum SNR that can distinguish a healthy from a degenerative cartilage pixel (accounting for error) is approximately 23.

Additionally, a simulation was performed to determine whether omitting the last two echo times (TE = 60 and TE = 70) yields more accurate T₂ values. The third simulation demonstrates the relationship between SNR of the first echo and calculated T₂ in one pixel using TE = 10-50 ms (Figure 4.3) in one pixel. The comparison of Figures 4.1, 4.2, and 4.3 demonstrates that using data from all of the echoes TE=10 - TE=70 provides a highest probability of distinguishing a healthy and degenerative cartilage pixel.

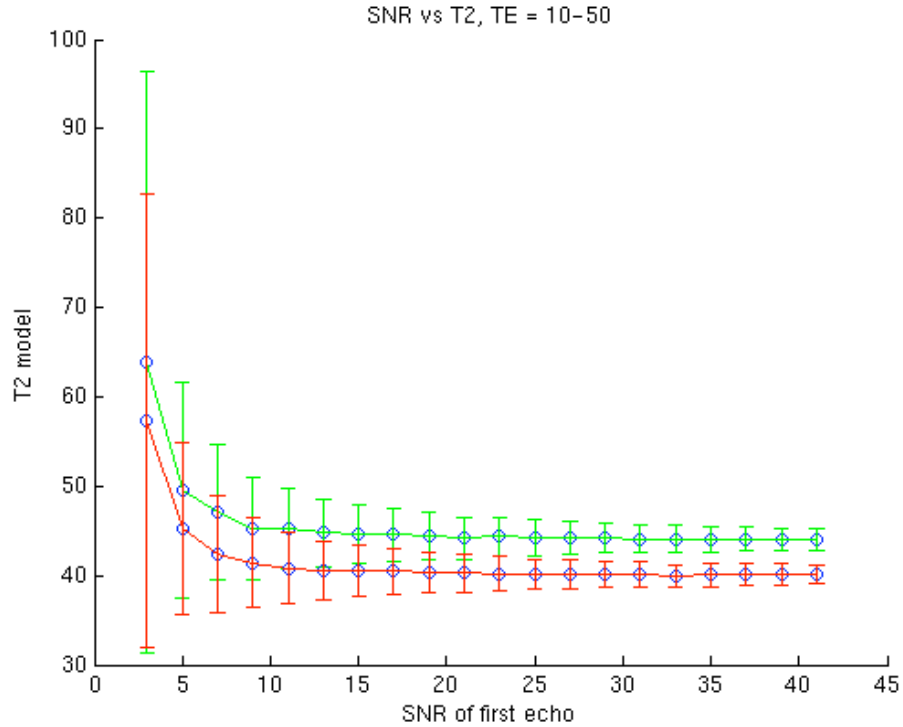


Figure 4.3: An illustration of the relationship between SNR of the first echo and calculated T_2 with $TE = 10-50$. The minimum SNR that can distinguish a healthy from a degenerative cartilage pixel (accounting for error) is approximately 25.

While Figures 4.1-4.3 depict the relationship between SNR and T_2 in a single pixel, the mean T_2 in the OAI data is calculated per pixel and then averaged per cartilage ROI. The average T_2 value per ROI is the average of the T_2 in the 200 pixels (Figure 4.4). The standard deviation (which is the error bar on the graph in Figure 4.4) is the standard deviation of the T_2 of the 200 pixels. The graph illustrates that the standard deviation is significantly decreased when averaging the T_2 values per ROI. Therefore, the minimum SNR of the first echo that can both distinguish healthy from degenerative cartilage ROI and maintain accurate quantification is about 12. The standard deviation of T_2 values calculated per pixel and calculated per ROI are compared in Figure 4.5.

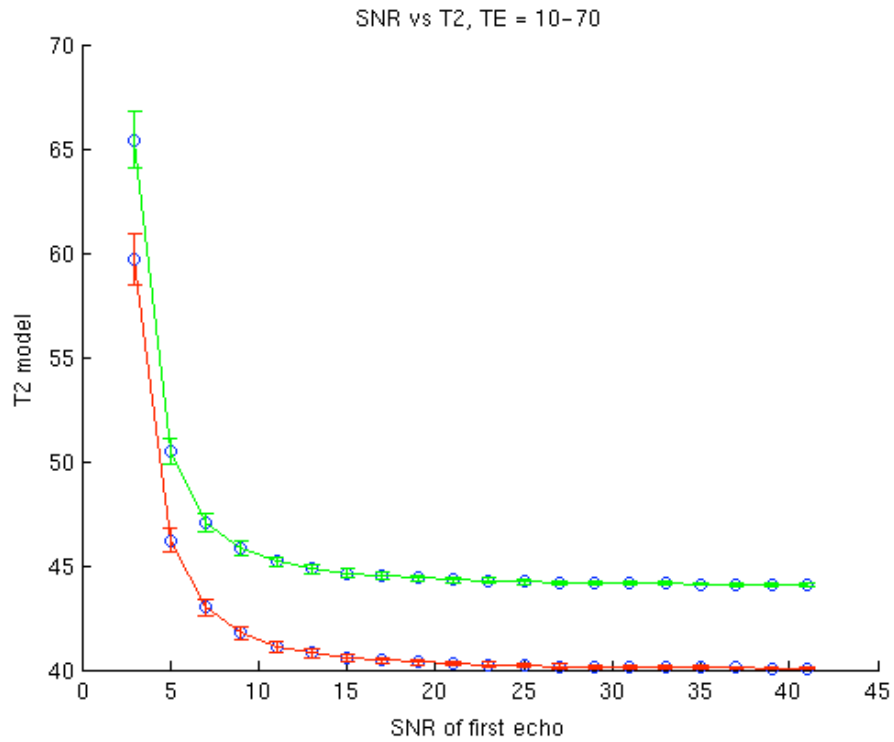


Figure 4.4: An illustration of the relationship between SNR of the first echo and calculated T_2 with $TE = 10-70$, in an ROI. The ROI consists of 200 pixels. The minimum SNR that can be used to calculate accurate T_2 values and distinguish healthy cartilage from degenerative cartilage is about 15.

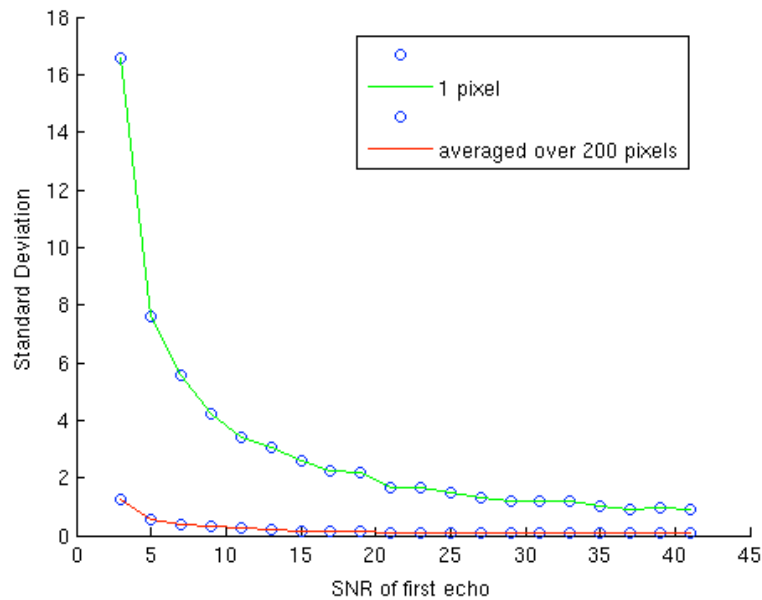


Figure 4.5: The standard deviation of T_2 values calculated per pixel, and calculated per ROI that consists of 200 pixels. The standard deviation is much lower when evaluating T_2 values averaged over 200 pixels.

4.3 Fitting Techniques

4.3.1 Image Analysis

MR images of the knee joint including sagittal 3D DESSwe (TR = 16.3 ms, TE = 4.7 ms, interpolated in-plane resolution = 0.365 x 0.365 mm, slice thickness = 0.7 mm) and sagittal 2D MSME (TR = 2700 ms, TE₁-TE₇ = 10-70 ms) images were analyzed. Articular cartilage was segmented using a spline-based, semi-automatic technique in six regions: medial and lateral tibia, medial and lateral femur, trochlea, and patella (Figure 4.6) in 13 subjects from the progression cohort of the OAI. Additional details about the image acquisition parameters have are provided by Peterfy and colleagues (3).

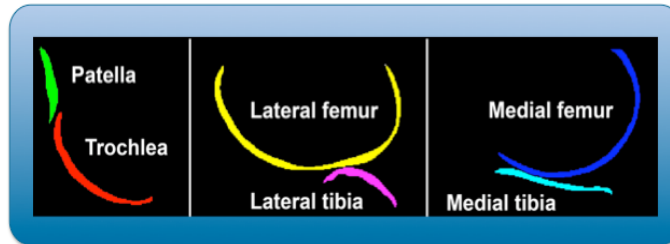
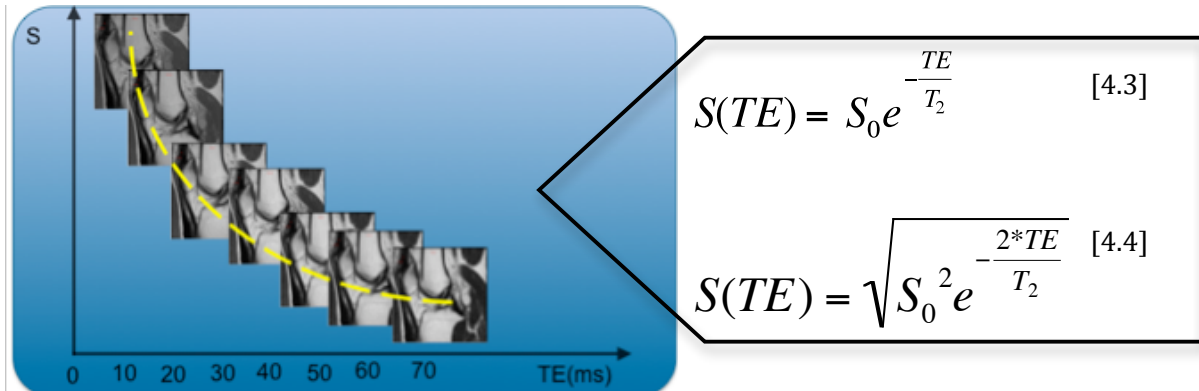


Figure 4.6: An illustration of the segmented cartilage regions.

4.3.2 Impact of Fitting Routine on T_2 Calculation

The T_2 values were calculated using 2- and 3-parameter fitting routines (Equations 4.3 and 4.4).




S is the cartilage signal intensity from a T_2 -weighted image with a chosen TE . S_0 is the signal intensity when $TE=0$ ms. Using each equation, the T_2 is quantified on a pixel by pixel basis, using the Levenberg-Marquardt algorithm(4). Both equations 3 and 4 are two parameter fitting algorithms. However, equation 3 is the standard T_2 decay curve that does not account for noise, while equation 4 is a signal equation (derived from power images) that accounts for noise (5). Using this method, an image that is “free of noise-induced bias” can be produced by squaring the magnitude image and subtracting an average value of the background noise from the entire image (5). This method will produce a corrected image from which the T_2 can be calculated.

Equations 5 and 6 will be used as metrics to evaluate the goodness of fit for T_2 quantification, calculated using noise corrected and non-noise corrected images, all assuming mono-exponential decay.



[4.5]



[4.6]

S_i represents the measured value at the i th TE, \hat{S}_i represents the predicted value at the i th TE, \bar{S} is the mean of the measured values, n is the number of echoes, and m is the number of fitted coefficients estimated from the measured values ($m=2$; S_0 and T_2).

4.3.3 Statistical Analysis

A linear mixed-effects regression analysis (6,7) of MR parameters (mean T_2 , RMSE, Adjusted R^2) on the model type (noise correction, no noise correction) was performed with subject specific random effects to account for multiple cartilage compartments within each subject. This model was implemented to determine if there is a significant difference in MR parameters between each type of model.

4.3.4 Results

Figure 4.7 illustrates the mean T_2 values in each patient (averaged over compartment) calculated using the two fitting algorithms (no noise correction, noise correction). The algorithm without noise correction yielded greater T_2 values in 5/13 subjects, while the noise

correction algorithm yielded greater T_2 values in 8/13 subjects. The random effects model did not demonstrate a significant difference when comparing T_2 values from the fitting routines ($p > 0.05$).

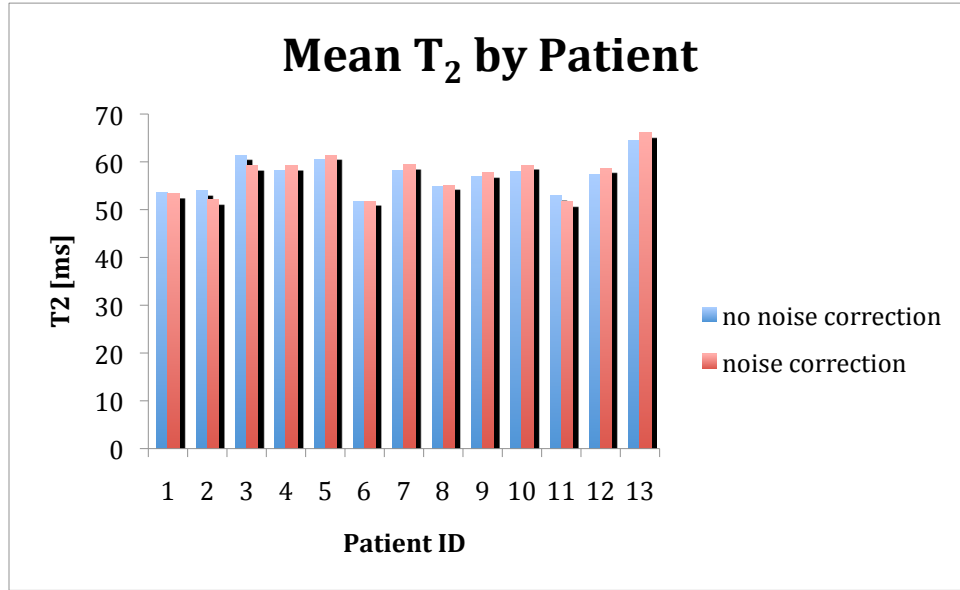


Figure 4.7: An illustration of the T_2 values in each patient calculated the two fitting routines (no noise correction, noise correction).

The RMSE's were lower when using the noise correction algorithm as compared to the standard T_2 fitting algorithm without noise correction in each patient (Figure 4.8). The random effects model demonstrated a significant difference in RMSE between the fitting routines.

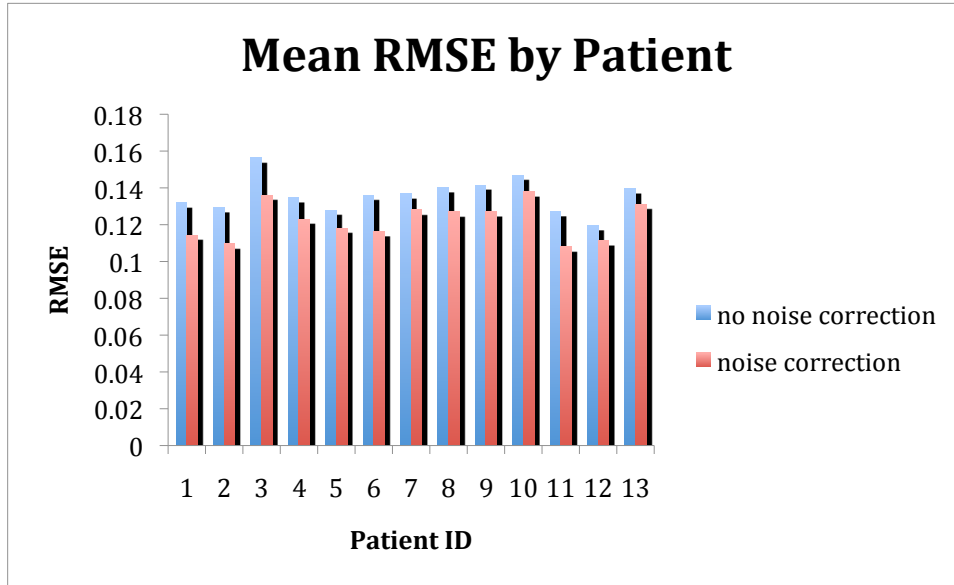


Figure 4.8: An illustration of the RMSE values in each patient calculated using the two fitting algorithms (no noise correction, noise correction). The graph demonstrates that the RMSE's are lower using the noise correction algorithm, demonstrating a greater goodness of fit.

The mean adjusted R^2 was lower in 12/13 subjects when using the standard T_2 fitting technique; however, this trend did not reach significance ($p > 0.05$, Figure 4.9).

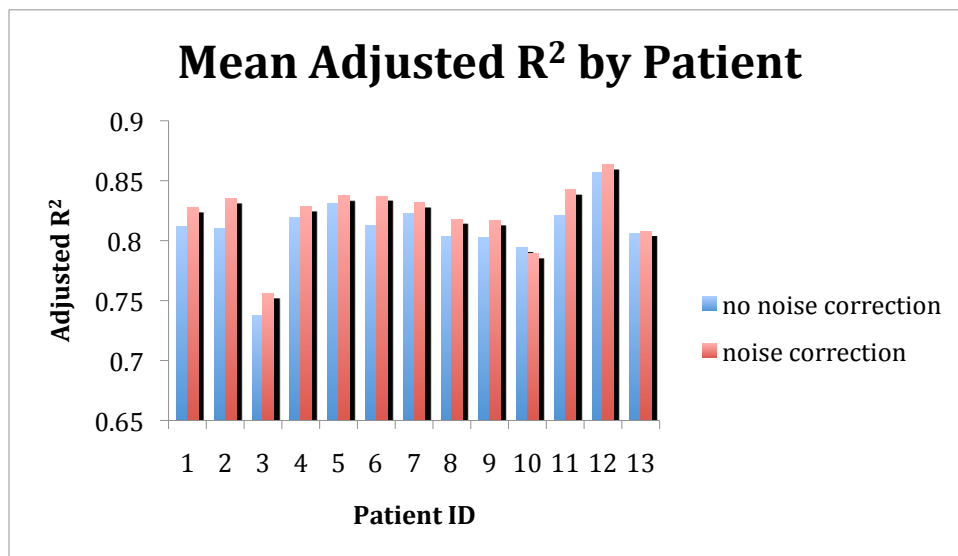


Figure 4.9: An illustration of the mean adjusted R^2 values in each patient calculated using the two fitting algorithms (no noise correction, noise correction). The graph demonstrates that most of the RMSE's are lower (12/13) using the T_2 fitting algorithm without noise correction.

4.4 Discussion and Conclusion

This study investigated the impact of SNR on the accuracy of T_2 quantification as well as the impact of noise correction on the T_2 fitting. Simulations were performed to determine the minimum SNR that can be used to distinguish healthy cartilage from degenerative cartilage. The results demonstrated that a minimum SNR (of the first echo) of 12 can be used to accurately calculate and distinguish healthy from degenerate cartilage. Since the SNR of the first echo in the OAI images is approximately 20, the SNR is adequate for assessment of OA.

The results of this study demonstrated that the goodness of fit was improved using a power images with noise correction, but did not make a significant impact on the T_2 values. The power images correction yielded lower RMSE's and higher Adjusted R^2 values than the standard T_2 fitting technique without noise correction. However, there was no significant difference in mean T_2 values between fitting routines.

4.5 References

1. Mosher TJ, Dardzinski BJ. Cartilage MRI T_2 relaxation time mapping: overview and applications. *Semin Musculoskelet Radiol* 2004;8(4):355-368.
2. Graham SJ, Stanchev PL, Bronskill MJ. Criteria for analysis of multicomponent tissue T_2 relaxation data. *Magnetic resonance in medicine* 1996;35(3):370-378.
3. Peterfy CG, Schneider E, Nevitt M. The osteoarthritis initiative: report on the design rationale for the magnetic resonance imaging protocol for the knee. *Osteoarthritis Cartilage* 2008;16(12):1433-1441.
4. Mor JJ. The Levenberg-Marquardt algorithm: implementation and theory. *Lecture notes in mathematics* 1977;630:105-116.
5. Miller AJ, Joseph PM. The use of power images to perform quantitative analysis on low SNR MR images. *Magn Reson Imaging* 1993;11(7):1051-1056.

6. McCulloch CE, Searle SR. Generalized, linear, and mixed models: Wiley-Interscience; 2004.
7. Littell RC, Milliken GA, Stroup WW, Wolfinger RD. SAS system for mixed models: SAS Institute, Cary, NC; 1996.

Chapter 5: A Pilot, Two-Year Longitudinal Study of the Interrelationship between Trabecular Bone and Articular Cartilage in the Osteoarthritic Knee

5.1 Introduction

Osteoarthritis (OA) is a degenerative joint disease in which bone and cartilage morphological and biochemical changes cause abnormal biomechanical loading patterns, leading to joint deformity, pain, stiffness, crepitus, and decreased mobility (1). OA affects roughly 80% of the population over 75 years (2) and can be caused by many factors such as joint malalignment, obesity, prior surgery or trauma, meniscal abnormality, or cruciate ligament tears (3-6).

During joint loading, the tissues of the knee including cartilage, bone, muscle, and ligament interact to sustain weight-bearing stresses. Specifically, cartilage acts as a “cushion,” which absorbs impacts and distributes loads along the joint surface (7). Although it sustains less force than the surrounding bone and muscle tissues during locomotion (6), its degeneration is significant in the pathogenesis of OA. For example, previous studies have shown that joint space narrowing, an indication of OA progression, is related to cartilage degradation (8). In addition, Wluka et al. showed that tibial cartilage volume decreases about five percent per year in osteoarthritic patients (9). Such progressive osteoarthritic changes are associated with increased bone resorption (10) and abnormal trabecular architecture (11). Moreover, increased subchondral bone stiffness has been associated with cartilage deterioration (12-14), linking bone and cartilage structural changes to the development of OA.

Given the morphological changes occurring in bone and cartilage are interdependent (15), measurements of bone or cartilage structural parameters, individually, may be insufficient to determine the pathogenesis and implications of OA. In a previous cross-sectional study of trabecular bone and articular cartilage, Lindsey et al. used MRI to determine that cartilage degeneration in the knee joint is associated with changes in trabecular bone structure (15). As a further investigation, it would be important to study how such a relationship changes over time. Therefore, the purpose of this study is to examine the relationship between structural changes of trabecular bone and cartilage, in patients with varying degrees of OA over two years, using MR imaging.

5.2 Methods

5.2.1 Subjects

A total of thirty-eight subjects (mean age = 58 years, range = 28-81 years, % female = 39.5%) were scanned at baseline and twelve months. Of these subjects, twenty-one (mean age = 60 years, range = 28-81 years, % female = 42.8%) were scanned again at twenty-four months (drop-outs due to death, knee replacement, and unwillingness to continue). All patients completed a WOMAC (Western Ontario and McMaster Universities Arthritis Index) questionnaire of pain, function, and stiffness (16). A summary of baseline OA subject characteristics is presented in Table 5.1.

Table 5.1: OA subject characteristics at baseline.

	Weight (lbs)	Height (in)	BMI	Age	WOMAC Pain	WOMAC Stiffness	WOMAC Function
OA1 (n = 13)							
Women (n = 7)							
Mean	125.57	63.14	26.04	64.43	76.71	68.43	192.73
SD	56.57	2.41	3.50	10.11	61.53	86.20	186.09
Men (n = 6)							
Mean	211.17	68.67	31.53	56.50	115.67	184.50	288.59
SD	31.69	3.67	4.80	12.57	72.78	87.07	358.72
OA2 (n = 17)							
Women (n = 5)							
Mean	162.75	68.00	24.83	68.00	50.67	54.67	148.00
SD	14.50	2.45	2.88	5.52	56.13	43.19	226.13
Men (n = 12)							
Mean	194.75	71.58	27.78	63.67	97.09	138.64	135.91
SD	28.27	2.39	4.22	12.26	45.12	79.93	86.96

Subjects were recruited by an orthopaedic surgeon based on clinical investigation and diagnosis from antero-posterior weight-bearing radiographs. All subjects (except controls) displayed symptoms of OA, as evaluated by a radiologist. The severity of each subject's OA at baseline was evaluated using the x-ray based Kellgren-Lawrence (KL) scale (17): KL scores of 1 and 2 were considered mild OA and classified as OA1 (n = 13, mean age = 61 years, range = 46-81 years, % female = 53.8%); KL scores of 3 and 4 were considered severe OA and classified as OA2 (n = 17, mean age = 65 years, range = 43-76 years, % female = 29.4%). A summary of the OA subject cohort is presented in Figure 5.1. Additionally, a group of control subjects (OA0) with no radiographic evidence of OA (n = 8, mean age = 39 years, range = 28-70 years, % female = 37.5%) was included in the study. This study was approved by the Committee on Human Research, and all patients signed an informed consent.

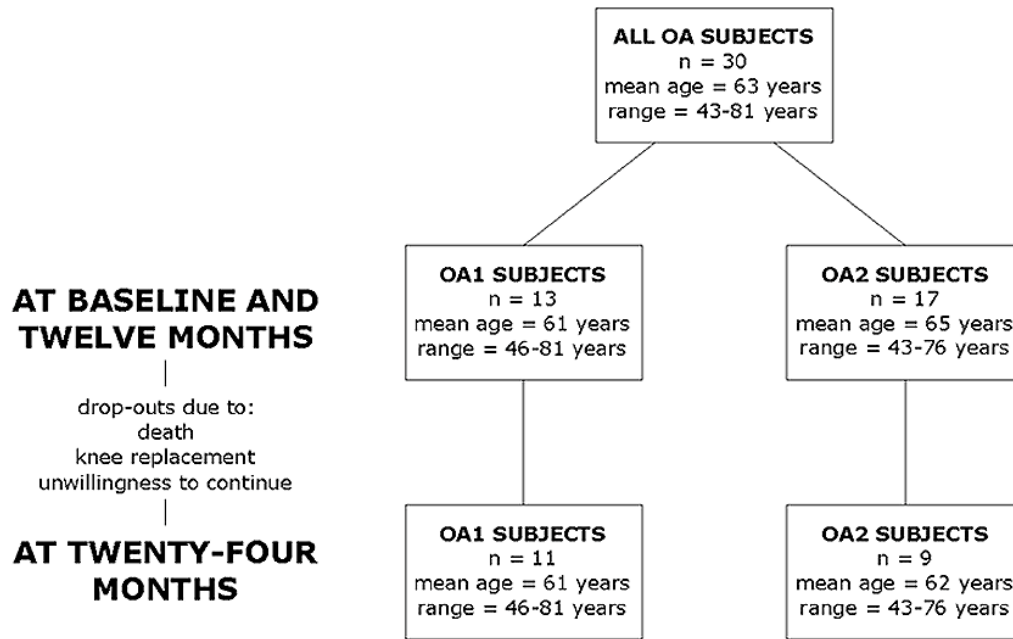


Figure 5.1: A tree diagram of OA subject characteristics at baseline.

5.2.2 Magnetic Resonance Imaging

A GE SIGNA 1.5 Tesla echo-speed system (GE Medical Systems, Waukesha, WI) and bilateral dual-phased array coil (USA Instruments, Cleveland, OH) were used to acquire images.

The subject was positioned supine in the scanner, and his or her knee was secured using a knee-holder (constructed in-house) that allowed the knee to flex 30 ± 1 degrees. The receiver coils were secured to and centered at the knee joint, so that signal to noise ratio was maximized. High-resolution, axial images (Figure 5.2) were acquired for assessing trabecular bone structure, using a 3-D fast gradient echo (FGRE) sequence (18) (TE = 4.5 ms, TR = 30 ms, flip angle = 40° , resolution = $.195 \times .195 \times 1 \text{ mm}^3$, FOV = 10 cm, scan time = 18:26 minutes). High-resolution, fat-suppressed, sagittal images were acquired for assessing cartilage structure, using a 3-D spoiled gradient echo (SPGR) sequence (TE = 3.3 ms, TR = 30 ms, flip angle = 30° , resolution = $.234 \times .234 \times 2 \text{ mm}^3$, FOV = 12 cm, scan time = 9:31 minutes). In a subset of the patients ($n_{\text{total}} = 12$, $n_{\text{OA1}} = 5$, $n_{\text{OA2}} = 7$, mean age = 59

years, range = 43-76 years, % female = 33.3%), sagittal images were acquired for measuring T_2 relaxation time, using a 2-D dual echo spin echo (SE) sequence ($TE_1/TE_2 = 10/45$ ms, TR = 1500 ms, resolution = $.468 \times .468 \times 4$ mm³, FOV = 12 cm, scan time = 5:24 minutes). All twelve subjects had a baseline and follow-up scan, averaging 680 days between scans (range = 400-1050 days).

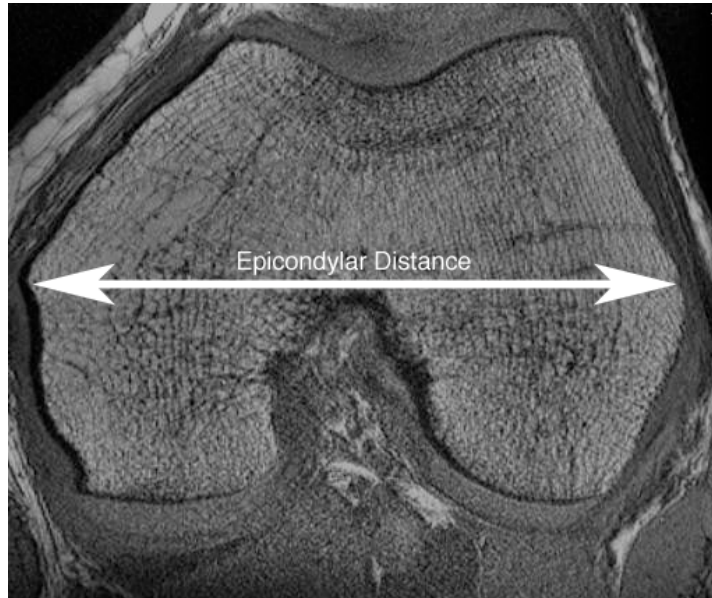


Figure 5.2: A high-resolution, axial image acquired for assessing trabecular bone structure, using a 3-D fast gradient echo sequence ($TE = 4.5$ ms, TR = 30 ms, flip angle = 40° , resolution = $.195 \times .195 \times 1$ mm³, FOV = 10 cm, scan time = 18:26 minutes). The epicondylar distance is labeled.

5.2.3 Image Analysis

All images were transferred to a Sun Workstation (Sun Microsystems, Mountain View, CA), which was used to perform analysis. To correct for non-uniform signal intensity, a 3-D low pass filter was applied to the images (19).

Trabecular bone analysis was performed using an in-house program created with IDL (Research Systems, Boulder, CO) (20). Regions of interest (ROI), consisting of trabecular

bone and marrow, were segmented (based on the axial images) in the femur, medial and lateral condyles, tibia, and medial and lateral tibia, as in a previous study (Figure 5.3) (15).

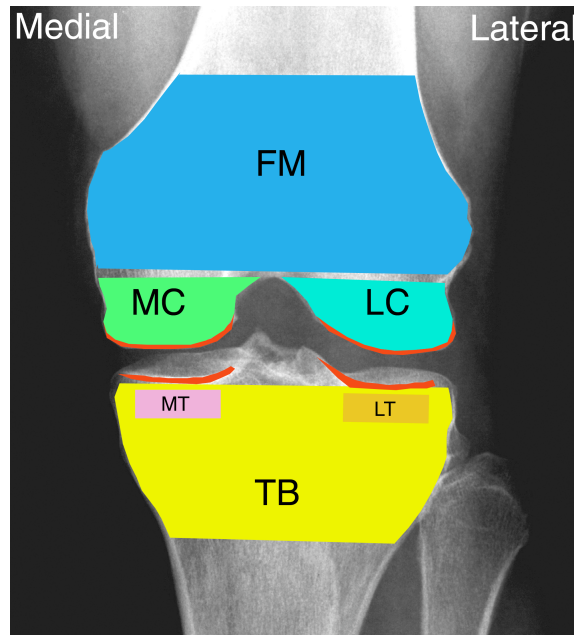


Figure 5.3: A graphical representation of the segmented bone and cartilage regions. The femur (FM, blue), tibia (TB, yellow), medial condyle (MC, green), lateral condyle (LC, turquoise), medial tibia (MT, pink), lateral tibia, (LT, orange) and cartilage compartments (red) are shown.

The first slice was defined at the proximal end of the tibia, and the last slice was defined at the distal end of the femur. The femur was defined, beginning with the slice where the condyles meet and concluding five slices before the end of the volume, so as to minimize coil signal drop-off effects. The medial and lateral condyles were defined beginning with the slice where the condyles appear and ending at the slice where the condyles meet. The tibia was defined starting from the fifth slice and ending at the joint line. The medial and lateral tibia were segmented using a 1x3 grid that fit within the tibial plateau (15). The first and third boxes, defined on five consecutive slices of the tibial plateau, were representative sections of the medial and lateral tibia. Figure 5.3 shows a representation of all the segmented regions. To adjust the ROI for variation in bone size among the subjects, the

dimensions of the grid were standardized by the epicondylar distance (15). For example, the width and height of each box was calculated using the following equation:

$$\text{Width[mm]} = \text{Height[mm]} = \text{Epicondylar Distance[mm]} * (2/9) \quad [5.1]$$

Each segmented region was analyzed to measure the following parameters: apparent trabecular number (app. Tb.N) [1/mm], apparent trabecular thickness (app. Tb.Th) [mm], apparent bone volume fraction (app. BV/TV), and apparent trabecular separation (app. Tb.Sp) [mm] (21-23). In order to distinguish the trabecular bone from the marrow, a threshold that assumed a biphasic model using a dual-reference limit, as previously described (24,25), was applied. This threshold was employed to generate a binary image of bone and marrow phases. Reproducibility results for trabecular bone structure analysis have been previously published (20); the coefficient of variation (CV) was 2.20% for app. BV/TV, 2.20% for app. Tb.N, 3.20% for app. Tb.Sp, and 2.90% for app. Tb.Th.

Cartilage segmentation was performed using an in-house program created with Matlab (Mathworks, Natick, MA). Based on the sagittal images, articular cartilage was segmented using a spline-based, semi-automatic technique and was defined in four distinct regions: medial and lateral tibia, and medial and lateral femur (Figure 5.3). The analysis of the femur was performed by a single observer, and the analysis of the tibia was performed by a different, but single observer. The root mean square CV for intra-observer reproducibility was 2.40% for femoral thickness, 2.18% for femoral volume, 3.69% for tibial thickness, and 2.61% for tibial volume (15). An iterative minimization process was used to calculate total cartilage volume and average thickness for each region. Following segmentation, the image was transformed into a mask in which the cartilage appeared white and the rest of the image appeared black. Second, edge detection and skeletonization were used to determine the

boundaries of the cartilage so that a medial line could be generated. Finally, the cartilage thickness was determined by calculating the minimum distance from each point on the medial line to a cartilage boundary. The average thickness was calculated for each slice and then averaged for all the slices. The cartilage volume was determined by multiplying the total number of voxels encompassing the cartilage by the volume of each voxel.

Studies have shown that variations in joint size have a larger effect on cartilage volume than cartilage thickness (26). Therefore, cartilage volume was normalized by the epicondylar distance in order to minimize variation due to joint size.

Dual-echo, spin-echo images were used to generate sagittal T_2 maps, using custom software (IDL, Research Systems, Boulder, CO), assuming mono-exponential signal decay with echo time. The cartilage segmentation was re-sampled and superimposed on the T_2 map, to define the region of interest for T_2 assessment (27). There were twelve OA subjects ($n_{OA1} = 5$, $n_{OA2} = 7$, mean age = 59 years, range = 43-76 years, % female = 33.3%) from which follow-up T_2 maps were obtained, as there was often considerable knee movement between the high-resolution scan and the dual-echo scan. The cartilage compartments were determined, as previously described, and classified as the medial and lateral tibial, and medial and lateral femoral compartments. For qualitative comparison, three normal volunteers (mean age = 44 years, range = 28-70 years, % female = 33.3%) were scanned and similarly analyzed. The intra-observer T_2 reproducibility results indicate that the coefficients of variation (CV) for the femur and tibia are 1.5% and 2.0%, respectively (28).

5.2.4 Statistical Analysis

In this study, group-specific mean values as well as correlations between annual percentage changes of bone and cartilage structural parameters were evaluated. Partial

Spearman correlations were obtained between the percentage changes in cartilage parameters in each compartment as well as between the percentage changes in trabecular bone parameters in each compartment, adjusting for age, gender, and OA group. Mixed random effects models (29) were used to compute the percentage changes from baseline to followup-1, and followup-1 to followup-2, for each trabecular bone and cartilage parameter, treating the study subject as the random effect. These models properly control for correlations resulting from age, gender, repeated measurements over time, and from multiple regional measurements from the same subject. The least squares mean change of these values was calculated for each parameter, in each region based on these models.

Mean T_2 values for both osteoarthritic and control subjects were calculated at baseline and follow-up. The paired Student's *t*-test was used to compare the T_2 values between the baseline and follow-up exams for each cartilage compartment, in OA subjects.

The correlations between the changes in cartilage and bone parameters were also investigated. Correlations were based on the entire longitudinal data, including the percentage changes from baseline to follow-up 1, and follow-up 1 to follow-up 2. Similar to the theory of partial correlation coefficients for normally distributed data, residuals of mixed effects models (30) were used to calculate partial Pearson's correlation coefficients between the parameters of interest and age (after removing both individual and design effects, such as repeated measurements from individual participants and different age distributions for two measurements). The corresponding *p*-value was calculated based on Fisher's *z*-transformation (31). Effective degrees of freedom were used in calculating the significance of these correlations.

Because of the exploratory nature and limited sample size of this study, *p*-values were not adjusted for multiple tests.

5.3 Results

5.3.1 Patient Characteristics

The following trends in baseline patient characteristics were observed (Table 5.1): The OA1 males have greater average 1) weight, 2) height, 3) BMI, 4) WOMAC pain score, 5) WOMAC stiffness score, and 6) WOMAC function score than OA1 females. (However, the average age of OA1 females was greater than that of OA1 males). All these trends hold true for the OA2 subjects, except the OA2 females have a greater average WOMAC function score than the OA2 males.

5.3.2 Cartilage and Bone Structure Parameters

A large variation in bone and cartilage parameters is evident among individual subjects in each group, however group-specific means demonstrate decreasing trends (in bone and cartilage parameters) in OA subjects (representative examples are shown in Figure 5.4). In OA1 subjects, a trend of decreasing mean values for apparent bone volume fraction (app. BV/TV), apparent trabecular number (app. Tb.N), and apparent trabecular thickness (app. Tb.Th) in the femur, medial and lateral condyles, and tibia, and increasing apparent trabecular separation (app. Tb.Sp) was evident over two years. OA2 subjects exhibited similar trends; however, they were less pronounced. Decreases in mean values of cartilage volume and thickness in all the cartilage compartments (medial and lateral tibia, and medial and lateral femur) were evident in osteoarthritic subjects over two years, but were more

pronounced in OA2 subjects. The mean values for bone and cartilage parameters in control subjects showed mild variations, but no trends were observed.

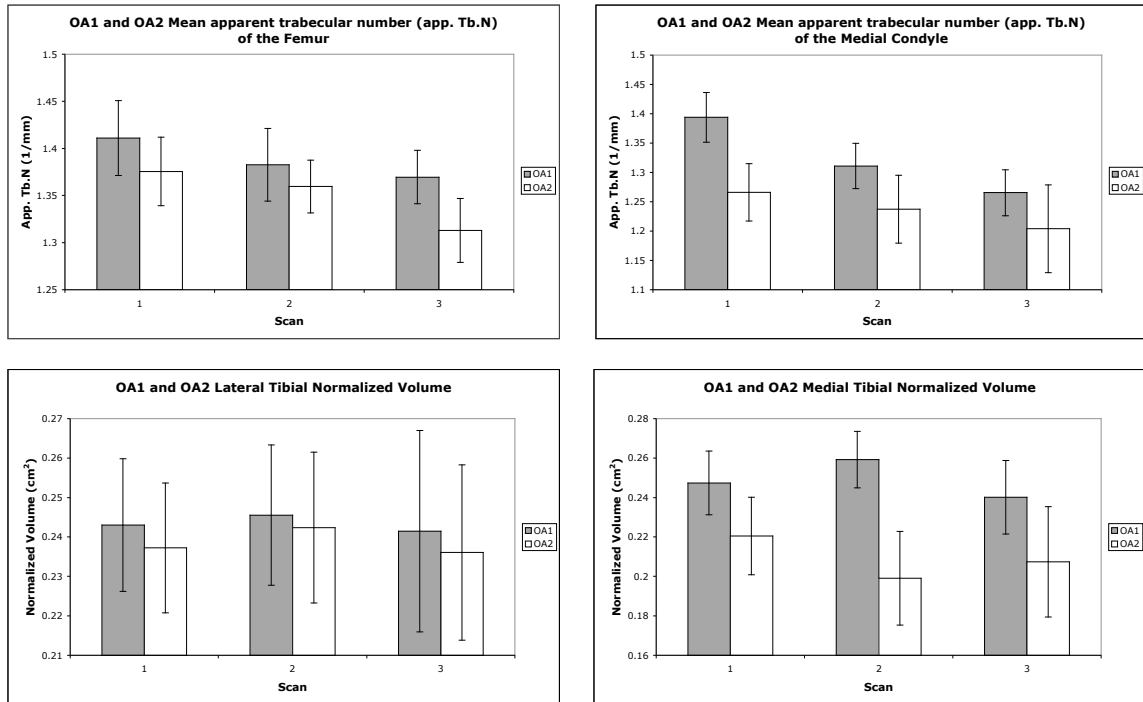


Figure 5.4: A Comparison of OA1 and OA2 mean bone and cartilage parameters over two years. The graphs show (1) a decrease in mean apparent trabecular number (app. Tb.N) of the femur, (2) a decrease in mean app. Tb.N of the medial condyle, and (3) a decrease in medial and lateral tibial normalized cartilage volume over two years. The error bars represent standard error of the mean.

Examination of individual OA subject data showed that nine out of ten OA1 subjects had reduced medial femoral cartilage thickness (mean = -19.04%, range = (-0.63 to -39.78%)), and all ten OA1 subjects had reduced lateral femoral cartilage thickness (mean = -19.94%, range = (-6.22 to -35.52%)) over two years. Eight out of ten OA1 subjects showed a reduction in medial femoral cartilage volume (mean = -32.80%, range = (-7.91% to -63.07%)), and all ten OA1 subjects showed a reduction in lateral femoral cartilage volume (mean = -15.67%, range = (-0.88% to -40.24%)) over two years. Similar changes were found for OA2 subjects, but they were less pronounced. The percent changes in bone parameters

varied among individual osteoarthritic subjects over two years; however, nine out of eleven OA1 subjects showed decreases in apparent bone volume fraction (app. BV/TV) of the femur (mean = -12.14%, range = (-0.71% to 37.91%)) and the medial condyle (mean = -22.86%, range = (-4.72% to 46.91%)). The individual control subjects showed mild variations in bone and cartilage parameters, but no trends were observed.

Using parameter differences from baseline to followup-1, and followup-1 to followup-2, least squares mean percentage changes for each group were calculated, as shown in Table 5.2. The wide range of values in the longitudinal changes between subjects in each group is demonstrated by the standard errors in Table 5.2.

Table 5.2: Least squares mean percentage change of cartilage parameters (standard error in parenthesis) for OA0 (n = 8), OA1 (n =13), and OA2 (n=17) subjects over two years. A decrease in cartilage thickness and volume in the femoral condyles was evident in both osteoarthritic groups. However, the relative difference in the least squares mean percentage change of only cartilage thickness between the osteoarthritic and control groups approached marginal significance ($p = 0.083$ for the lateral condyle and $p = 0.068$ for the medial condyle).

		Cartilage Thickness	Cartilage Volume
Lateral Condyle	<u>OA0</u>	2.6 (11.9)	7.2 (11.2)
	<u>OA1</u>	-10.5 (11.0)	-7.0 (5.8)
	<u>OA2</u>	-9.4 (11.2)	-5.3 (7.3)
Medial Condyle	<u>OA0</u>	8.6 (11.6)	8.2 (16.1)
	<u>OA1</u>	-7.7 (10.3)	-10.2 (14.2)
	<u>OA2</u>	-2.5 (10.4)	-5.4 (14.5)

A decrease in cartilage thickness and volume in the femoral condyles was evident in both osteoarthritic groups. However, the relative difference in the least squares mean change of only cartilage thickness between the osteoarthritic and control groups approached marginal significance ($p < 0.10$). The least squares mean changes of trabecular bone structural

parameters for all regions, as well as cartilage structural parameters for the medial and lateral tibia were insignificant ($p > 0.10$).

5.3.3 Cartilage T_2

The mean T_2 increased significantly ($p < 0.05$) between the baseline and follow-up exams for all cartilage compartments except the lateral tibia (Figure 5.5) for both osteoarthritic groups. For qualitative comparison, the osteoarthritic subjects had a higher mean T_2 value compared to normal volunteers in all cases, except for the baseline scan of the medial tibia.

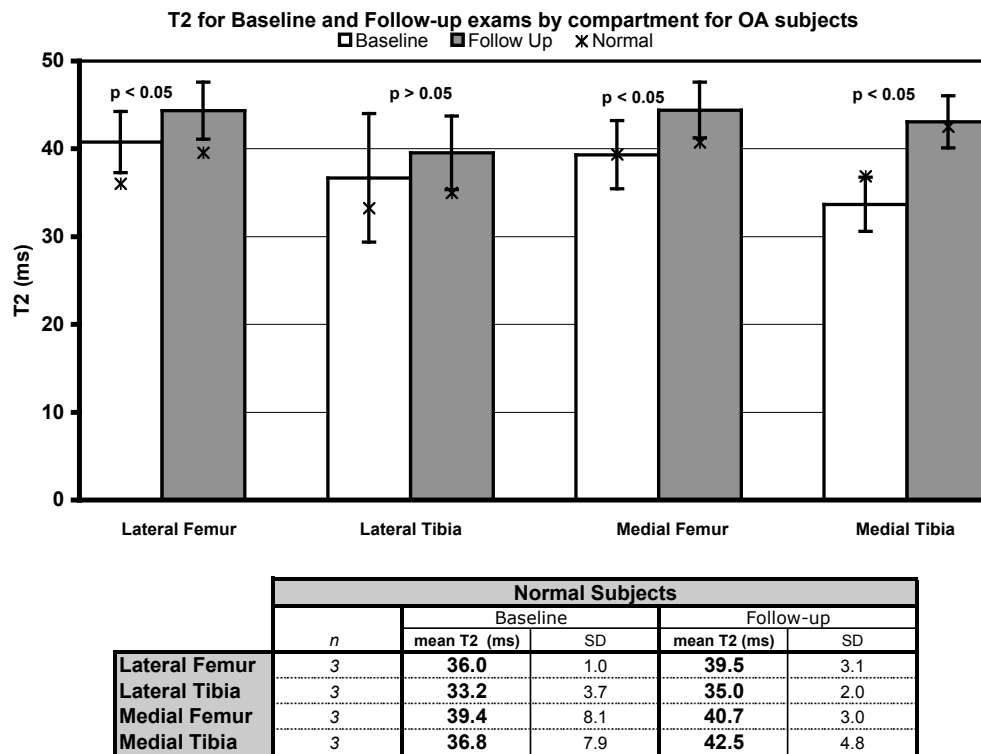


Figure 5.5: A comparison of mean T_2 values (\pm one standard deviation) across twelve patients in the knee cartilage compartments at baseline and follow-up. The T_2 was observed to significantly ($p < 0.05$) increase over time for all compartments except the lateral tibia. Mean T_2 values for three normal volunteers (standard deviations are listed in the table) are shown for qualitative comparison, and are lower in all cases except the baseline scan of the medial tibia.

5.3.4 Correlations Between Cartilage and Bone Structure

The correlation between percentage changes in medial femoral cartilage T_2 and medial tibial cartilage T_2 was $r = 0.81$ ($p < 0.05$). Additionally, a negative correlation ($r = -0.75$, $p < 0.05$) was established between percentage changes in medial femoral cartilage thickness and medial femoral cartilage T_2 (Table 5.3).

Table 5.3: Significant ($**0.00 < p \leq 0.05$; $*0.05 < p \leq 0.10$) Spearman correlations between changes in cartilage thickness and between changes in T_2 in different regions.

Parameter	Parameter	Correlation Coefficient
Medial Tibial Cartilage Thickness	Lateral Tibial Cartilage Thickness	0.49
Medial Femoral Cartilage Thickness	Medial Femoral Cartilage T_2	-0.75
Medial Tibial Cartilage T_2	Medial Femoral Cartilage T_2	0.81

The correlations between percentage changes in cartilage thickness, in different regions, and percentage changes in bone structural parameters, also in different regions, are shown in Tables 3 and 4, respectively. Significant ($p < 0.05$) correlations were evident between the medial and lateral tibial cartilage thickness ($r = 0.49$). Similarly, a positive relationship was established between changes in bone structure in different regions. The highest correlations ($r \sim 0.65$) were established between the bone structure of the medial and lateral tibia, suggesting a strong interdependence. The remaining significant correlations of interest are moderate and are listed in Table 5.4.

Table 5.4: Significant ($p < 0.05$) Spearman correlations between percentage changes in bone parameters (apparent bone volume fraction (app. BV/TV), apparent trabecular number (app. Tb.N), apparent trabecular thickness (app. Tb.Th), and apparent trabecular separation (app. Tb.Sp)) from baseline to follow-up 1. The table shows that a positive relationship was established between bone structure changes in the femur and tibia, the femur and the medial condyle, and the lateral and medial tibia. The highest correlations were established between bone structure of the medial and lateral tibia, suggesting a strong interdependence. The * signifies that $p < 0.0001$.

	Femur vs. Tibia	Femur vs. Medial Condyle	Lateral Tibia vs. Medial Tibia
App. BV/TV vs. App. BV/TV	0.47	0.44	0.63
App. BV/TV vs. App. Tb.N		0.59	0.63
App. BV/TV vs. App. Tb.Th	0.36		0.58
App. BV/TV vs. App. Tb.Sp	-0.46	-0.49	-0.61
App. Tb.N vs. App. BV/TV		0.38	0.54
App. Tb.N vs. App. Tb.N		0.67 *	0.57
App. Tb.N vs. App. Tb.Th			0.45
App. Tb.N vs. App. Tb.Sp		-0.50	-0.55
App. Tb.Th vs. App. BV/TV	0.51	0.43	0.73 *
App. Tb.Th vs. App. Tb.N	0.39	0.39	0.70 *
App. Tb.Th vs. App. Tb.Th	0.42	0.44	0.71 *
App. Tb.Th vs. App. Tb.Sp	-0.50	-0.40	-0.69 *
App. Tb.Sp vs. App. BV/TV		-0.44	-0.60
App. Tb.Sp vs. App. Tb.N		-0.68 *	-0.61
App. Tb.Sp vs. App. Tb.Th			-0.53
App. Tb.Sp vs. App. Tb.Sp		0.54	0.59

Overall, a positive relationship was established between cartilage changes and localized bone changes closest to the joint line, while a negative relationship was established between cartilage changes and global bone changes farthest from the joint line, in both osteoarthritic groups. For example, the medial tibial cartilage volume was positively correlated with app. Tb.N of the medial ($r = 0.36, p < 0.05$) and lateral ($r = 0.41, p < 0.05$) tibia, and with app. Tb.Th of the medial ($r = 0.32, p < 0.10$) and lateral ($r = 0.45, p < 0.10$) condyles, while negatively correlated with the app. BV/TV of the tibia ($r = -0.53, p < 0.05$) and femur ($r = -0.50, p < 0.05$).

Significant positive correlations were established between changes in lateral cartilage thickness and changes in medial femoral bone structure. Furthermore, significant positive correlations were established between changes medial cartilage thickness and changes in lateral tibial bone structure.

5.4 Discussion and Conclusion

In this longitudinal study, MRI was used to track the changes in cartilage and bone structure and to determine their relationship over two years. Although a large variation in bone and cartilage parameters is evident in individual subjects, group-specific means show a reduction in both cartilage and (femoral, medial femoral, lateral femoral, and tibial) bone structural parameters in the OA subjects. These results indicate a loss of cartilage and a deterioration of bone structure in OA subjects over time. In addition, the correlations between changes in cartilage and bone structure demonstrate interdependence between these parameters in the progression of OA.

Previous studies have established that cartilage degeneration is one of the characteristics of OA progression (8,15). For example, Raynauld et al. determined that tibial cartilage volume decreased 6.1 % over two years in osteoarthritic patients and showed that the rate of cartilage depletion varies (32,33); in their study of osteoarthritic knees, 21 patients' cartilage depleted less than 2.0% over two years, while 11 patients' cartilage depleted more than 15.0% over two years. Similarly, our study exhibited a group of fast and slow progressors: the average annual rate of change of cartilage thickness in the medial condyle was -7.7% for OA1 subjects and -2.5% for OA2 subjects. (The difference between these rates of change is not statistically significant; however, this may be attributed to a limited sample size). In both studies, the majority of fast progressors are female; however, it

is difficult to make other comparisons because Raynauld et al. based most of their categorical characterizations on clinical information such as Western Ontario and McMaster Universities Arthritis Index (WOMAC) scores, while ours were based on KL score, determined at baseline.

When examining the variation of cartilage thickness in individual subjects over two years, the thickness tended to increase after the baseline scan, but decreased substantially by the last scan. The initial increase of cartilage thickness can be explained by the common incidence of cartilage hydration and swelling in early stages of OA (6,34). This initial swelling, or increase in cartilage thickness, is followed by a more pronounced decreasing trend, exhibited by the decreasing mean values and decreasing rates of change of cartilage volume and thickness.

In a subset of the study population, T_2 increased significantly ($p < 0.05$) between the baseline and follow-up scans, in all compartments, (medial and lateral femur, medial tibia) except the lateral tibia. These results, along with the negative correlation established between medial femoral cartilage thickness and medial femoral T_2 , concur with previous studies (35,36) and support the hypothesis that osteoarthritic cartilage has increased mobile water, and hence higher T_2 (27). When examining the correlations between changes in T_2 over time, the strongest correlation was established between the medial tibial cartilage T_2 and the medial femoral cartilage T_2 ($r=0.81$, $p < 0.05$), suggesting that varus malalignment significantly affects the femoral and tibial cartilage of the medial compartment.

Previous studies have shown that bone and cartilage function as a unit, working together to sustain the mechanical forces associated with joint loading (15,37,38). Thus, this study explored the relationship between cartilage degeneration and morphologic changes in

bone structure. Positive correlations were established between cartilage morphology and localized bone changes closest to the joint line, while negative correlations were established between cartilage morphology and global bone changes farthest from the joint line. These relationships could be explained by the following hypothesis: osteoarthritic knees with cartilage degeneration have high incidence of subchondral plate sclerosis, (39-42) which could cause osteopenia in the subarticular bone (41,43) due to decreased load transmission. This localized osteopenia may lead to reactive bone formation farther from the joint line, compensating for the localized bone loss. This hypothesis is supported by Wolff's Law, which states that tissues will adapt to changes in mechanical loading by altering their structural properties (44).

The results of this study show an association between medial tibial cartilage depletion and both medial and lateral tibial bone structure degradation. These results could be influenced by factors such as subchondral plate sclerosis and focal cartilage lesions (that may be in the vicinity of the representative slices). Therefore, these correlations show that if medial cartilage volume or thickness decreases, localized areas of tibial bone structure may degrade, however, the overall structural parameters of the femur and tibia increase significantly ($p < 0.05$).

Sharma et al. (4) showed that joint malalignment increases the probability of developing medial and lateral OA. To explore how varus and valgus alignment affects the progression of OA, this study included a subject cohort with both types of malalignment. Significant positive correlations are evident between changes in lateral cartilage and medial femoral bone structure. This relationship demonstrates that if lateral cartilage thickness decreases, the bone structure of the medial condyle is likely to degrade, while (moderately

significant correlations indicate that) reactive bone structural formation will develop in the lateral condyle. Such developments may be attributed to valgus alignment, which causes greater forces in the lateral compartment and causes unloading in the medial compartment (14). These increased forces cause bone formation in the diseased compartment (45), while the decreased forces cause bone resorption in the contra-lateral compartment (4,5) (15). Similar, but moderately significant correlations, were established in subjects with varus OA; if medial cartilage volume and thickness decreases, the lateral tibial bone structure is likely to weaken. The relationship between cartilage degeneration in one compartment and weakening of bone structure in the contra-lateral compartment further shows that alignment plays a significant role in the progression of OA.

Potential confounds of this study include long scan time, modest subject sample size, limited follow-up rate, uneven gender distribution, and wide age distribution in OA subjects. The long scan time may have influenced the quantity of follow-up T₂ data available, as knee motion between the high-resolution scan and the dual-echo scan could preclude follow-up T₂ analysis. Due to the small sample size, the trends in baseline OA subject characteristics may not be generalized to the OA subjects. Despite these confounds, this pilot study demonstrates significant trends and correlations, and therefore, substantiates the need for further longitudinal studies.

In conclusion, this study quantifies the changes in bone and cartilage structural parameters over time, and demonstrates a longitudinal relationship between the morphological changes in bone and cartilage structure in patients with varying degrees of OA. Although a large variation of bone and cartilage changes is apparent among subjects, significant correlations between changes in bone and cartilage parameters in osteoarthritic

subjects are evident in a limited sample size, with a relatively short follow-up duration. This study also emphasizes the role of quantitative MRI as a potential tool for monitoring cartilage and bone structure in degenerative joint disease.

5.5 References

1. Mollenhauer JA, Erdmann S. Introduction: molecular and biomechanical basis of osteoarthritis. *Cell Mol Life Sci* 2002;59(1):3-4.
2. Recht MP, Resnick D. Magnetic resonance imaging of articular cartilage: an overview. *Top Magn Reson Imaging* 1998;9(6):328-336.
3. Felson DT, Lawrence RC, Dieppe PA, Hirsch R, Helmick CG, Jordan JM, Kington RS, Lane NE, Nevitt MC, Zhang Y, Sowers M, McAlindon T, Spector TD, Poole AR, Yanovski SZ, Ateshian G, Sharma L, Buckwalter JA, Brandt KD, Fries JF. Osteoarthritis: new insights. Part 1: the disease and its risk factors. *Ann Intern Med* 2000;133(8):635-646.
4. Sharma L, Song J, Felson DT, Cahue S, Shamiyeh E, Dunlop DD. The role of knee alignment in disease progression and functional decline in knee osteoarthritis. *Jama* 2001;286(2):188-195.
5. Sharma L. Local factors in osteoarthritis. *Curr Opin Rheumatol* 2001;13(5):441-446.
6. Arokoski JP, Jurvelin JS, Vaatainen U, Helminen HJ. Normal and pathological adaptations of articular cartilage to joint loading. *Scand J Med Sci Sports* 2000;10(4):186-198.
7. Disler DG, Recht MP, McCauley TR. MR imaging of articular cartilage. *Skeletal Radiol* 2000;29(7):367-377.
8. Cicuttini FM, Wluka AE, Forbes A, Wolfe R. Comparison of tibial cartilage volume and radiologic grade of the tibiofemoral joint. *Arthritis Rheum* 2003;48(3):682-688.
9. Wluka AE, Stuckey S, Snaddon J, Cicuttini FM. The determinants of change in tibial cartilage volume in osteoarthritic knees. *Arthritis Rheum* 2002;46(8):2065-2072.

10. Bettica P, Cline G, Hart DJ, Meyer J, Spector TD. Evidence for increased bone resorption in patients with progressive knee osteoarthritis: longitudinal results from the Chingford study. *Arthritis Rheum* 2002;46(12):3178-3184.
11. Kamibayashi L, Wyss U, Cooke D, Zee B. Trabecular micro-structure in the medial condyle of the proximal tibia of patients with knee osteoarthritis. *Bone* 1995;17:27-35.
12. Radin E, Rose R. Role of subchondral bone in the initiation and progression of cartilage damage. *Clinical orthopedics and Related research* 1986;213:34-40.
13. Lajeunesse D, Reboul P. Subchondral bone in osteoarthritis: a biologic link with articular cartilage leading to abnormal remodeling. *Curr Opin Rheumatol* 2003;15(5):628-633.
14. Wada M, Maezawa Y, Baba H, Shimada S, Sasaki S, Nose Y. Relationships among bone mineral densities, static alignment and dynamic load in patients with medial compartment knee osteoarthritis. *Rheumatology (Oxford)* 2001;40(5):499-505.
15. Lindsey CT, Narasimhan A, Adolfo JM, Jin H, Steinbach LS, Link T, Ries M, Majumdar S. Magnetic resonance evaluation of the interrelationship between articular cartilage and trabecular bone of the osteoarthritic knee(1). *Osteoarthritis Cartilage* 2004;12(2):86-96.
16. Bellamy N, Buchanan W, Goldsmith C, et.al. Validation study of WOMAC: a health status instrument for measuring clinically important patient relevant outcomes to anti-rheumatic drug therapy in patients with osteoarthritis of the hip and knee. *J Rheumatology* 1988;15:1833-1840.
17. Kellgren J, Lawrence J. Radiologic assessment of osteoarthritis. *Ann Rheum Dis* 1957;16:494-502.
18. Beuf O, Ghosh S, Newitt DC, Link TM, Steinbach L, Ries M, Lane N, Majumdar S. Magnetic resonance imaging of normal and osteoarthritic trabecular bone structure in the human knee. *Arthritis Rheum* 2002;46(2):385-393.
19. Wald LL, Carvajal L, Moyher SE, Nelson SJ, Grant PE, Barkovich AJ, Vigneron DB. Phased array detectors and an automated intensity-correction algorithm for high-resolution MR imaging of the human brain. *Magn Reson Med* 1995;34(3):433-439.

20. Newitt DC, Van Rietbergen B, Majumdar S. Processing and analysis of in vivo high resolution MR images of trabecular bone for longitudinal studies: reproducibility of structural measures and micro-finite element analysis derived mechanical properties. *Osteoporosis International* 2002;13(4):278-287.
21. Majumdar S, Newitt D, Mathur A, Osman D, Gies A, Chiu E, Lotz J, Kinney J, Genant H. Magnetic resonance imaging of trabecular bone structure in the distal radius: relationship with X-ray tomographic microscopy and biomechanics. *Osteoporos Int* 1996;6(5):376-385.
22. Majumdar S, Genant HK, Grampp S, Newitt DC, Truong VH, Lin JC, Mathur A. Correlation of trabecular bone structure with age, bone mineral density, and osteoporotic status: in vivo studies in the distal radius using high resolution magnetic resonance imaging. *J Bone Miner Res* 1997;12(1):111-118.
23. Goldstein SA, Goulet R, McCubbrey D. Measurement and significance of three-dimensional architecture to the mechanical integrity of trabecular bone. *Calcif Tissue Int* 1993;53 Suppl 1(3):S127-132; discussion S132-133.
24. Majumdar S, Newitt D, Jergas M, Gies A, Chiu E, Osman D, Keltner J, Keyak J, Genant H. Evaluation of technical factors affecting the quantification of trabecular bone structure using magnetic resonance imaging. *Bone* 1995;17(4):417-430.
25. Majumdar S, Genant HK. A review of the recent advances in magnetic resonance imaging in the assessment of osteoporosis. *Osteoporosis International* 1995;5(2):79-92.
26. Faber SC, Eckstein F, Lukasz S, Muhlbauer R, Hohe J, Englmeier KH, Reiser M. Gender differences in knee joint cartilage thickness, volume and articular surface areas: assessment with quantitative three-dimensional MR imaging. *Skeletal Radiol* 2001;30(3):144-150.
27. Dunn T, Lu Y, Jin H, Ries M, Majumdar S. MR Quantification of Cartilage T2 Variation with Severity of Osteoarthritis in the Knee. *Radiology*, 2004;Accepted,.
28. Ghosh S. Magnetic Resonance Imaging based on Evaluation of Articular Cartilage in Osteoarthritis. San Francisco, CA: University of California, San Francisco; 2001. 265 p.

29. Diggle P, Liang K-Y, Zeger SL. Analysis of longitudinal data. OxfordNew York: Clarendon Press ;Oxford University Press; 1994. xi, 253 p.
30. Laird NM, Ware JH. Random-effects models for longitudinal data. *Biometrics* 1982;38(4):963-974.
31. Daniel WW. Biostatistics : a foundation for analysis in the health sciences. New York: Wiley; 1999. xiv, 755, [152] p.
32. Raynauld JP. Quantitative magnetic resonance imaging of articular cartilage in knee osteoarthritis. *Curr Opin Rheumatol* 2003;15(5):647-650.
33. Raynauld JP, Martel-Pelletier J, Berthiaume MJ, Labonte F, Beaudoin G, de Guise JA, Bloch DA, Choquette D, Haraoui B, Altman RD, Hochberg MC, Meyer JM, Cline GA, Pelletier JP. Quantitative magnetic resonance imaging evaluation of knee osteoarthritis progression over two years and correlation with clinical symptoms and radiologic changes. *Arthritis Rheum* 2004;50(2):476-487.
34. Gandy SJ, Dieppe PA, Keen MC, Maciewicz RA, Watt I, Waterton JC. No loss of cartilage volume over three years in patients with knee osteoarthritis as assessed by magnetic resonance imaging. *Osteoarthritis Cartilage* 2002;10(12):929-937.
35. Buckwalter JA, Mankin HJ. Articular cartilage: degeneration and osteoarthritis, repair, regeneration, and transplantation. *Instr Course Lect* 1998;47:487-504.
36. Lusse S, Claassen H, Gehrke T, Hassenpflug J, Schunke M, Heller M, Gluer CC. Evaluation of water content by spatially resolved transverse relaxation times of human articular cartilage. *Magn Reson Imaging* 2000;18(4):423-430.
37. Ding M, Dalstra M, Linde F, Hvid I. Mechanical properties of the normal human tibial cartilage-bone complex in relation to age. *Clin Biomech (Bristol, Avon)* 1998;13(4-5):351-358.
38. Issever AS, Walsh A, Lu Y, Burghardt A, Lotz JC, Majumdar S. Micro-computed tomography evaluation of trabecular bone structure on loaded mice tail vertebrae. *Spine* 2003;28(2):123-128.

39. Layton MW, Goldstein SA, Goulet RW, L.A. Feldkamp, Kabinsky DJ, Bole GG. Examination of subchondral bone architecture in experimental osteoarthritis by microscopic computed tomography. *Arthritis and Rheumatism* 1988;31:1400-1405.
40. Pessis E, Drape JL, Ravaud P, Chevrot A, Dougados M, Ayrat X. Assessment of progression in knee osteoarthritis: results of a 1 year study comparing arthroscopy and MRI. *Osteoarthritis Cartilage* 2003;11(5):361-369.
41. Buckland-Wright C. Subchondral bone changes in hand and knee osteoarthritis detected by radiography. *Osteoarthritis Cartilage* 2004;12 Suppl A:10-19.
42. Pastoureau P, Leduc S, Chomel A, De Ceuninck F. Quantitative assessment of articular cartilage and subchondral bone histology in the meniscectomized guinea pig model of osteoarthritis. *Osteoarthritis Cartilage* 2003;11(6):412-423.
43. Karvonen RL, Miller PR, Nelson DA, Granda JL, Fernandez-Madrid F. Periarticular osteoporosis in osteoarthritis of the knee. *J Rheumatol* 1998;25(11):2187-2194.
44. Wolff J. *Das Gesetz der Transformation der Knochen*. Berlin: Hirschwald; 1892.
45. Christensen P, Kjaer J, Melsen F, Nielsen HE, Sneppen O, Vang PS. The subchondral bone of the proximal tibial epiphysis in osteoarthritis of the knee. *Acta Orthop Scand* 1982;53(6):889-895.

Chapter 6: The Feasibility of Characterizing the Spatial Distribution of Cartilage T_2 using Texture Analysis

6.1 Introduction

Quantitative T_2 relaxation time has been used as a non-invasive marker of cartilage degeneration, as it is sensitive to tissue hydration and biochemical composition. In early cartilage degeneration, changes in the extracellular matrix (e.g. disorganization and breakdown of collagen network) increase the mobility of water, thus increasing T_2 relaxation time. Previous studies have demonstrated elevated T_2 relaxation time in OA subjects as compared to healthy subjects (1,2), have reported spatial variations in T_2 values from the radial zone to the articular cartilage surface (3), and have shown different visual patterns of T_2 values in pre-arthritic, early arthritic, and healthy hip cartilage (4). Dray et al. (5) found no difference between mean T_2 values in OA cartilage however, they showed visual differences in the spatial distribution of the T_2 values. These results demonstrate the necessity to characterize and quantify the spatial distribution of cartilage T_2 values.

Texture analysis based on the grey level co-occurrence matrix (GLCM) is a method developed by Haralick et al. (6) that can be used to examine the spatial distribution of pixel values in an image. Recent studies have characterized the distribution of cartilage pixel values in anatomic images (7) and T_2 relaxation maps (8). Blumenkrantz et al. (8) demonstrated that mild OA patients (n=8) had significantly elevated GLCM entropy and reduced angular second moment (ASM) of cartilage T_2 than controls (n = 14). Based on these results, we hypothesize that texture measures can be used to characterize and quantify cartilage degeneration in early OA and may complement measures of mean cartilage T_2 . The purpose of this study was (i) to characterize the spatial distribution of cartilage T_2 in

postmenopausal OA patients and age-matched healthy subjects using second order texture measures at baseline and (ii) to analyze changes in the texture of cartilage T₂ after 9 months in both groups.

6.2 Methods

6.2.1 Subjects

Eight female OA patients (age = 55.7 ± 7.3 years) and ten age-matched female controls (57.6 ± 6.2 years) participated in the study. In all subjects, standing anteroposterior radiographs of the knee were obtained and evaluated using the Kellgren Lawrence (KL) (9) grading scale for OA severity. The inclusion criteria required that patients had a KL score of 2 or 3 in one knee, and an equal or lower KL score in the contralateral knee); frequent knee symptoms (pain, aching or stiffness), or used medication (all types) to treat knee pain on most days during the past year; and a body-mass-index (BMI) $> 30 \text{ kg/m}^2$. The OA patients were not undergoing any type of treatment during the study. The inclusion criteria required that control subjects did not have radiological and clinical evidence of knee OA in either knee (KL score 0) and had a BMI $< 30 \text{ kg/m}^2$. This study was performed in accordance with the rules and regulations from the local Human Research Committee, and all subjects provided informed consent.

MR Imaging

6.2.2 Magnetic Resonance Imaging

MR imaging was performed on a 3.0 Tesla system (Signa, GE Medical systems, Waukesha, WI) using a knee coil that was specifically developed for this study (Clinical MR

Solutions, Brookfield, WI, USA). Subjects were positioned supine in the scanner and imaged at baseline and 9 months.

High-resolution, fat-suppressed, 3D spoiled gradient-echo (SPGR) sagittal MR images (TE = 7.5 ms, TR = 20 ms, resolution = .293 x .293 x 1.5 mm³, FOV = 15 cm) were acquired for assessing cartilage morphology. 2D dual echo fast spin echo (FSE) sagittal images (TE₁/TE₂ = 8.5/34.1 ms, TR = 3600 ms, resolution = 0.625 x 0.625 x 3 mm³, FOV = 16 cm) were acquired for measuring cartilage T₂ relaxation time and to determine the Whole-Organ Magnetic Resonance Imaging Scores (WORMS) (10).

6.2.3 Image Analysis

All images were analyzed using a Sun Workstation (Sun Microsystems, Palo Alto, CA). Knee cartilage was segmented from the SPGR images using a spline-based, semi-automatic technique (Bezier splines and edge detection) (11) developed using Matlab (Mathworks, Natick, MA). Five regions including the medial and lateral tibia, and medial and lateral femur, and trochlea were defined. Shape-based interpolation was used to generate isotropic voxels from which three-dimensional cartilage thickness and volume maps were computed.

T₂ maps were computed on a pixel-by-pixel basis from the dual-echo, fast spin-echo images, using the following equation:

$$S(TE) \propto \exp(-TE/T_2) \quad [6.1]$$

The T₂ maps were registered to the SPGR images using a rigid-body algorithm (to reduce the effects of knee movement from the SPGR sequence to the T₂ mapping sequence). The segmented regions of interest were re-sampled and superimposed on the T₂ maps. The

segmented regions of interest that included partial volume effects due to fluid were manually excluded.

Texture analysis was performed on a slice-by-slice basis on the cartilage T₂ maps. This method is based on the grey level co-occurrence matrix (GLCM) as described by Haralick et al. (6). The GLCM determines the frequency that neighboring grey-level values occur in an image. Analysis can be performed at a defined orientation (e.g. 0 degrees, 90 degrees) and a defined spacing (e.g. spacing = 1 for nearest-neighbor pixels). Texture parameters including angular second moment (ASM) and entropy are calculated from the co-occurrence matrix. ASM is a measure of order of an image, while entropy is a measure of disorder in an image. The equations for ASM and entropy are shown below (6.2 and 6.3). P represents the probability of the co-occurrence of pixel values i and j in an image. N represents the total number of pixel value co-occurrences in the image, and R is a normalizing constant.

$$ASM = \sum_{i=1}^N \sum_{j=1}^N \left(\frac{P(i,j)}{R} \right)^2 \quad [6.2]$$

$$Entropy = \sum_{i=1}^N \sum_{j=1}^N P(i,j)(-\ln P(i,j)) \quad [6.3]$$

Texture analysis was performed on the cartilage T₂ maps in the lateral femur, lateral tibia, medial femur, medial tibia, and trochlea. A grey level co-occurrence matrix was defined for each cartilage region and used for texture analysis. Second order texture measures including entropy and ASM, were calculated at 0° (corresponding to the anterior-posterior axis) and at 90° (corresponding to the superior-inferior axis), with pixel offsets

ranging from 1-3 pixels. The pixel offset range was chosen based on the fact that approximately 3 to 4 pixels span the cartilage thickness.

6.2.4 Statistical Analysis:

At baseline, t-tests were used to compare texture parameters in OA patients and controls. A one-way analysis of variance (ANOVA) was employed to evaluate texture parameters in different cartilage compartments (using JMP software (SAS institute, Cary, NC). Pearson correlations were calculated to determine the relationship between (1) ASM and entropy of cartilage T_2 , (2) texture parameters at different orientations, and (3) texture parameters at different pixel offsets. Paired t-tests were used to compare texture parameters of cartilage T_2 in OA patients at 0 and 90 degrees.

The reproducibility (root mean square coefficient of variation percentage (CV%)) for cartilage segmentation and T_2 quantification was less than 5% and is described in detail by Stahl et al. (12).

The longitudinal data analysis was performed using SAS Version 9.1 software (SAS Institute, Cary, North Carolina). Least square means (LSMean) and Standard Errors (SE) at baseline and 9 months were estimated for mean T_2 , standard deviation of T_2 , entropy and ASM of cartilage T_2 , and cartilage volume and thickness. These variables were compared with multivariate analysis of variance (MANOVA) after adjusting the effects between visits and among measurement locations, and after excluding the repeated measurement errors in the same subjects with SAS GLM procedure. The changes in outcome variables between baseline and 9 months were evaluated using the same MANOVA model.

6.3 Baseline Results

6.3.1 Baseline Patient Characteristics

The OA subjects (n = 8) and controls (n = 10) were similar in age (OA subjects = 55.7 ± 7.3 years, controls = 57.6 ± 6.2 years, $p = 0.574$), but had significantly different BMI's (OA subjects = 34.4 ± 4.9 , controls = 23.2 ± 2.1 , $p < 0.0001$). Four OA subjects had a KL score of 2, and the other four had a KL score of 3.

6.3.2 Baseline T_2 and Texture Analysis

At baseline, the mean and the standard deviation of cartilage T_2 values were greater in OA subjects than in controls ($p < 0.05$ in all compartments combined and in the lateral femur). There were no significant differences in cartilage thickness or volume between patients and controls at baseline ($p > 0.05$).

The ASM of cartilage T_2 was greater in control subjects than in OA patients in all compartments combined ($p < 0.05$ for 0° , 1 pixel offset), the lateral femur ($p < 0.05$ for 90° , 3 pixel offset), and the medial tibia ($p < 0.05$ for 90° , 1 pixel offset). Entropy of cartilage T_2 was greater in OA patients than in control subjects in all compartments combined ($p < 0.05$ for 0° , 1-3 pixel offsets), the lateral femur ($p < 0.05$ for 0° , 1-3 pixel offset; and for 90° , 2-3 pixel offset), and the medial tibia ($p < 0.05$ for 90° , 1-3 pixel offset). Representative examples of images and texture parameters from two OA patients (with cartilage WOMBS scores of 5 and 1) and control are shown in Figure 6.1. Figure 6.2 illustrates the differences in entropy and ASM of cartilage T_2 (at 0° and 90°) between OA patients and controls.

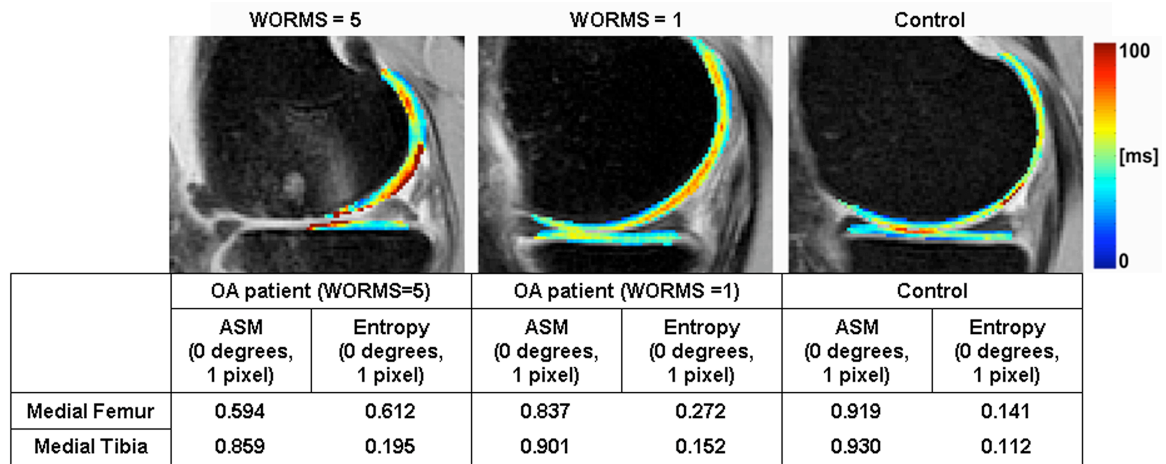


Figure 6.1: Representative T_2 colormaps overlaid on T_2 -weighted images of an advanced OA patient (cartilage WORMS = 5) (left), a mild OA patient (cartilage WORMS = 1) (center), and a control subject (right). The entropy and ASM of cartilage T_2 for the OA patients and control subject are listed in the table. The OA patients both have greater entropy and lower ASM than the control subject.

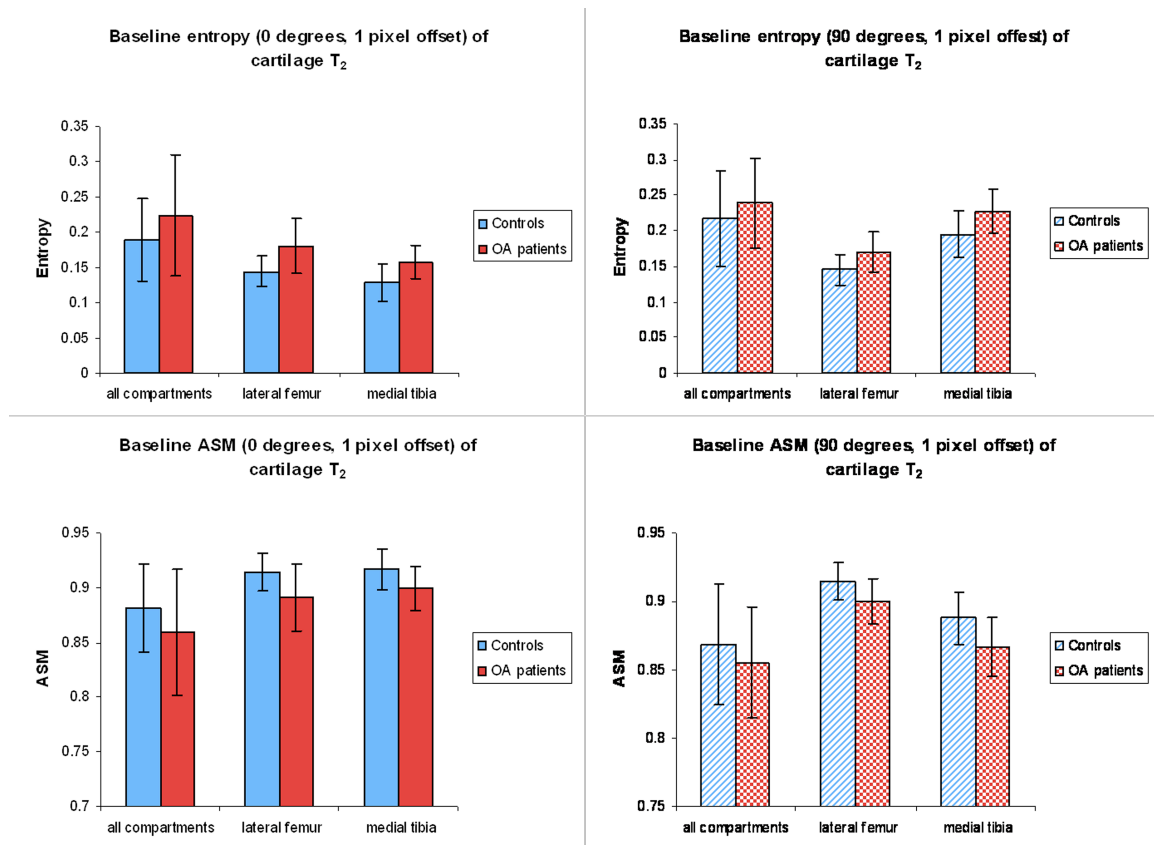


Figure 6.2: Entropy (top row) of cartilage T_2 is greater in OA patients than in controls in all compartments combined, and the lateral and medial tibia at 0 degrees (top left) and 90 degrees (top right). ASM (bottom row) of cartilage T_2 greater in controls than in OA patients in all compartments combined and the lateral and medial tibia at 0 degrees (bottom left) and 90 degrees (bottom right). The ‘ \ast ’ indicates a significant difference ($p < 0.05$) between OA patients and controls. The ‘ Δ ’ indicates that ($p < 0.10$).

In OA patients, entropy and ASM of cartilage T_2 was significantly different between cartilage compartments. ASM of cartilage T_2 was greatest in the medial tibia and lowest in the medial femur. ASM (0° , 1 pixel offset) was significantly greater in the lateral femur than both the medial femur and trochlea ($p < 0.05$). Entropy of cartilage T_2 was greatest in the medial femur and lowest in the medial tibia. Entropy (0° , 1 pixel offset) was significantly greater in the medial femur than the medial tibia, lateral femur, and lateral tibia ($p < 0.05$). Entropy (0° , 1 pixel offset) was significantly greater in the trochlea

than both the medial tibia and the lateral femur ($p < 0.05$). Significant differences between 0° and 90° in ASM and entropy of cartilage T_2 were demonstrated in the lateral tibia, medial tibia, and trochlea.

6.3.3 Correlations Between Measurements

A positive relationship was demonstrated between texture parameters at different pixel offsets. In addition, strong positive correlations were found between texture parameters at different orientations (0° and 90°). Negative correlations were demonstrated between ASM and entropy (table 6.1).

Table 6.1: Correlations between texture parameters of cartilage T_2 are shown in the table.

	Texture parameter	Orien- tation	Pixel offset	Texture Parameter	Orientation	Pixel Offset	Correlation	P value
Effects of pixel offset	ASM	0	1	ASM	0	2	0.997	<0.0001
	ASM	0	1	ASM	0	3	0.993	<0.0001
Effects of orientation	ASM	90	1	ASM	0	1	0.618	<0.0001
	ENT	90	1	ENT	0	1	0.497	<0.0001
Effects of texture parameter	ASM	0	1	ENT	0	1	-0.986	<0.0001
	ASM	90	1	ENT	90	1	-0.985	<0.0001

A positive correlation was established between entropy (90° , 2 pixel offset) of cartilage T_2 and the standard deviation of cartilage T_2 ($r = 0.313$, $p < 0.05$). A negative correlation was established between mean cartilage T_2 and standard deviation of cartilage T_2 ($r = 0.307$, $p < 0.05$).

No significant correlations were evident between baseline texture parameters and longitudinal changes in cartilage thickness and volume.

6.3.4 WORMS Scoring

Texture parameters were evaluated in patients with different degrees of cartilage degeneration (determined by cartilage WORMS scores). Cartilage WORMS score was

determined in each cartilage compartment. The subject cohort was subdivided into three groups: controls, those with a WORMS score of 1, and those with a WORMS score of ≥ 2 , (corresponding to normal, inhomogeneous cartilage signal, and morphologic cartilage degeneration, respectively). Cross-sectional analysis of the combined data from baseline and follow-up showed that entropy was greatest (and ASM was lowest) in patients with the greatest WORMS score. Representative examples are shown in Figure 6.1. The mean \pm standard error of ASM (0° , 1 pixel offset) was 0.877 ± 0.004 in controls, 0.868 ± 0.014 in patients with WORMS score of 1, and 0.858 ± 0.006 in patients with WORMS ≥ 2 ($p = 0.03$). The mean \pm standard error of entropy (0° , 1 pixel offset) was 0.192 ± 0.006 in controls, 0.208 ± 0.020 in patients with WORMS score of 1, and 0.226 ± 0.009 in patients with WORMS ≥ 2 ($p = 0.009$).

6.4 Longitudinal Results

6.4.1 Mean and standard deviation of cartilage T_2

Using the combined data from baseline and 9 months, the LSMean analysis showed significant differences ($p < 0.05$) in mean and standard deviation of cartilage T_2 between OA patients and controls (Table 6.2). Overall, the mean T_2 was 42.329 ± 0.521 ms in patients and was 40.035 ± 0.485 ms in controls ($p = 0.002$). The standard deviation of cartilage T_2 was 14.259 ± 0.275 ms in patients and was 12.884 ± 0.256 ms in controls ($p < 0.001$).

Table 6.2: Least square means (LSMeans) analysis (baseline and follow-up combined) of ASM and entropy of cartilage T₂, mean and standard deviation of cartilage T₂, and cartilage volume and thickness between OA patients and controls using data from baseline and 9 months are shown in the table.

Variable	Control		Patient		P
	LSMean	SE	LSMean	SE	
ASM	0.851	0.003	0.841	0.003	0.037
Entropy	0.243	0.004	0.257	0.005	0.034
T₂ SD	12.884	0.256	14.259	0.275	0.0003
T₂ Mean	40.035	0.485	42.329	0.521	0.002
Thickness	1.565	0.033	1.570	0.036	0.914
Volume	1.615	0.067	1.716	0.072	0.307

The LSMean model demonstrated longitudinal decreases in mean T₂ (all compartments combined) which approached significance (p = 0.06) in OA patients, but not in controls (p = 0.51). The standard deviation of cartilage T₂ significantly (p < 0.05) increased from baseline to 9 months in OA patients (Table 6.3). No significant longitudinal changes in the standard deviation of cartilage T₂ were evident in controls.

6.4.2 Cartilage Thickness and Volume

Using the combined data from baseline and 9 months, LSMean analysis showed that cartilage volume and thickness was not significantly different between OA patients and controls (table 6.2). Overall, the mean cartilage thickness was 1.570 ± 0.036 mm in patients and was 1.565 ± 0.033 mm in controls (p = 0.87) in all compartments. The mean cartilage volume was 1.716 ± 0.072 cm³ in patients and was 1.615 ± 0.067 cm³ in controls (p = 0.30).

Cartilage thickness and volume decreased in OA patients over time; however these differences were not significant (p = 0.70 for thickness, p = 0.71 for volume) (Table 6.3). Cartilage volume and thickness increased in control subjects over time; however these differences were also insignificant (p = 0.47 for thickness, p = 0.91 for volume).

6.4.3 Texture Analysis

Using the data from baseline and 9 months, LSMeans analysis showed that ASM and entropy of cartilage T₂ were both significantly different between OA patients and controls (Table 6.2). Overall, the ASM of cartilage T₂ was 0.841 ± 0.003 in patients and was 0.851 ± 0.003 in controls ($p = 0.037$). The entropy of cartilage T₂ was 0.257 ± 0.005 in patients and was 0.243 ± 0.004 in controls ($p = 0.034$).

Longitudinal increases in the ASM ($p = 0.061$), and decreases in entropy ($p = 0.035$) of cartilage T₂ in OA patients were observed (Figure 6.3, Table 6.3). Figure 6.3 illustrates the changes in entropy and ASM of cartilage T₂ in OA patients at 0 and 90 degrees. There were no significant changes in entropy or ASM of cartilage T₂ in controls from baseline to 9 months.

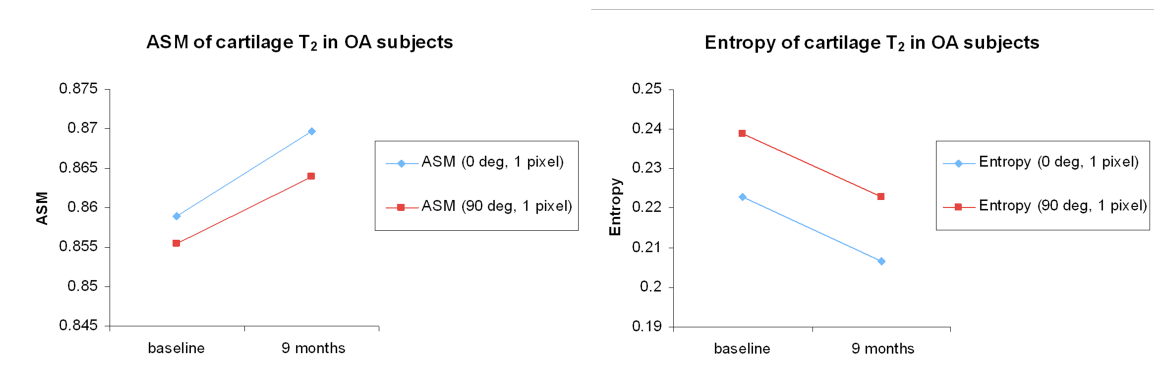


Figure 6.3: Increased ($p < 0.10$) cartilage T₂ ASM was evident in OA patients from baseline to 9 months. Decreased ($p < 0.10$) cartilage T₂ entropy was evident in OA patients from baseline to 9 months.

Table 6.3: The longitudinal changes in ASM and entropy of cartilage T₂, mean and standard deviation of cartilage T₂, and cartilage volume and thickness in OA patients are shown in the table. The standard deviation of T₂ and entropy of T₂ significantly decreased from baseline to 9 months. Control subjects did not show significant changes in these parameters.

Variable	Patient (LSMean±SE)		P
	Baseline	9 months	
ASM	0.835 ± 0.004	0.847 ± 0.004	0.061
Entropy	0.268 ± 0.007	0.247 ± 0.007	0.035
T ₂ SD	14.89 ± 0.388	13.70 ± 0.388	0.032
T ₂ Mean	43.37 ± 0.736	41.40 ± 0.736	0.060
Thickness	1.585 ± 0.051	1.557 ± 0.051	0.701
Volume	1.744 ± 0.102	1.691 ± 0.102	0.715

6.5 Discussion and Conclusion

This study demonstrated the feasibility of using texture analysis to characterize the spatial distribution of T₂ values in articular cartilage in OA patients and controls. Entropy and ASM showed significant differences between mild OA patients and controls, demonstrating that these parameters may be able to differentiate osteoarthritic from healthy cartilage. The mean T₂ values, their standard deviation, and their entropy were greater in OA patients than in controls, indicating that the T₂ values in osteoarthritic cartilage are not only elevated, but also more heterogeneous than those in healthy cartilage. Over 9 months, the standard deviation and entropy of cartilage T₂ significantly ($p < 0.05$) decreased in OA patients, while no significant changes were evident in cartilage thickness or volume. The longitudinal results demonstrate that changes in texture parameters of cartilage T₂ may precede morphological changes in thickness and volume in the progression of OA.

The results of this study are consistent with those of previous studies, which have reported elevated T₂ values in OA cartilage (1,2), and increased entropy and decreased ASM of cartilage T₂ and T_{1ρ} values in OA subjects compared to controls (13). T₂ relaxation time in cartilage has been associated with many factors including the mobility of water (14) (which

is affected by the breakdown of the extracellular matrix), water content (15), and collagen fiber orientation (16). Both *in vitro* (17) and *in vivo* studies (14,18-20) have observed differences in T_2 values from the deep to superficial layers of cartilage. Characterizing the heterogeneity of T_2 values (using standard deviation and texture analysis) provides a means to quantify their distribution. Standard deviation, which evaluates the deviation of T_2 values from their mean, characterizes the spread of T_2 values, while second order texture measures examine the differences in neighboring T_2 pixel values. Together, these measurements can be used to quantify the distribution of cartilage T_2 values on both a global and focal scale, which is essential, given the heterogeneity of biochemical changes that occur in osteoarthritic cartilage. Based on the cross-sectional data, the mean, standard deviation, and entropy of cartilage T_2 values were elevated in OA subjects as compared to controls. The increases in mean cartilage T_2 suggest that the mobility of water is elevated in osteoarthritic cartilage; the increases in standard deviation and entropy suggest that the changes to the extracellular matrix are both globally and spatially heterogeneous throughout the degenerated cartilage.

Longitudinally, the standard deviation and entropy of cartilage T_2 significantly decreased in OA patients. There were no significant changes in mean, standard deviation, ASM or entropy of cartilage T_2 in controls. The mechanisms responsible for the longitudinal decreases of cartilage T_2 entropy are difficult to isolate in an *in vivo* imaging study. These longitudinal results were unexpected; however, we speculate that decreased entropy of cartilage T_2 in OA patients over 9 months is related to swelling of cartilage in the early stages of OA, or short-term changes in disease progression. For example, figure 6.4 illustrates the progression of cartilage degeneration in an OA patient from baseline to 9 months. At baseline, the cartilage signal is inhomogeneous, and at 12 months, a cartilage defect (which

has a more homogeneous signal) has developed. The changes in intensity and spatial distribution of pixel values are evidenced by increased entropy of cartilage T_2 . These results demonstrate that changes in cartilage T_2 are heterogeneous during the evolution of OA.

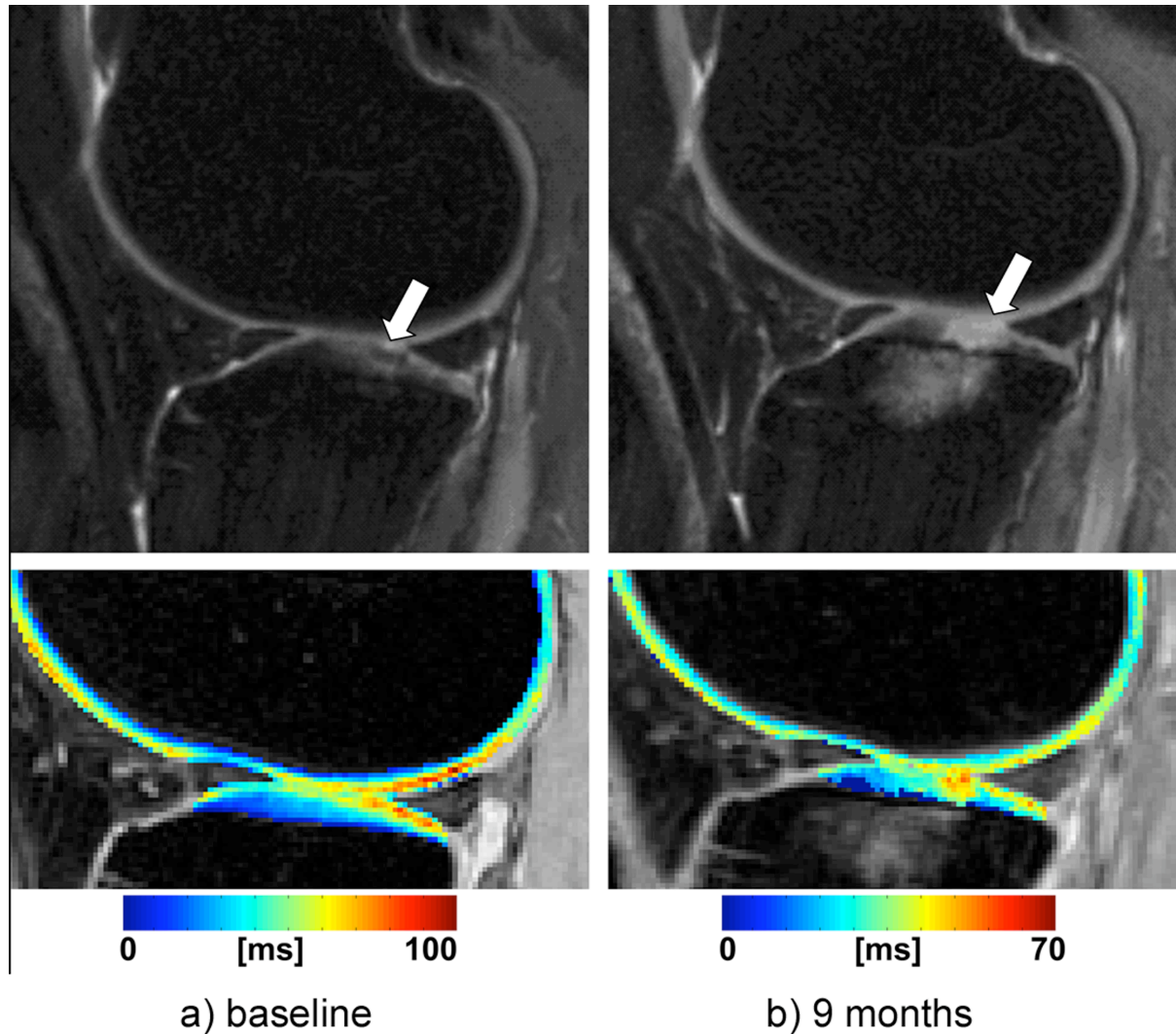


Figure 6.4: Sagittal T_2 -weighted FSE images (top row) and cartilage T_2 maps overlaid on T_2 -weighted FSE images (bottom row) of an OA patient at baseline and 9 months. At baseline, the cartilage signal at the posterior lateral tibia (arrow) is inhomogeneous (a) and at 9 months, an extensive cartilage defect with a more homogeneous signal has developed in the same area (arrow in (b)). An extensive adjacent bone marrow edema pattern is also evident. Visually, there is a decrease in the heterogeneity of T_2 values from baseline to follow-up.

The goal of this study was to establish a method that can be used to quantify and compare the distribution of T_2 pixels in osteoarthritic and healthy cartilage. Since GCLM texture analysis yields a numerical result, it facilitates a simple means for comparison between subject groups. The short-term changes in the spatial distribution of cartilage T_2 values motivate a long-term follow-up study. A further study with a larger patient cohort, and multiple follow-up durations (such as the Osteoarthritis Initiative) is therefore clearly warranted, and would be essential to understand the time-course of T_2 changes in OA. There were no significant cross-sectional differences or longitudinal changes in cartilage thickness or volume in OA patients and controls. This may be because the time-course of cartilage volume and thickness changes are slower than changes in mean, standard deviation, and texture of cartilage T_2 in OA.

The limitations of this pilot study include a small subject sample size (8 OA patients, and 10 controls), short follow-up duration (9 months) and the use of two echo times in calculating the T_2 map. While additional echo times would increase the accuracy of cartilage T_2 and texture quantification, two echo times were used due to constraints in imaging duration. Due to the limited spatial resolution of the T_2 mapping sequence, only approximately 3 to 4 pixels spanned the cartilage thickness (21-23). Increased spatial resolution would decrease partial volume effects at the cartilage-bone surface and would improve the accuracy of the texture analysis particularly perpendicular to the cartilage surface. Because the patient's knee cannot be in an identical position during the baseline and follow-up scans, registration of these scans would ensure that the same region of cartilage is evaluated at both visits. Therefore, improved registration and segmentation techniques would increase the accuracy of cartilage volume, thickness, and T_2 measurements. Another

limitation to this study is the fact that the OA patients had a significantly greater mean BMI than controls. The excess fat tissue in the knee may affect the signal received by the coils, and may affect the calculated T_2 values. Future studies should be designed to include both age and BMI-matched patients and controls.

In this study, the orientation of the texture analysis was performed with respect to the imaging plane, rather than with respect to bone surface. Therefore, 0 degrees may not be considered parallel to the bone surface, especially given the curvature of the femoral condyles. Future studies will define the texture analysis coordinates with respect to the bone surface – 0 degrees will be parallel to the bone surface, while 90 degrees will be perpendicular. This could be accomplished by flattening out the cartilage, thereby facilitating texture analysis at a greater pixel offset in the horizontal plane.

A recent study by Qazi et al. (7) quantified the homogeneity of cartilage signal from T_1 -weighted knee images obtained on a 0.18 T scanner. This study calculated first-order entropy of cartilage using a histogram-based method, and demonstrated a significant difference in cartilage entropy between mild OA patients and healthy controls. Though both studies evaluate the pixel distribution of OA cartilage, the field strength, thus the contrast-to-noise, resolution and other factors are different between our study and the above-mentioned study, which makes direct comparison difficult. Perhaps, future studies could combine histogram and co-occurrence-based measurements to investigate their collective sensitivity to cartilage degeneration.

In summary, the results show that OA patients have higher and more heterogeneous cartilage T_2 values than healthy controls. Over 9 months, the standard deviation and entropy of T_2 values decreased in OA patients, which may reflect the change of heterogeneity in

cartilage structure in the evolution of OA. The T_2 quantification sequence, the number of echoes, the fitting routine, and the impact of noise are all factors, which may affect the calculation of texture parameters. While we have established the feasibility of using texture measures to quantify regional heterogeneity in cartilage T_2 , the time-course and evolution of these measures are likely to be complex; therefore, further studies examining texture analysis in a larger cohort are warranted.

6.6 References

1. Dunn TC, Lu Y, Jin H, Ries MD, Majumdar S. T_2 Relaxation Time of Cartilage at MR Imaging: Comparison with Severity of Knee Osteoarthritis. *Radiology* 2004;232(2):592-598.
2. Blumenkrantz G, Lindsey CT, Dunn TC, Jin H, Ries MD, Link TM, Steinbach LS, Majumdar S. A pilot, two-year longitudinal study of the interrelationship between trabecular bone and articular cartilage in the osteoarthritic knee. *Osteoarthritis Cartilage* 2004;12(12):997-1005.
3. Mosher TJ, Dardzinski BJ, Smith MB. Human articular cartilage: influence of aging and early symptomatic degeneration on the spatial variation of T_2 --preliminary findings at 3 T. *Radiology* 2000;214(1):259-266.
4. Nishii T, Tanaka H, Sugano N, Sakai T, Hananouchi T, Yoshikawa H. Evaluation of cartilage matrix disorders by T_2 relaxation time in patients with hip dysplasia. *Osteoarthritis Cartilage* 2007.
5. Dray N, Williams A, Prasad PV, Sharma L, Burstein D. T_2 in an OA population: Metrics for reporting data? ; 2005; Miami, FL. p 1995.
6. Haralick RM, Shanmugam K, Dinstein I. Textural Features for Image Classification. *IEEE Transactions on Systems, Man, and Cybernetics* 1973;SMC-3(6):610-618.
7. Qazi AA, Folkesson J, Pettersen PC, Karsdal MA, Christiansen C, Dam EB. Separation of healthy and early osteoarthritis by automatic quantification of cartilage homogeneity. *Osteoarthritis Cartilage* 2007.

8. Blumenkrantz G, Dunn TC, Carballido-Gamio J, Link TM, Majumdar S. Spatial Heterogeneity of Cartilage T2 in Osteoarthritic Patients. 2005; Boston, MA.
9. Kellgren J, Lawrence J. Radiologic assessment of osteoarthritis. *Ann Rheum Dis* 1957;16:494-502.
10. Peterfy CG, Guermazi A, Zaim S, Tirman PF, Miaux Y, White D, Kothari M, Lu Y, Fye K, Zhao S, Genant HK. Whole-Organ Magnetic Resonance Imaging Score (WORMS) of the knee in osteoarthritis. *Osteoarthritis Cartilage* 2004;12(3):177-190.
11. Carballido-Gamio J, Bauer J, Lee KY, Krause S, Majumdar S. Combined image processing techniques for characterization of MRI cartilage of the knee. *Conf Proc IEEE Eng Med Biol Soc* 2005;3:3043-3046.
12. Stahl R, Blumenkrantz G, Carballido-Gamio J, Zhao S, Munoz T, Hellio Le Graverand-Gastineau M-P, Li X, Majumdar S, Link TM. MRI-derived T2 relaxation times and cartilage morphometry of the tibio-femoral joint in subjects with and without osteoarthritis during a one-year follow-up. *Osteoarthritis Cartilage* 2007;in press.
13. Pai A, Blumenkrantz G, Majumdar S, Link TM, Ma CB, Li X. Assessment on Spatial heterogeneity of Cartilage T1rho and T2 in Patients with Osteoarthritis using Texture Analysis. 2006; San Diego, CA.
14. Mosher TJ, Liu Y, Yang QX, Yao J, Smith R, Dardzinski BJ, Smith MB. Age dependency of cartilage magnetic resonance imaging T2 relaxation times in asymptomatic women. *Arthritis Rheum* 2004;50(9):2820-2828.
15. Liess C, Lusse S, Karger N, Heller M, Gluer CC. Detection of changes in cartilage water content using MRI T2-mapping in vivo. *Osteoarthritis Cartilage* 2002;10(12):907-913.
16. Xia Y. Magic-angle effect in magnetic resonance imaging of articular cartilage: a review. *Invest Radiol* 2000;35(10):602-621.
17. Xia Y, Moody JB, Alhadlaq H. Orientational dependence of T2 relaxation in articular cartilage: A microscopic MRI (microMRI) study. *Magn Reson Med* 2002;48(3):460-469.
18. Smith HE, Mosher TJ, Dardzinski BJ, Collins BG, Collins CM, Yang QX, Schmithorst VJ, Smith MB. Spatial variation in cartilage T2 of the knee. *J Magn Reson Imaging* 2001;14(1):50-55.

19. Mosher TJ, Smith HE, Collins C, Liu Y, Hancy J, Dardzinski BJ, Smith MB. Change in knee cartilage T2 at MR imaging after running: a feasibility study. *Radiology* 2005;234(1):245-249.
20. Mosher TJ, Collins CM, Smith HE, Moser LE, Sivarajah RT, Dardzinski BJ, Smith MB. Effect of gender on in vivo cartilage magnetic resonance imaging T2 mapping. *J Magn Reson Imaging* 2004;19(3):323-328.
21. Adam C, Eckstein F, Milz S, Schulte E, Becker C, Putz R. The distribution of cartilage thickness in the knee-joints of old-aged individuals -- measurement by A-mode ultrasound. *Clin Biomech (Bristol, Avon)* 1998;13(1):1-10.
22. Eckstein F, Winzheimer M, Hohe J, Englmeier KH, Reiser M. Interindividual variability and correlation among morphological parameters of knee joint cartilage plates: analysis with three-dimensional MR imaging. *Osteoarthritis Cartilage* 2001;9(2):101-111.
23. Muhlbauer R, Lukasz TS, Faber TS, Stammberger T, Eckstein F. Comparison of knee joint cartilage thickness in triathletes and physically inactive volunteers based on magnetic resonance imaging and three-dimensional analysis. *Am J Sports Med* 2000;28(4):541-546.

Chapter 7: Longitudinal Changes in the Spatial Distribution of Cartilage MR T₂ in a Subset of Patients from the Osteoarthritis Initiative

7.1 Introduction

The Osteoarthritis Initiative (OAI; <http://www.oai.ucsf.edu/>) is a multi-center, longitudinal study aimed at assessing biomarkers in osteoarthritis (OA) including those derived from magnetic resonance (MR) imaging. The OAI is a cross-sectional and longitudinal dataset that includes both MRI and radiographic images of subjects scanned annually over 5 years. MR images that can be used to assess cartilage morphology and T₂ are available. This database provides a means to study and longitudinally evaluate MRI biomarkers including T₂ relaxation time, in the development and progression of OA, thus providing a wealth of information on OA development progression.

While previous studies have evaluated the longitudinal changes in cartilage T₂, their results have varied (3,8,12,13). These diverse findings highlight the heterogeneous nature of cartilage changes in the progression of OA. In order to systematically examine the pathogenesis of cartilage degeneration, a thorough evaluation of the joint structure and function is valuable. This study evaluates both the morphologic and biochemical changes in cartilage using MR imaging as well as clinical data from the OAI. The assessment of both the imaging and clinical aspects of OA facilitates a comprehensive evaluation of the disease state. The purpose of this study is to [1] examine changes in MR knee cartilage parameters including thickness, T₂, and spatial distribution of cartilage T₂ and [2] examine whether these baseline MR parameters predict change in knee pain.

7.2 Methods

7.2.1 Subjects

Thirteen subjects from the OAI with radiographic OA at baseline (mean age = 55.7±10.6 years, BMI = 30.1±3.7, Kellgren-Lawrence grade = 2-3, right knee) were evaluated. All subjects were from the progression cohort.

7.2.2 Clinical Assessment

Western Ontario and McMaster Universities (WOMAC) pain score was assessed in each patient at baseline, year 1, and year 2.

7.2.3 Magnetic Resonance Imaging

MR images of the knee joint including sagittal 3D DESSwe (TR = 16.3 ms, TE = 4.7 ms, interpolated in-plane resolution = 0.365 x 0.365 mm, slice thickness = 0.7 mm) and sagittal 2D MSME (TR = 2700 ms, TE1-TE7 = 10-70 ms) images were analyzed.

7.2.3 Image Analysis

Articular cartilage was segmented from the DESSwe images in six regions: medial and lateral tibia, medial and lateral femur, trochlea, and patella, using a spline-based, semi-automatic technique. 3D cartilage thickness was calculated from the DESSwe segmentations. The 2D MSME images were used to generate T₂ maps assuming mono-exponential signal decay (Figure 7.1).

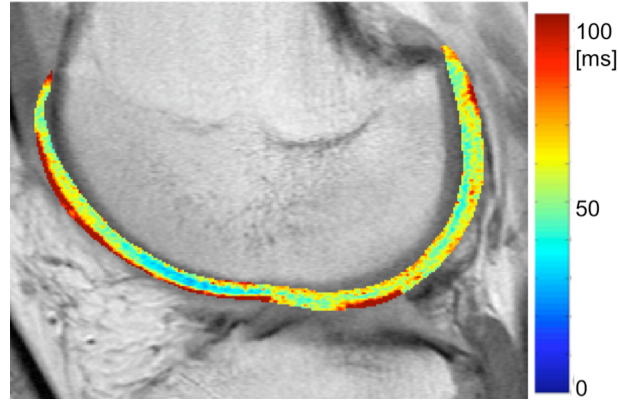


Figure 7.1: A representative T_2 map overlaid on the first echo ($TE = 10$ ms) of the MSME sequence.

Using the MSME first echo and DESSwe to compute a rigid-body transformation, T_2 maps were registered to the DESSwe images, and the segmented regions of interest were superimposed on the registered T_2 maps. Median cartilage T_2 was calculated in each region. Texture analysis, a method developed by Haralick et al. (14), was used to examine the spatial distribution of T_2 relaxation times in an image. Texture analysis supplements standard measures of cartilage T_2 (such as mean and standard deviation), by providing information on the spatial association of T_2 values. Using this method, a grey level co-occurrence matrix (GLCM), which tabulates the frequency of co-occurrence of pairs of grey-level values of adjacent pixels in an image, was defined. Texture parameters including angular second moment (ASM), entropy, homogeneity, and contrast were calculated from the GLCM. Analysis was performed using a symmetric GLCM at different orientations (0° - corresponding to the anterior-posterior axis, 45° , 90° - corresponding to the superior-inferior axis, 135°). GLCM-ASM and GLCM-entropy are measures of orderliness, while GLCM-homogeneity and GLCM-contrast are measures of contrast in an image.

7.2.4 Statistical Analysis

Statistical analysis was performed using JMP 7.0 software (SAS Institute, Cary, NC, USA). Cartilage parameters were averaged in all compartments except the lateral tibia based on their positive correlation, in order to reduce multiple testing issues. Mixed random effects approaches (treating the subject as a random effect) were used to model the annual rate-of-change in cartilage parameters and to test for an association of baseline cartilage parameters with change in WOMAC pain score over the two years of follow-up.

7.3 Results

7.3.1 Cartilage Thickness

Longitudinal decreases in mean cartilage thickness were evident in all cartilage compartments over two years. The annual rate of cartilage loss was significant ($p < 0.05$, Table 7.2) in the lateral femur (-2.66% per year), lateral tibia (-1.41% per year), and medial tibia (-3.63% per year).

Table 7.1: Annual percentage changes in cartilage thickness, calculated using data from baseline, 1-year and 2-year follow-up.

Compartment	Cartilage thickness	
	Annual % change	P value
Lateral femur	-2.66	0.007
Medial femur	-1.28	0.440
Lateral tibia	-1.41	0.049
Medial tibia	-3.63	0.009
Patella	-4.00	0.097
Trochlea	-1.71	0.442

7.3.2 Cartilage T_2

The mean cartilage T_2 showed little change over time, with exception of the lateral tibia, which decreased -4.00% annually ($p < 0.05$).

7.3.3 Texture Analysis of Cartilage T_2

Texture analysis of cartilage T_2 using GLCM showed longitudinal increases in mean contrast and entropy, and decreases in mean ASM and homogeneity. Entropy of cartilage T_2 at baseline (all compartments combined except the lateral tibia) was associated with an increase in WOMAC pain score over 2 years ($p < 0.05$). Figure 7.2 shows the fitted model of the effect of baseline entropy on WOMAC pain score over 2 years in three cases: average baseline entropy, above-average baseline entropy, and below-average baseline entropy. The model illustrates that patients with high entropy at baseline have a greater longitudinal rate-of-change in WOMAC pain score.

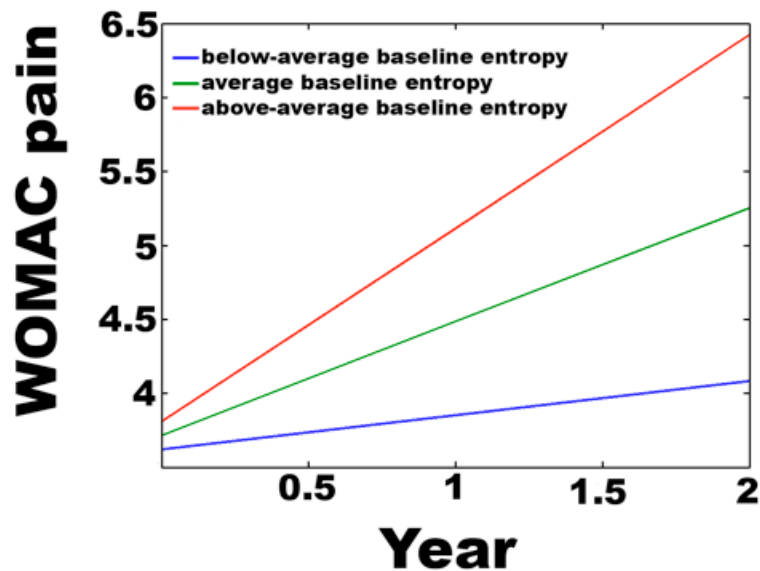


Figure 7.2: A model illustrating the effect of baseline entropy of cartilage T_2 on changes in WOMAC pain over time.

7.4 Discussion and Conclusion

In this study, OA patients from the progression cohort of the OAI exhibited a significant decrease in cartilage thickness over two years, demonstrating morphologic OA progression over time. Of all MR parameters evaluated (including cartilage thickness and mean T_2), only the baseline entropy of cartilage T_2 was significantly associated with longitudinal rate-of-change in pain.

The results of this pilot study suggest that the cascade of events leading to pain in OA may encompass changes in the internal structure and organization of cartilage, as measured by the entropy of cartilage T_2 . Further long-term studies investigating the relationship between spatial distribution of cartilage T_2 and the onset of OA in the incidence cohort, are underway

7.5 References

1. NIAMS Osteoarthritis Handout on Health; 2006.
2. Dijkgraaf LC, de Bont LG, Boering G, Liem RS. The structure, biochemistry, and metabolism of osteoarthritic cartilage: a review of the literature. *J Oral Maxillofac Surg* 1995;53(10):1182-1192.
3. Blumenkrantz G, Lindsey CT, Dunn TC, Jin H, Ries MD, Link TM, Steinbach LS, Majumdar S. A pilot, two-year longitudinal study of the interrelationship between trabecular bone and articular cartilage in the osteoarthritic knee. *Osteoarthritis Cartilage* 2004;12(12):997-1005.
4. Dardzinski BJ, Mosher TJ, Li S, Van Slyke MA, Smith MB. Spatial variation of T_2 in human articular cartilage. *Radiology* 1997;205(2):546-550.

5. Dray N, Williams A, Prasad PV, Sharma L, Burstein D. T2 in an OA population: Metrics for reporting data? ; 2005; Miami, FL. p 1995.
6. Dardzinski BJ, Laor T, Schmithorst VJ, Klosterman L, Graham TB. Mapping T2 relaxation time in the pediatric knee: feasibility with a clinical 1.5-T MR imaging system. *Radiology* 2002;225(1):233-239.
7. Dunn TC, Lu Y, Jin H, Ries MD, Majumdar S. T2 Relaxation Time of Cartilage at MR Imaging: Comparison with Severity of Knee Osteoarthritis. *Radiology* 2004;232(2):592-598.
8. Blumenkrantz G, Stahl R, Carballido-Gamio J, Zhao S, Lu Y, Munoz T, Hellio Le Graverand-Gastineau MP, Jain SK, Link TM, Majumdar S. The feasibility of characterizing the spatial distribution of cartilage T(2) using texture analysis. *Osteoarthritis Cartilage* 2008;16(5):584-590.
9. Li X, Pai A, Blumenkrantz G, Carballido-Gamio J, Link T, Ma B, Ries M, Majumdar S. Spatial distribution and relationship of T1rho and T2 relaxation times in knee cartilage with osteoarthritis. *Magn Reson Med* 2009;61(6):1310-1318.
10. Carballido-Gamio J, Stahl R, Gabrielle B, Adan R, Sharmila M. Spatial Analysis of Magnetic Resonance T1rho and T2 Relaxation Times Improves Classification Between Subjects With and Without Osteoarthritis. . *Med Phys* 2009;in press.
11. Carballido-Gamio J, Gabrielle B, John L, Link TM, Sharmila M. Longitudinal Analysis of MRI T2 Knee Cartilage Lamellar Organization in a Subset of Patients from the Osteoarthritis Initiative. *Magn Reson Med* 2009;in press.
12. Stahl R, Blumenkrantz G, Carballido-Gamio J, Zhao S, Munoz T, Hellio Le Graverand-Gastineau MP, Li X, Majumdar S, Link TM. MRI-derived T2 relaxation times and cartilage morphometry of the tibio-femoral joint in subjects with and without osteoarthritis during a 1-year follow-up. *Osteoarthritis Cartilage* 2007;15(11):1225-1234.
13. Welsch GH, Mamisch TC, Marlovits S, Glaser C, Friedrich K, Hennig FF, Salomonowitz E, Trattnig S. Quantitative T2 mapping during follow-up after matrix-associated autologous chondrocyte transplantation (MACT): Full-thickness and zonal evaluation to visualize the maturation of cartilage repair tissue. *J Orthop Res* 2009.

14. Haralick RM, Shanmugam K, Dinstein I. Textural Features for Image Classification. IEEE Transactions on Systems, Man, and Cybernetics 1973;SMC-3(6):610-618.

Chapter 8: A Feasibility Study of In Vivo Magnetic Resonance T_{1ρ} Imaging of the Intervertebral Disc

8.1 Introduction

Low back pain is the most frequent cause of activity limitation for people under the age of 45 years in the United States (1). Low back pain is frequently associated with degenerative disc disease (DDD), which is characterized by biochemical and morphological changes in the intervertebral disc (2–4). The intervertebral disc is composed of three regions: (a) the nucleus pulposus; (b) the annulus fibrosus; and (c) cartilaginous end plates. The nucleus pulposus is a hydrated proteoglycan gel located in the center of the disc. It contains approximately 25% (dry weight) collagen and 50% (dry weight) proteoglycan (5). The negatively charged proteoglycans in the nucleus are responsible for an internal swelling pressure, which provides compressive stiffness to the disc. The annulus is composed of 15–25 concentric lamellae (6) and is located on the periphery of the disc. It contains 67% (dry weight) collagen (5) and a low concentration of proteoglycans (7). The collagen in the annulus resists the swelling pressure from the nucleus and provides tensile and shear strength. The end plates separate the disc from the bordering vertebral bone.

The process of disc degeneration is characterized by a loss of cellularity, degradation of the extracellular matrix (ECM) and, as a result, morphological changes and alterations in biomechanical properties. The most consistent chemical changes observed with aging are loss of proteoglycans and concomitant loss of water and disc pressure (8). Secondary changes due to redistribution of tissue stress include fibrocartilage production with disorganization of the annular architecture and increases in type II collagen (9). Together, degeneration-associated changes in the nucleus and the annulus are fundamental to the development of a

number of spinal pathologies. For instance, changes in proteoglycan content within the nucleus lead to reduced imbibition of water, depressurization and flattening of the disc. The annulus may then bulge into the spinal canal and neural foramen. Disc height loss also results in narrowing of the spinal canal and unfolding of the ligamentum flavum, contributing directly to the development of spinal stenosis (which may result in constriction of spinal nerves or spinal cord). Herniation of the intervertebral disc leading to disc protrusion and extrusion can occur as a result of mechanical annular disruption and fissuring due to chronic nonphysiologic stress secondary to nuclear dehydration.

Various techniques have been proposed to assess the competence of the disc in vivo with particular emphasis on developing objective surgical indications. Radiographs are the first line of investigation in vertebral spine trauma but are of limited value in assessing suspected lumbar prolapsed intervertebral disc disease. While pain provocation using discography/CT discography (10–12) has been shown to improve the odds of a positive surgical outcome, there has been a reported high incidence of false positives (13) and there remains a significant number of severely degenerated discs that have been found to be asymptomatic (14).

Magnetic resonance imaging (MRI) has also been used as a noninvasive measure of disc degeneration visualizing early as well as more advanced changes. MRI allows the delineation of the annulus from the nucleus with high spatial resolution. Pfirrmann et al. (15) proposed a grading system for disc degeneration based on standard spin-echo sequences. With T₂-weighted spin-echo imaging sequences, healthy intervertebral discs show a bright signal from the nucleus pulposus and a low signal from the annulus fibrosus. Disc degeneration is demonstrated by a change in the signal of the nucleus pulposus to give an

irregular outline and a reduction in signal intensity. However, disc degeneration detected using MRI may not be associated with low back pain (16). In the intervertebral disc, the uptake of Gd-DTPA enhancement has been observed clinically often in normal-appearing discs (17), and there is a high prevalence of disc degeneration in asymptomatic populations (18). Stabler et al. (19) showed that a band-like contrast enhancement of the disc correlated with vascularization, often seen as a consequence of annular tears, and corresponded to pain, even in the absence of stenosis. Thus, the relationship between disc degeneration, MRI, and low back pain remains undefined.

In an effort to improve the capability of MR techniques to quantitatively assess disc degeneration, surrogate MR measures of tissue hydration, such as relaxation times (T_1 and T_2) and water diffusivity, are being studied. Investigators have demonstrated differences in T_1 between mechanically loaded and unloaded disc specimens (20) as well as correlations between $1/T_2$ and both water and collagen content for disc specimens (7). Since proteoglycan loss is an initiating factor of DDD, an in vivo imaging technique that reflects proteoglycan content would be ideal for the early detection of DDD. Quantitative $T_{1\rho}$ imaging probes the interaction between motionally restricted water molecules and their macromolecular environment; thus, the ECM in the intervertebral disc may potentially be investigated using these techniques. Previous studies have quantified $T_{1\rho}$ relaxation time in cartilage (21–26) as well as in intervertebral disc specimens in vitro (27–30) and have demonstrated a relationship between $T_{1\rho}$ relaxation and proteoglycan content (25,31). The purpose of this study was to test the feasibility of quantifying $T_{1\rho}$ relaxation time in phantoms and intervertebral discs of healthy volunteers using in vivo MR imaging at 3 T.

8.2. Materials and Methods

8.2.1 Phantom Design

To examine the performance of the $T_{1\rho}$ pulse sequence, three phantoms with varying concentrations of agarose gel (50 ml; 1%, 2% and 4%; weight/volume) were constructed. Agarose (Sigma Aldrich, St. Louis, MO, USA) was chosen because it is known to exhibit decreasing $T_{1\rho}$ relaxation time with increasing agarose concentration, as well as $T_{1\rho}$ relaxation times similar to those of biologic tissues [32].

8.2.2 Human Subjects

Eleven healthy volunteers (mean age=31.3 years; age range=23–60 years; gender: 5 females, 6 males) participated in the study. Among them, 3 volunteers were scanned twice to examine in vivo reproducibility. They were scanned once, allowed to leave the examination table, repositioned and scanned again. This study was approved by the Committee on Human Research, and all subjects provided informed consent.

8.2.3. Magnetic Resonance Imaging

The phantoms and volunteers were scanned using a GE SIGNA 3 T echo-speed system (GE Healthcare, Waukesha, WI, USA) and phased array spine coil. After a three-plane localizer, axial $T_{1\rho}$ -weighted images were acquired using a multislice spiral sequence [21]. The $T_{1\rho}$ imaging sequence is shown in Figure 8.1. It consists of $T_{1\rho}$ pre-encoding followed by spiral acquisition (bandwidth=100 kHz; interleaves=14/ slice; data points=4096/interleaf; spin lock (SL) frequency=300 Hz; TSL1/TSL2/TSL3/TSL4=20/50/80/110 ms). The decay during the SL period is due to transverse relaxation at a rate of $1/T_{1\rho}$. A crusher gradient dephases any residual transverse

magnetization. To eliminate T1 effects, an RF cycling technique was implemented [21,33]. The parameters for image acquisition were as 5.8/2000 ms and flip angle=90 degrees. The field of view (FOV) was 20 cm, and the slice thickness was 3 mm. The total scan time was 13 minutes. Additionally, axial T₂-weighted images (TE/TR=85/5200 ms; FOV=20 cm; slice thickness=3 mm; bandwidth=35.7 kHz; matrix=288 x 224; scan time ~5 min) were acquired.

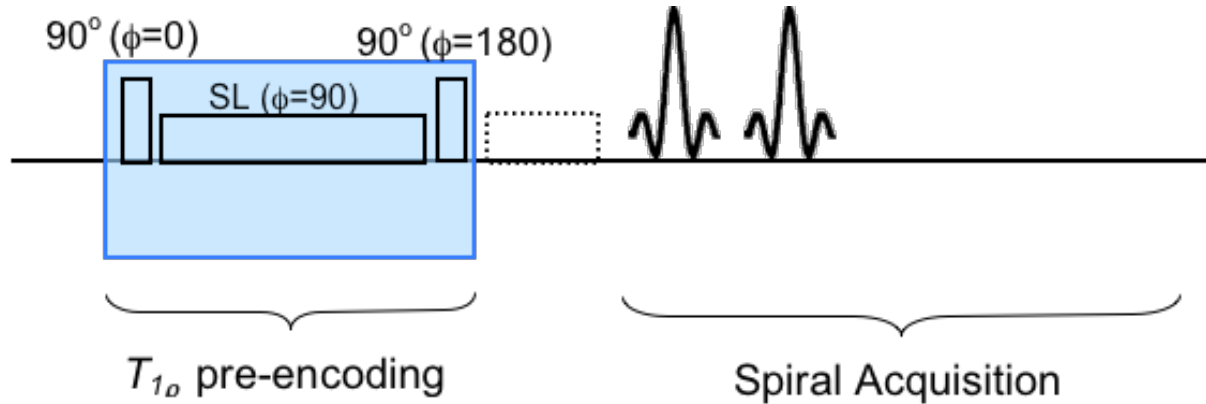


Figure 8.1:Diagram of T_{1ρ} imaging sequence.

8.2.4. Image Analysis

All images were processed using a Sun Workstation (Sun Microsystems, Palo Alto, CA, USA). T_{1ρ} maps were computed on a pixel-by-pixel basis using the following equation:

$$S(TSL) \propto \exp(-TSL/T_{1\rho}) \quad [8.1]$$

The signal to noise ratio (SNR) was calculated from T_{1ρ}-weighted images using the following equation:

$$SNR = \text{mean signal}/\text{standard deviation of background noise} \quad [8.2]$$

The nucleus pulposus and annulus fibrosus of the intervertebral disc were segmented from the T₂-weighted high-resolution images using a threshold-based method. The outside of the annulus was manually segmented from the T₂-weighted high-resolution image. Then, a histogram of the segmented region was generated, and a threshold, defined as the average intensity between the nucleus and annulus peaks, was identified. Lastly, the nucleus was

segmented using the chosen threshold, and the segmented region of interest (ROI) was superimposed on the $T_{1\rho}$ map (Figure 8.2).

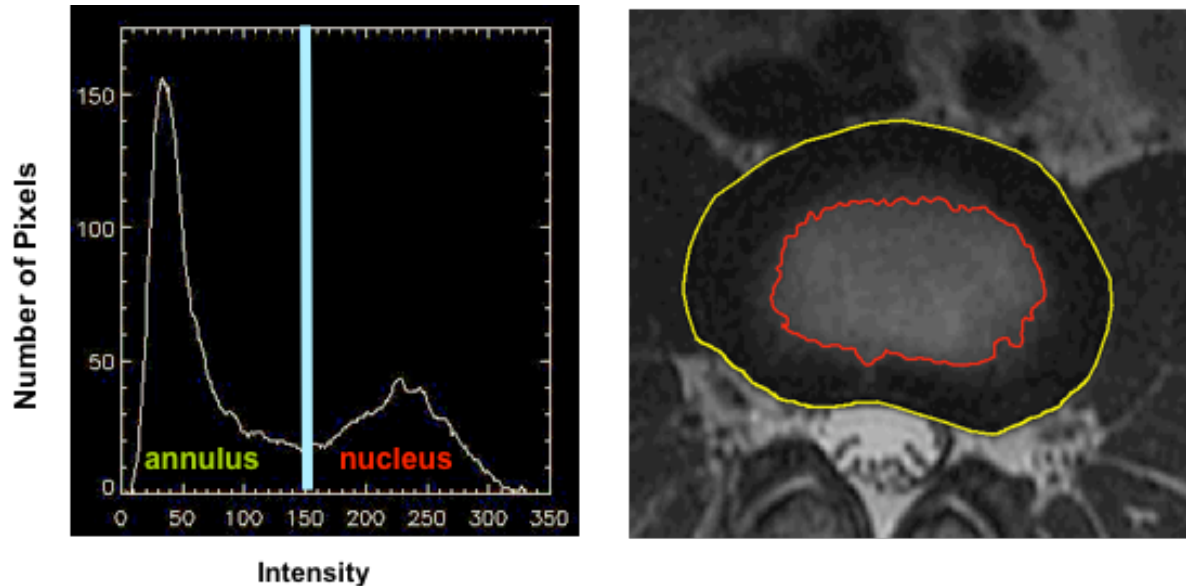


Figure 8.2: a, left) A histogram of the nucleus and annulus **b, right)** representation of the segmented nucleus (inner circle) and annulus (outer circle).

8.2.5. Reproducibility

The reproducibility of $T_{1\rho}$ quantification was examined by performing three experiments, two in vitro and one in vivo. First, axial $T_{1\rho}$ -weighted images of an agarose phantom were obtained to investigate SNR and $T_{1\rho}$ relative to the distance from the coil. Line profiles of the SNR and $T_{1\rho}$ from the base (closest to coil) to the apex (farthest from coil) of the phantom were examined to determine the effects of SNR on $T_{1\rho}$ quantification. Second, $T_{1\rho}$ quantification as a function of position along the coil was examined. Each phantom was scanned six times and was repositioned between scans: twice at the isocenter, twice at 3 cm superior to the isocenter and twice at 3 cm inferior to the isocenter (Figure. 8.3). Third, four volunteers were each scanned twice, and three discs from each volunteer were evaluated to

determine in vivo reproducibility.

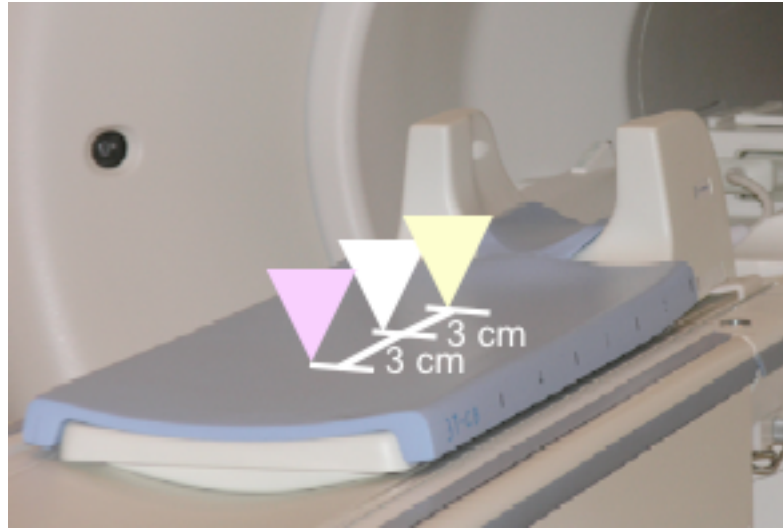


Figure 8.3: Three phantoms with different agarose concentrations, scanned at three different positions along the coil.

8.2.6. Statistical Analysis

Reproducibility was assessed using the coefficient of variation was defined using the following equation:

$$CV = \text{standard deviation of } T_{1\rho} / \text{average } T_{1\rho} \quad [8.3]$$

The median $T_{1\rho}$ values of the nucleus and the annulus of the intervertebral discs L3-L4, L4-L5 and L5-S1 were calculated for each subject. Statistical analysis was performed using JMP software (SAS institute, Cary, NC). A one-way analysis of variance (ANOVA) was employed to compare $T_{1\rho}$ values of different regions (nucleus and annulus) and disc levels. Pearson correlations were calculated to determine the relationship between age and $T_{1\rho}$ values in the nucleus and the annulus.

8.3. Results

8.3.1. Phantom

The median $T_{1\rho}$ values of the 1%, 2% and 4% agarose phantoms were 140.6, 83.8 and 56.0 ms, respectively. Figure 8.4 illustrates line profiles of SNR and $T_{1\rho}$ in a phantom as a function of distance from the coil. The SNR decreases by approximately 50% from 6 to 10 cm from the surface of the coil. This range corresponds to the approximate position of the intervertebral disc during axial imaging. However, the $T_{1\rho}$ values are within 1 S.D. of the median $T_{1\rho}$ value of the phantom. The phantom reproducibility data are shown in Table 8.1. The CV of each phantom, scanned twice at the isocenter, twice at 3 cm superior to the isocenter and twice at 3 cm inferior to the isocenter, was less than 3%.

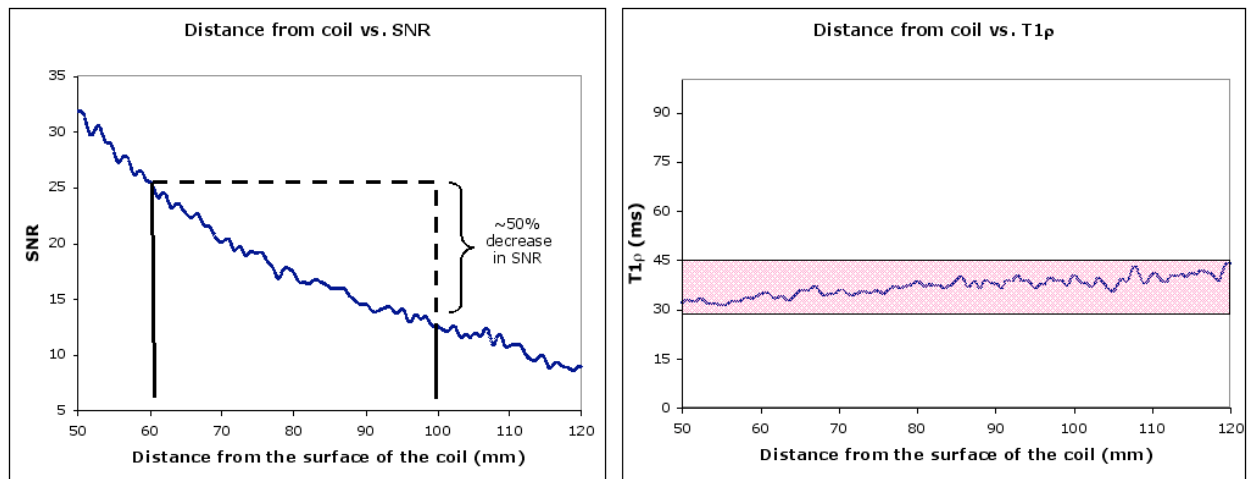


Figure 8.4: a, left) SNR in a phantom as a function of distance from the surface of the coil. The range of 60-100 mm represents the approximate position of the intervertebral disc. **b, right)** $T_{1\rho}$ in a phantom as a function of distance away from the coil. The shaded region represents the median $T_{1\rho} \pm$ standard deviation. The $T_{1\rho}$ values are within one standard deviation of the median $T_{1\rho}$ value of the phantom

Table 8.1: The coefficient of variation for three phantoms with different agarose concentrations scanned twice at isocenter, twice at 3 cm superior to isocenter, and twice at 3 cm inferior to isocenter (illustrated in Figure 8.3).

	Agarose Concentration (%)	Median $T_{1\rho}$ (ms)	CV(%)
Phantom A	4	52.5	2.97
Phantom B	2	83.8	2.04
Phantom C	1	140.6	1.63

8.3.2. In Vivo

A representative colormap that illustrates the spatial variation of the $T_{1\rho}$ values in the intervertebral disc is shown in Figure 8.5. A wide range of $T_{1\rho}$ values is evident in both the nucleus and the annulus, demonstrating the heterogeneity of $T_{1\rho}$ values in the disc.

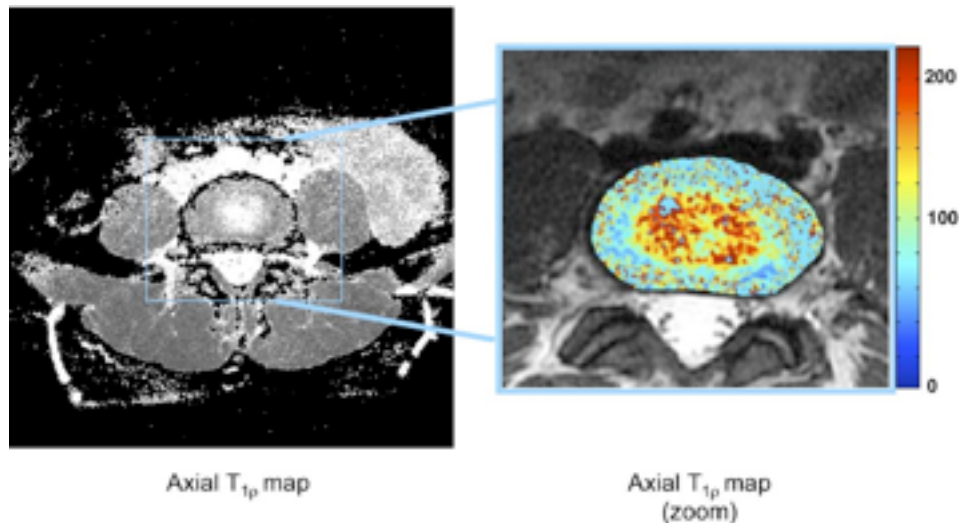


Figure 8.5. Axial $T_{1\rho}$ map and axial $T_{1\rho}$ color map of the intervertebral disc.

The coefficient of variation for *in vivo* reproducibility was 4.59%. This calculation

does not include the $T_{1\rho}$ values from the scans with obvious partial volume effects, in locations where the disc is not parallel to the axial imaging plane due to spinal curvature and positioning. The median $T_{1\rho}$ value was 116.6 ± 21.4 ms for the nucleus and 84.1 ± 11.7 ms for the annulus (Figure 8.6). The Student's t-tests showed that the median $T_{1\rho}$ value of the nucleus and annulus was significantly different ($p < 0.05$). The median $T_{1\rho}$ value for different discs are shown in Table 8.2.

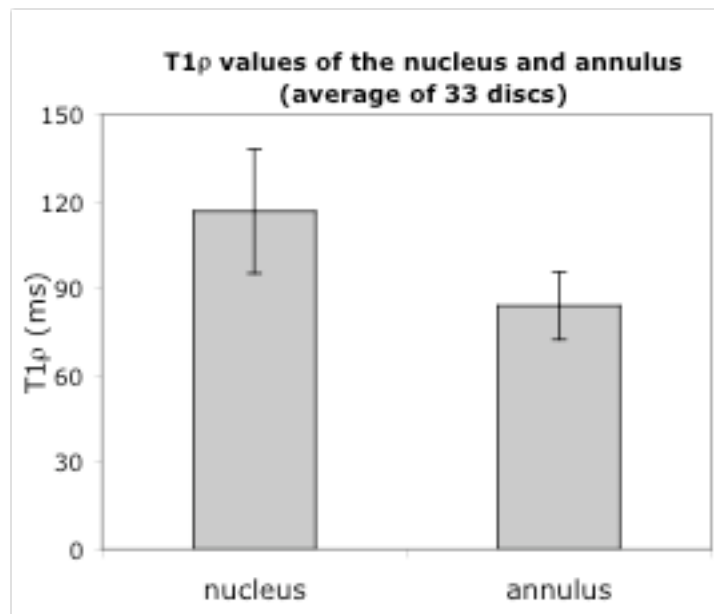


Figure 8.6: $T_{1\rho}$ values of the nucleus and annulus ($n = 11$, 33 discs, 3 from each subject). The error bar represents the standard deviation.

Table 8.2: Median $T_{1\rho}$ values in the nucleus and annulus of different discs. The standard deviation is in parentheses.

Disc	$T_{1\rho}$ (ms) nucleus	$T_{1\rho}$ (ms) annulus
S1/L5	110.4 (27.2)	74.3 (9.8)
L5/L4	115.2 (19.3)	84.6 (10.6)
L4/L3	123.1 (17.7)	91.6 (8.6)

A trend of decreasing $T_{1\rho}$ values from L3-L4 to L4-L5 to L5-S1 was evident. Pairwise comparisons with adjustment for multiple comparisons revealed a significant difference between the median $T_{1\rho}$ values of the annulus between discs L3-L4 and L5-S1, and L4-L5 and L5-S1. There was no significant difference in the median $T_{1\rho}$ value of the annulus between discs L4-L5 and L3-L4. No significant differences were evident between the median $T_{1\rho}$ value of the nucleus in different discs. The correlations between age and $T_{1\rho}$ relaxation time in the nucleus ($r^2=-0.82$, $p= 0.0001$) and annulus ($r^2=-0.37$, $p= 0.04$) were significant, however, the correlation in the annulus was lower than the correlation in the nucleus. Ten of the subjects that participated in this study ranged in age from 23-35 years and the eleventh subject was 60 years old. The median $T_{1\rho}$ value of the 60 year old subject ($T_{1\rho,\text{nucleus}} = 75.3$ ms, $T_{1\rho,\text{annulus}} = 72.3$ ms) was lower than the median $T_{1\rho}$ value of the younger subjects ($T_{1\rho,\text{nucleus}} = 123.2 \pm 17.3$ ms, $T_{1\rho,\text{annulus}} = 85.3 \pm 11.4$ ms). The correlation between age and $T_{1\rho}$ relaxation time in the nucleus of the younger subjects was lower than the correlation that included all the subjects, but still highly significant ($r^2=-0.62$, $p= 0.0037$). The correlation between age and $T_{1\rho}$ relaxation time in the annulus of the younger subjects was also lower than the correlation that includes all the subjects, however, it was insignificant ($r^2=-0.12$, $p= 0.323$).

8.4 Discussion and Conclusion

In this study, a $T_{1\rho}$ spiral sequence was used to quantify $T_{1\rho}$ relaxation time in the intervertebral disc of healthy volunteers. This study demonstrates the feasibility of using spiral imaging at 3T for *in vivo* $T_{1\rho}$ quantification of the intervertebral disc. The results indicate that median $T_{1\rho}$ value of the nucleus is greater than that of the annulus, which is consistent with the results from a recent *in vitro* study by Regatte et al (28). The results also

show highly significant correlations of $T_{1\rho}$ and age of the volunteers and a trend for decreasing $T_{1\rho}$ from L3/4 to L5/S1.

Based on $T_{1\rho}$ quantification in phantoms with different agarose concentrations, the $T_{1\rho}$ value decreases as agarose concentration increases. These results are consistent with other studies²¹. The phantom reproducibility results demonstrate that $T_{1\rho}$ values are consistent along the length of the coil, and that the accuracy of $T_{1\rho}$ quantification is not affected by distance along the coil. Despite the decrease in SNR with distance away from the coil, the $T_{1\rho}$ values in the phantom are within one standard deviation of the median $T_{1\rho}$ value of the phantom. Therefore, the accuracy of $T_{1\rho}$ quantification is minimally affected by changes in SNR.

The *in vivo* reproducibility results illustrate the feasibility of quantifying $T_{1\rho}$ in the intervertebral disc. In this study, the median $T_{1\rho}$ value of the nucleus was greater than that of the annulus. These results may be due to the differences in biochemical composition of the two regions: the nucleus has a greater concentration of proteoglycans, a lower concentration of collagen, and is more hydrated than the annulus. Moreover, the nucleus and annulus differ structurally in that the nucleus is composed of a hydrated gel, while the annulus is composed of concentric collagen lamellae. These contributing factors as well as macromolecular orientation²⁶, mechanical loading, and diffusion need to be further studied to fully assess the sensitivity of $T_{1\rho}$ relaxation in the intervertebral disc.

Assessment of $T_{1\rho}$ relaxation time may serve as a non-invasive marker of early degenerative changes in the intervertebral disc. A study by Johannessen et al.n (29) showed a strong correlation between $T_{1\rho}$ and GAG content ($r = 0.7$, $p < 0.01$), and a moderate correlation between T_2 and GAG content ($r = 0.5$, $p < 0.05$) in lumbar intervertebral disc

specimens. Furthermore, T_2 was significantly correlated to collagen, however it was not correlated to proteoglycan content in the intervertebral disc⁷. These studies demonstrate that $T_{1\rho}$ quantification may provide specific information regarding GAG content in the intervertebral disc. As proteoglycan loss is a marker of early disc degeneration, $T_{1\rho}$ may be useful in characterizing early biochemical changes in the disc. $T_{1\rho}$ relaxation time has also been quantified in osteoarthritic (OA) cartilage. Li et al. showed that OA patients had significantly greater $T_{1\rho}$ (but not T_2) than controls (21), and Regatte et al. reported that $T_{1\rho}$ has a higher dynamic range than T_2 (27,28). These studies demonstrate the potential of using $T_{1\rho}$ quantification to detect early biochemical changes in diseased tissue, and show that $T_{1\rho}$ may provide complementary information to T_2 in identifying early degenerative changes.

A negative relationship between age and $T_{1\rho}$ relaxation time was observed in this study. The median $T_{1\rho}$ value in the nucleus and the annulus of the older subject (60 years) was lower than the median $T_{1\rho}$ values in the younger subjects (23-35 years). Previous studies have reported various age-related changes in the intervertebral disc including decreased disc volume³⁴, dehydration, and decreased proteoglycan content (35). These compositional changes may be reflected in a decrease of $T_{1\rho}$ values with age. However, the relationship between the age-related biochemical changes and $T_{1\rho}$ relaxation time must be further investigated. In this study, a significant relationship between age and $T_{1\rho}$ was found in a small sample size of which a majority of the subjects ranged in age from 23-35 years. The results suggest that $T_{1\rho}$ may depict age-related changes in asymptomatic subjects.

A trend of decreasing $T_{1\rho}$ values from L3-L4 to L4-L5 to L5-S1 was evident, and the difference in the median $T_{1\rho}$ values of the annulus between L5-S1 and L4-L5, and L5-S1 and L3-L4 was significant. However, the median $T_{1\rho}$ value in the L4-L5 and L3-L4 discs was not

significantly different. These results may be influenced by the fact that the L5-S1 disc withstands greater mechanical stresses than the L3-L4 and L4-L5 discs (36). Mechanical signals may affect matrix synthesis and may potentially influence the turnover of the ECM (37). Thus, we speculate that the differences in $T_{1\rho}$ values between L5-S1 and both the L3-L4 and L4-L5 discs may be due to greater mechanical stresses in the L5-S1 disc. A limitation of this study, however, includes partial volume effects evident in some of the axial scans (especially in disc L5-S1) due to lumbar spine curvature. The imaging protocol used in the study was limited to axial acquisition because spiral acquisition precludes the use of an anti-aliasing filter, which would be necessary in both coronal and sagittal imaging. In future studies, sagittal acquisition will be used to minimize the effects of spine curvature and partial volume effects on $T_{1\rho}$ quantification.

The results of this study suggest that *in vivo* $T_{1\rho}$ quantification is feasible, shows age-related changes in the intervertebral disc, and may potentially be a clinical tool to identify early degenerative changes in the intervertebral disc. In the clinical setting, this technique may be useful to monitor both the progression of the disease and the efficacy of drug treatment. In the future, studies will be conducted to determine if $T_{1\rho}$ quantification can be used to differentiate patients with low back pain from healthy controls.

8.5 References

1. Kent PM, Keating JL. The epidemiology of low back pain in primary care. *Chiropr Osteopat* 2005;13:13.
2. van Blitterswijk WJ, van de Nes JC, Wuisman PI. Glucosamine and chondroitin sulfate supplementation to treat symptomatic disc degeneration: biochemical rationale and case report. *BMC Complement Altern Med* 2003;3:2.
3. Cohen SP, Larkin TM, Barna SA, Palmer WE, Hecht AC, Stojanovic MP. Lumbar

discography: a comprehensive review of outcome studies, diagnostic accuracy, and principles. *Reg Anesth Pain Med* 2005;30(2):163-83.

4. Martin MD, Boxell CM, Malone DG. Pathophysiology of lumbar disc degeneration: a review of the literature. *Neurosurg Focus* 2002;13(2):E1.

5. Cassinelli EH, Hall RA, Kang JD. Biochemistry of intervertebral disc degeneration and the potential for gene therapy applications. *Spine J* 2001;1(3):205-14.

6. Urban JP, Roberts S. Degeneration of the intervertebral disc. *Arthritis Res Ther* 2003;5(3):120-30.

7. Weidenbaum M, Foster RJ, Best BA, Saed-Nejad F, Nickoloff E, Newhouse J, Ratcliffe A, Mow VC. Correlating magnetic resonance imaging with the biochemical content of the normal human intervertebral disc. *J Orthop Res* 1992;10:552-561.

8. Pearce RH, Grimmer BJ, Adams ME. Degeneration and the chemical composition of the human lumbar intervertebral disc. *J Orthop Res* 1987;5:198-205.

9. Rufai A, Benjamin M, Ralphs JR. The development of fibrocartilage in the rat intervertebral disc. *Anat Embryol (Berl)* 1995;192(1):53-62.

10. Colhoun E, McCall IW, Williams L, Cassar Pullicino VN. Provocation discography as a guide to planning operations on the spine. *J Bone Joint Surg Br* 1988;70(2):267-71.

11. Patrick BS. Lumbar discography: a five year study. *Surg Neurol* 1973;1(5):267-73.

12. Simmons EH, Segil CM. An evaluation of discography in the localization of symptomatic levels in discogenic disease of the spine. *Clin Orthop Relat Res* 1975(108):57-69.

13. Walsh TR, Weinstein JN, Spratt KF, Lehmann TR, Aprill C, Sayre H. Lumbar discography in normal subjects. A controlled, prospective study. *J Bone Joint Surg Am* 1990;72(7):1081-8.

14. Wiesel SW, Tsourmas N, Feffer H. Study of computer-assisted tomography: I. The incidence of positive CAT scans in an asymptomatic group of patients. *Spine* 1984;9(6):549-556.

15. Pfirrmann CW, Metzdorf A, Zanetti M, Hodler J, Boos N. Magnetic resonance classification of lumbar intervertebral disc degeneration. *Spine* 2001;26(17):1873-8.

16. Beattie P. The relationship between symptoms and abnormal magnetic resonance images of lumbar intervertebral disks. *Phys Ther* 1996;76(6):601-8.

17. Hwang GJ, Suh JS, Na JB, Lee HM, Kim NH. Contrast enhancement pattern and frequency of previously unoperated lumbar discs on MRI. *Jour Magn Res Imag* 1997;7:575-578.
18. Jensen MC, Brant-Zawadzki MN, Obuchowski N, Modic MT, Malkasian D, Ross JS. Magnetic resonance imaging of the lumbar spine in people without back pain [see comments]. *N Engl J Med* 1994;331(2):69-73.
19. Stabler A, Krimmel K, Seiderer M, Gartner C, Fritsch S, Raum W. [The nuclear magnetic resonance tomographic differentiation of osteoporotic and tumor-related vertebral fractures. The value of subtractive TR gradient-echo sequences, STIR sequences and Gd-DTPA]. *Rofo Fortschr Geb Rontgenstr Neuen Bildgeb Verfahr* 1992;157(3):215-21.
20. Chiu EJ, Newitt DC, Hu SS, Lotz JC, Majumdar S. MRI measurement of water diffusion in the human intervertebral disc with compression. 1997; San Francisco, CA. Orthopaedic Research Society. p 123.
21. Li X, Han ET, Ma CB, Link TM, Newitt DC, Majumdar S. In vivo 3T spiral imaging based multi-slice T(1rho) mapping of knee cartilage in osteoarthritis. *Magn Reson Med* 2005;54(4):929-36.
22. Akella SV, Regatte RR, Gougoutas AJ, Borthakur A, Shapiro EM, Kneeland JB, Leigh JS, Reddy R. Proteoglycan-induced changes in T1rho-relaxation of articular cartilage at 4T. *Magn Reson Med* 2001;46(3):419-23.
23. Regatte RR, Akella SV, Wheaton AJ, Lech G, Borthakur A, Kneeland JB, Reddy R. 3D-T1rho-relaxation mapping of articular cartilage: in vivo assessment of early degenerative changes in symptomatic osteoarthritic subjects. *Acad Radiol* 2004;11(7):741-9.
24. Regatte RR, Akella SV, Borthakur A, Kneeland JB, Reddy R. In vivo proton MR three-dimensional T1rho mapping of human articular cartilage: initial experience. *Radiology* 2003;229(1):269-74.
25. Regatte RR, Akella SV, Borthakur A, Kneeland JB, Reddy R. Proteoglycan depletion-induced changes in transverse relaxation maps of cartilage: comparison of T2 and T1rho. *Acad Radiol* 2002;9(12):1388-94.
26. Menezes NM, Gray ML, Hartke JR, Burstein D. T2 and T1rho MRI in articular cartilage systems. *Magn Reson Med* 2004;51(3):503-9.
27. Regatte R, Akella S, Dodge G, Reddy R. Spin-Lock (t1rho) MRI of the sand rat: a

new approach to study this model of disc degeneration. 2004; Canada.

28. Regatte R, Akella S, Borthakur A, Reddy R. High Resolution T1rho Relaxation and Dispersion Imaging of Intervertebral Disc. 2004.

29. Johannessen W, Auerbach JD, Wheaton AJ, Kurji A, Reddy R, Borthakur A, Elliott DM. Non-Invasive Determination of Nucleus Pulposus Proteoglycan Content Using T1rho MRI. 2005; Switzerland.

30. Keshari K, Blumenkrantz G, Li X, Majumdar S. *T1rho-weighted imaging to characterize intervertebral disc degeneration*. ISMRM 2005; Miami.

31. Wheaton AJ, Dodge GR, Elliott DM, Nicoll SB, Reddy R. Quantification of cartilage biomechanical and biochemical properties via T1rho magnetic resonance imaging. *Magn Reson Med* 2005;54(5):1087-93.

32. Nugent AC, Johnson GA. T1rho imaging using magnetization-prepared projection encoding (MaPPE). *Magn Reson Med* 2000;43(3):421-8.

33. Wright GA, Brittain JH, Stainsby JA. Preserving T1 or T2 contrast in magnetization preparation sequences. 1996; New York. p 1474.

34. Anderson DG, Tannoury C. Molecular pathogenic factors in symptomatic disc degeneration. *Spine J* 2005;5(6 Suppl):260S-266S.

35. Roughley PJ. Biology of intervertebral disc aging and degeneration: involvement of the extracellular matrix. *Spine* 2004;29(23):2691-9.

36. Ong A, Anderson J, Roche J. A pilot study of the prevalence of lumbar disc degeneration in elite athletes with lower back pain at the Sydney 2000 Olympic Games. *Br J Sports Med* 2003;37(3):263-6.

37. Urban JPG, Roberts S, Ralphs JR. *The Nucleus of the Intervertebral Disc from Development to Degeneration*. 1999; Denver, CO.

Chapter 9: In Vivo 3.0 Tesla Magnetic Resonance $T_{1\rho}$ and T_2 Relaxation Mapping in Subjects with Intervertebral Disc Degeneration and Clinical Symptoms

9.1 Introduction

It is difficult to compare the clinical symptoms experienced by various individuals with IVDD, since pain and physical ability are subjective by nature with varying tolerances and expectations between individuals. A number of questionnaires, including the SF-36 Health Survey (1) and Oswestry Disability Index (O.D.I) (2), aim to quantify the severity of physical limitation and disability, thus providing a standardized and comparable measure of clinical symptoms. These questionnaires have been shown to provide reliable quantitative scoring systems in previous studies (3,4). The SF-36 and O.D.I questionnaires have been widely used in patient studies, and their reliability and the validity have been studied extensively (3,4).

Despite the high prevalence of IVDD worldwide, diagnosis in the early stages of symptomatic disease is elusive in clinical practice. The traditional methods for imaging disc degeneration, including radiography, magnetic resonance imaging (MRI), and computed tomography (CT), are limited to depicting late-stage, gross morphologic changes. Ideally, a method that detects the initial biochemical changes in disc degeneration would be valuable in preventing disease progression. Such a method would improve diagnostic capabilities and enable preventive measures to be taken at the early stages of the disease.

MRI has been widely used to detect IVDD because it is non-invasive, provides superior soft tissue contrast, and can be used to assess tissue hydration. To date, MRI has

been mostly used for morphologic, qualitative assessment of IVDD. Pfirrmann et al. (5) proposed a grading system for disc degeneration based on standard spin-echo sequences. With T_2 -weighted spin-echo imaging sequences, healthy intervertebral discs exhibit a bright signal from the nucleus pulposus and a low signal from the annulus fibrosus.

While the Pfirrmann grading system provides a semi-quantitative evaluation of disc degeneration, which is beneficial for morphological evaluation, MRI relaxation time measurements offer a quantitative assessment of disc composition. Quantitative relaxation time measurements are beneficial in that they compute a tissue material property, which should be scanner-independent (6). In addition, quantitative techniques are able to detect subtle differences in tissue composition that may not be apparent with qualitative or semi-quantitative measurements.

MRI T_2 relaxation time is a quantitative parameter that is sensitive to changes in collagen and water content in cartilage (7) and in the intervertebral disc (8). Studies have shown that T_2 relaxation time decreases with disc degeneration (9-13). Perry et al. measured T_2 in five subjects using an FSE sequence, and reported that the average T_2 values were greater in normal discs as compared to those graded as Pfirrmann Grade III or IV (12). Karakida et al. investigated diurnal changes in the disc by measuring T_2 in the morning and evening, and reported that degenerative discs had lower T_2 than healthy discs at both time points (14). These studies demonstrate that T_2 relaxation time may be a non-invasive biomarker for IVDD that is sensitive to changes in collagen and hydration in early disc degeneration.

Recent studies have proposed that MRI $T_{1\rho}$ relaxation time is associated with loss of macromolecules (15), which is an initiating factor in IVDD. $T_{1\rho}$ imaging, which probes the

interaction between water molecules and their macro-molecular environment, has the potential to identify early biochemical changes in the intervertebral disc. Recent *in vitro* studies have reported correlations between $T_{1\rho}$ and glycosaminoglycan (GAG) content (15), and have demonstrated a relationship between $T_{1\rho}$ and disc mechanical properties (9), suggesting that $T_{1\rho}$ may be sensitive to early biochemical changes in disc degeneration. *In vivo* studies have demonstrated differences in mean $T_{1\rho}$ values between the nucleus and the annulus (16), and have shown a correlation between $T_{1\rho}$ and degenerative grade in an asymptomatic population at 1.5 Tesla (10), thus demonstrating the feasibility of quantifying $T_{1\rho}$ in human subjects.

The purpose of this study was to [1] determine the relationship between $T_{1\rho}$ & T_2 relaxation time and degenerative grade in intervertebral discs using *in vivo* MR imaging at 3 Tesla, and to [2] determine the relationship between $T_{1\rho}$ & T_2 relaxation time and clinical findings as quantified by the SF-36 questionnaire and Oswestry Disability Index.

9.2 Methods

9.2.1 Subjects

Sixteen subjects (mean age = 40.2 ± 12.4 years, 10 males and 6 females, age range = 25- 60 years) participated in this study. Each subject completed the Oswestry Disability Index (O.D.I) (2) and SF-36 Health Survey Questionnaires (1). The patient inclusion criteria included: radiologic screening and MRI confirmation of degenerative disc disease in the lumbar spine at one or more levels, and clinical symptoms of discogenic back pain, having failed conservative management for more than 3 months (n=10). Additionally, a group of subjects (n=6) that had no clinical symptoms of back pain or sciatic pain participated in the study. Patients with prior back surgery, spine fractures, sacroiliac arthritis, degenerative

spondylolisthesis, metabolic bone disease, spinal infection, rheumatoid arthritis, active malignancy, and pregnancy were excluded from the study. Written informed consent was obtained from all patients after the nature of the examinations had been fully explained. All exams were performed in accordance with the rules and regulations from the local Human Research Committee.

9.2.2 Magnetic Resonance Imaging

MR imaging was performed using a GE SIGNA 3.0 Telsa echo-speed system (GE Healthcare, Waukesha, WI, USA). Single slice sagittal images for $T_{1\rho}$ mapping were acquired using a fast spin-echo sequence (TSL₁/TSL₂/TSL₃/TSL₄ (time of spin lock) = 0/40/80/120 ms, acquisition matrix = 256 x 192, resolution = 0.78 x 0.78 mm², spin lock (SL) power = 300 Hz, ETL = 8, FOV = 20 cm, BW = 31.25 KHz, slice thickness = 8mm, PE direction = A/P). Single slice sagittal images for T_2 mapping (TE₁-TE₇ = 9.6-77.2 ms, acquisition matrix = 256 x 192, resolution = 0.78 x 0.78 mm², FOV = 20cm, BW = 31.25 KHz, slice thickness = 8mm, PE direction = A/P) were acquired using a MSME (17). $T_{1\rho}$ quantification was performed in 16 patients (77 discs) while T_2 was quantified in only a subset of patients (9 patients, 44 discs) due to limitations in scan time. Additionally, sagittal T_2 -weighted images were acquired using a fast spin-echo sequence (TR/TE = 5000/70 ms, acquisition matrix = 320 x 224, resolution = 0.39 x 0.39 mm², ETL = 16, FOV = 20 cm, BW = 31.25 KHz, slice thickness=4mm, PE direction = A/P) were acquired for Pfirrmann grading (5) in all patients.

9.2.3 Image Analysis

Five intervertebral discs per subject were examined (80 discs total); however, discs with artifacts in the images due to patient motion were excluded in the analysis ($T_{1\rho}$ scans: 3

out of 80 discs, T₂ scans: 1 out of 45 discs). T_{1ρ} and T₂ maps were computed on a pixel-by-pixel basis using the following equations, respectively: $S(\text{TSL}) \propto \exp(-\text{TSL}/T_{1\rho})$, $S(\text{TE}) \propto \exp(-\text{TE}/T_2)$. Median T_{1ρ} and T₂ values were calculated in a 5-mm diameter section that was drawn manually in the center of the nucleus in discs L5/S1, L4/L5, L3/L4, L2/L3, and L1/L2 in each subject. This type of segmentation has been performed previously (9,10) demonstrating high inter-observer agreement ($r = 0.95$) for T_{1ρ} values. Figure 9.1 illustrates the procedure for T_{1ρ} mapping and creating the regions of interest (ROIs). Pfirrmann grading (5) was performed (by one musculoskeletal radiologist with 20 years of experience in musculoskeletal imaging) based on the T₂-weighted images; grades ranged from healthy (Pfirrmann grade 1) to severely degenerate (Pfirrmann grade 5).

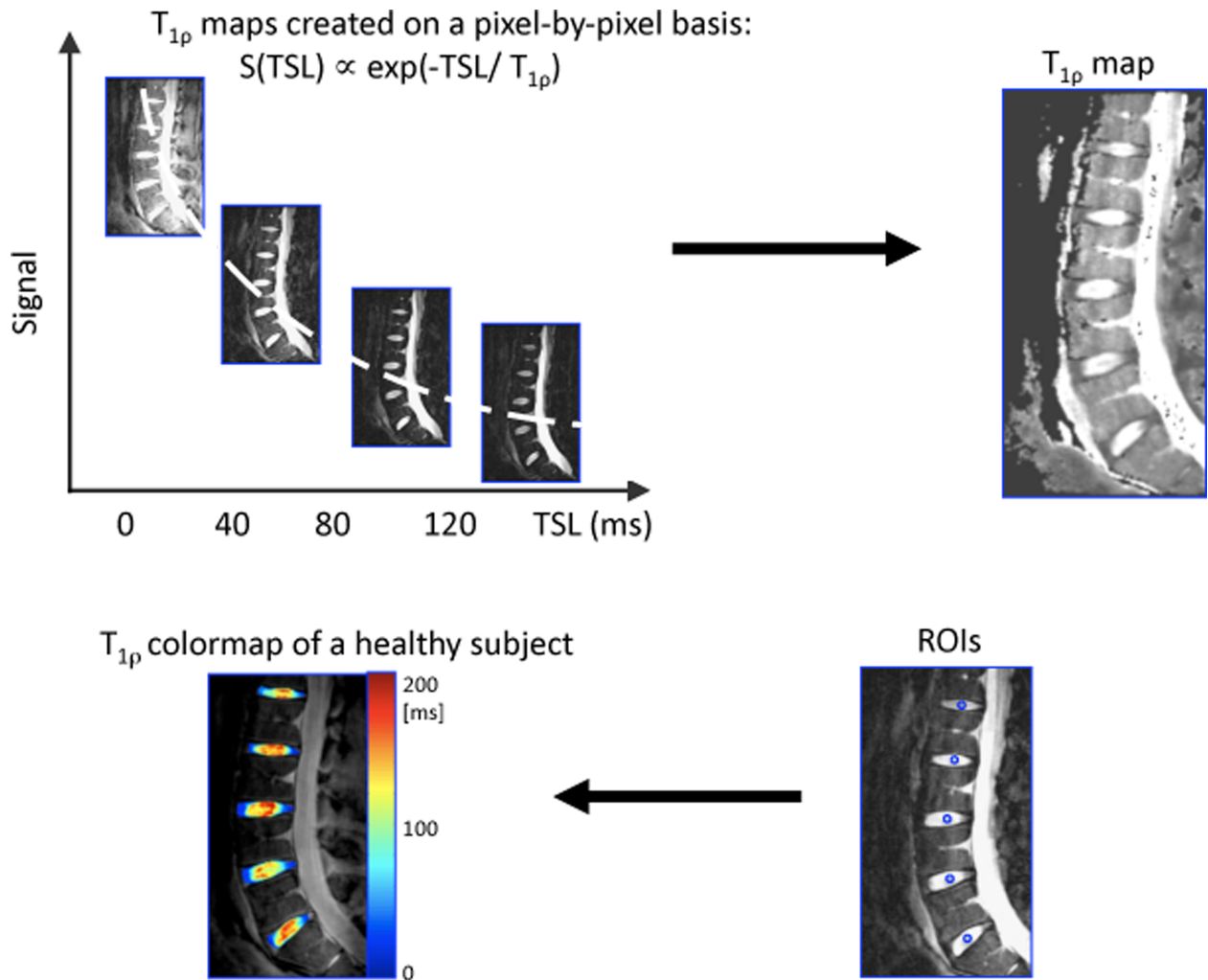


Figure 9.1: An illustration of the $T_{1\rho}$ fitting and quantification procedure. First, sagittal images for $T_{1\rho}$ mapping were acquired, and $T_{1\rho}$ maps were created on a pixel-by-pixel basis. A representative $T_{1\rho}$ map is shown. Median $T_{1\rho}$ and T_2 values were calculated in 5-mm diameter regions of interest (ROI's) that were drawn manually in the center of the nucleus in discs L5/S1, L4/L5, L3/L4, L2/L3, and L1/L2 in each subject. A $T_{1\rho}$ colormap of the intervertebral discs in a healthy subject is shown. T_2 maps were created analogously.

9.2.4 Statistical Analysis

A linear mixed-effects regression analysis (18,19) of MR parameters ($T_{1\rho}$ and T_2) on Pfirrmann Grade (with subject specific random effects to account for multiple discs measured within each subject) was performed to determine the relationship between $T_{1\rho}$ (or T_2) and degenerative grade. Mixed effects models provide explicit estimates of the amount and nature of the between- and within- person variation through explicit modeling of fixed and

random effects. The primary motivation for this modeling approach is that lumbar measurements have more variability between subjects than they do within subject. Pfirrmann grade is modeled as a fixed effect, i.e. differences in Pfirrmann grade between intervertebral discs (both within and between subjects) are modeled as having a constant change in $T_{1\rho}$ (or T_2). The random effect component models the mean of a subject's $T_{1\rho}$ (or T_2) (after accounting for Pfirrmann score) as a Gaussian (normal) distributed random observation from a population distribution. Individual lumbar measurements are then modeled as having an additional *within-subject* variation component (independently and identically distributed zero mean Gaussian variables). Additionally, confirmatory Spearman correlations (between Pfirrmann grade and $T_{1\rho}$ and Pfirrmann grade and T_2) were performed providing some insurance that the results were not unduly influenced by the Gaussian assumption.

Mixed effects models of MR parameters ($T_{1\rho}$, T_2 , Pfirrmann grade) regressed on clinical questionnaire scores (O.D.I and SF-36 Physical Health) were used to determine the relationship between $T_{1\rho}$ (or T_2 , or Pfirrmann grade) and clinical finding scores.

Spearman correlations were used to assess the relationship between $T_{1\rho}$ and T_2 values. Spearman correlations were also performed between the mean $T_{1\rho}$ (or T_2 or Pfirrmann Grade) in each subject and age, and between clinical questionnaire scores and age. All statistical analysis was performed using JMP Software (SAS Institute, Cary, NC, USA).

9.3 Results

9.3.1 T_2 and $T_{1\rho}$ versus Pfirrmann Grade

In this study, the intervertebral discs were categorized as Pfirrmann grade 1 (healthy, $n = 12$), grade 2 ($n = 42$), grade 3 ($n = 22$), grade 4 ($n = 3$) and grade 5 (severely degenerated, $n=1$, (80 discs total)). Representative $T_{1\rho}$ colormaps of a healthy subject, a subject with

moderate disc degeneration, and a subject with severe disc degeneration are shown in Figure 9.2.

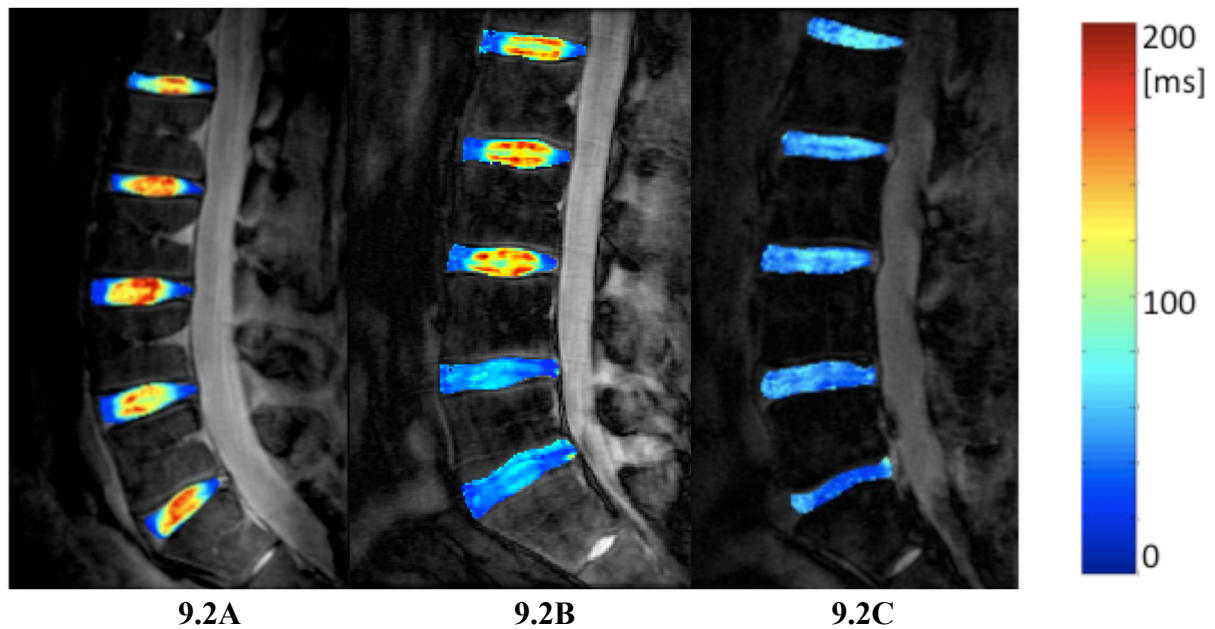


Figure 9.2: Representative $T_{1\rho}$ colormaps from 2A) a 24-year old subject with non-degenerated discs (Pfirrmann Grades L5/S1=1, L5/L4=1, L4/L3 = 1, L3/L2 =1; L2/L1 = 2) and an Oswestry Disability Index (O.D.I) score of 0; 2B) a 32-year old subject with mildly degenerated discs (Pfirrmann Grades L5/S1=3, L5/L4=3, L4/L3 = 2, L3/L2 =2; L2/L1 = 2) and an O.D.I score of 12; 2C) a 65-year old subject with mild and severely degenerated discs (Pfirrmann Grades L5/S1=5, L5/L4=4, L4/L3 = 3, L3/L2 =3; L2/L1 = 3) and an O.D.I score of 20. The $T_{1\rho}$ values in the healthy discs are greater than those in the degenerative discs.

Graphs of the median $T_{1\rho}$ and T_2 values of the discs are shown in Figures 9.3 and 9.4, respectively. Trends of decreasing $T_{1\rho}$ and T_2 values with increasing grade of degeneration were evident.

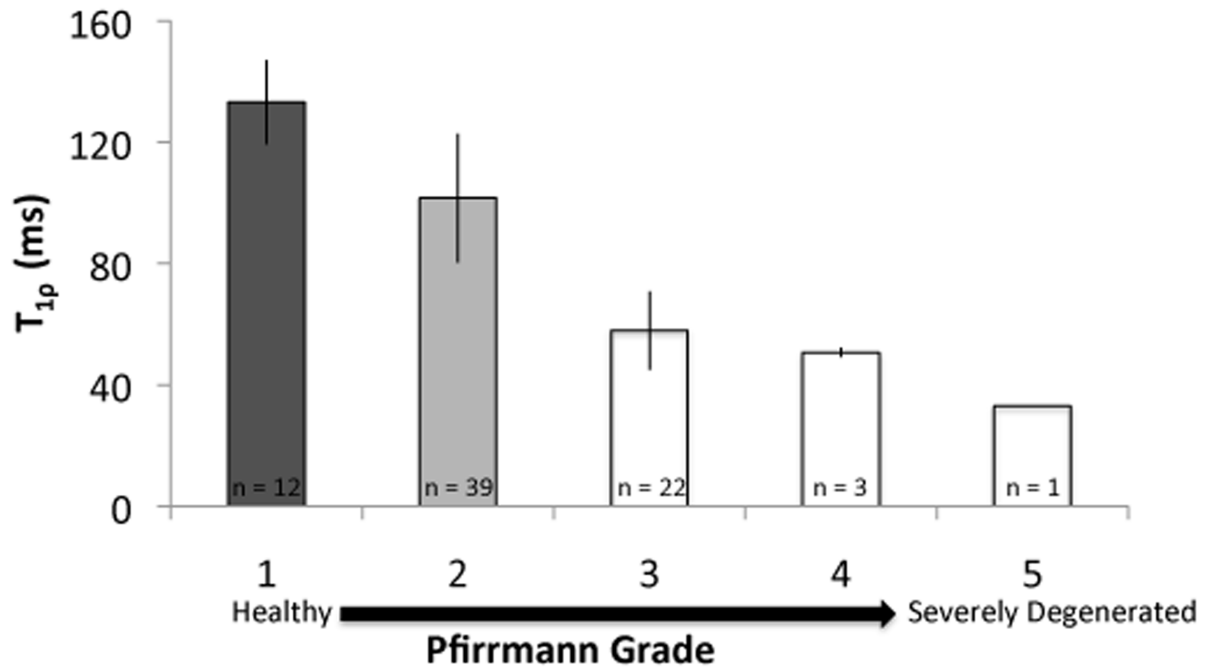


Figure 9.3: Median $T_{1\rho}$ values (\pm standard deviation) in each Pfirrmann grade are illustrated in the graph (16 patients, 77 discs). The plot is limited because it ignores differences between lumbar regions and is unable to properly account for the within- and between-subject structure of the data. However, the plot does provide a striking illustration of the behavior of $T_{1\rho}$ values with respect to Pfirrmann grade. Groups that are significantly different ($p < 0.05$) are categorized by different colors, as determined from the linear regression model. Note that the $T_{1\rho}$ values in the Pfirrmann grade 2 discs were significantly different from those in Pfirrmann grade 1, as evidenced by the mixed-effects regression model (which allows for subject-specific random effects), suggesting that $T_{1\rho}$ relaxation time may be sensitive to early degenerative changes.

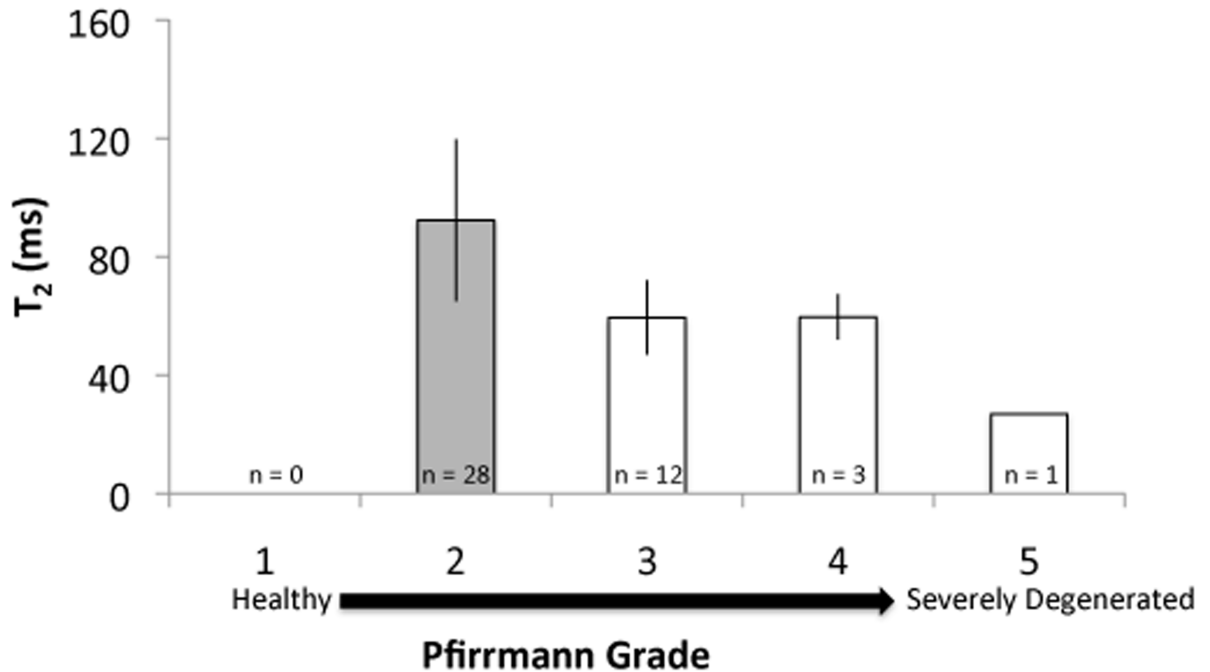


Figure 9.4: Median T_2 values (\pm standard deviation) in each Pfirrmann grade are illustrated ($n = 9$ patients, 44 discs) in the graph. The plot is limited because it ignores differences between lumbar regions and is unable to properly account for the within- and between-subject structure of the data. However, the plot does provide an illustration of the behavior of T_2 values with respect to Pfirrmann grade. Groups that are significantly different ($p < 0.05$) are categorized by different colors, as determined from the linear regression model.

The mean $T_{1\rho}$ values in discs with Pfirrmann grades 1 ($n = 12$), 2 ($n = 39$), 3 ($n = 22$), 4 ($n=3$), and 5 ($n=1$) were 133.1 ± 13.8 ms, 101.5 ± 21.2 ms, 57.9 ± 12.9 ms, 50.6 ± 1.52 ms, 33 ms, respectively. The mean T_2 values in discs with Pfirrmann grades 1 ($n = 0$), 2 ($n = 28$), 3 ($n = 12$), 4 ($n=3$), and 5 ($n=1$) were 92.3 ± 27.2 ms, 59.5 ± 12.5 ms, 59.6 ± 7.6 ms, 37 ms, respectively. The linear mixed-effects regression analysis showed a significant ($p < 0.05$) difference in relaxation time ($T_{1\rho}$ and T_2) values among the Pfirrmann grade groups. A significant difference in the $T_{1\rho}$ values between Pfirrmann grade 1 and all the other grades was evident ($p < 0.05$). The T_2 values showed similar trends: the T_2 values in Pfirrmann grade 2 discs were significantly different from those in more degenerative grades (Pfirrmann grade

> 2). (Note that, of the subset of patients that had T₂ mapping scans (n=9, 44 discs), none had discs that were graded as Pfirrmann 1.) Spearman correlations demonstrated that Pfirrmann grade was correlated with both T_{1ρ} (r = -0.84, p<0.01) and T₂ (r = -0.61, p<0.01). Subject age was also associated with T_{1ρ} (r = -0.81, p<0.01), T₂ (r = -0.51, p>0.05), and Pfirrmann Grade (r = 0.64, P<0.01). The correlation between T_{1ρ} and T₂ values was r = 0.76 (p<0.01), Table 9.1.

Table 9.1: Spearman correlations (r) between MR parameters, clinical questionnaire scores, and subject age.

Parameter	Parameter	r	p
T _{1ρ}	T ₂	0.76	< 0.01
T _{1ρ}	Pfirrmann Grade	-0.84	< 0.01
T ₂	Pfirrmann Grade	-0.61	< 0.01
T _{1ρ}	Age	-0.81	< 0.01
T ₂	Age	-0.51	> 0.05
Pfirrmann Grade	Age	0.64	< 0.01
O.D.I	Age	0.62	< 0.05
SF-36	Age	-0.61	< 0.05

9.3.2 MR Parameters Versus Clinical Findings

The MR parameters (T_{1ρ}, T₂, Pfirrmann Grade) were highly correlated with clinical questionnaire scores (O.D.I, and SF-36 Physical Health, Table 2). However, only the correlations between T_{1ρ} and the clinical questionnaire scores (O.D.I and SF-36 Physical health) were significant (p < 0.05). The relationship between T_{1ρ} and O.D.I was r² = 0.56 (p < 0.05) and the relationship between T_{1ρ} and SF-36 was r² = 0.55 (p<0.05). A significant

relationship was not found between T_2 and clinical questionnaire scores or between Pfirrmann Grade and clinical questionnaire scores.

Table 9.2: Relationship (R^2) between Clinical Questionnaire Scores (O.D.I. and SF-36 Physical Health) and MR parameters ($T_{1\rho}$, T_2 , and Pfirrmann Grade). The R^2 value, calculated using the JMP procedure for mixed effects models, accounts for both within- and between-subject variation.

		MR Parameters (R^2)		
		$T_{1\rho}$	T_2	Pfirrmann Grade
Clinical Questionnaires	Disability Index (O.D.I)	0.56*	NS	NS
	Physical Health (SF-36)	0.55*	NS	NS

* $p < 0.05$;

NS = not significant

9.3.3 T_2 and $T_{1\rho}$ by Disc Level

Decreasing $T_{1\rho}$ and T_2 values from L1/L2 to L5/S1 were evident. The average $T_{1\rho}$ values in discs L1/L2, L2/L3, L3/4, L4/L5, and L5/S1 were 106.3 ± 22.2 ms, 102.6 ± 31.0 ms, 97.6 ± 29.5 ms, 79.3 ± 30.5 ms, and 72.3 ± 36.4 ms, respectively. The average T_2 values in discs L1/L2, L2/L3, L3/4, L4/L5, and L5/S1 were 99.1 ± 39.3 ms, 85.4 ± 26.2 ms, 84.3 ± 22.4 ms, 68.8 ± 18.9 ms, and 61.7 ± 23.7 ms, respectively (Figure 9.5).

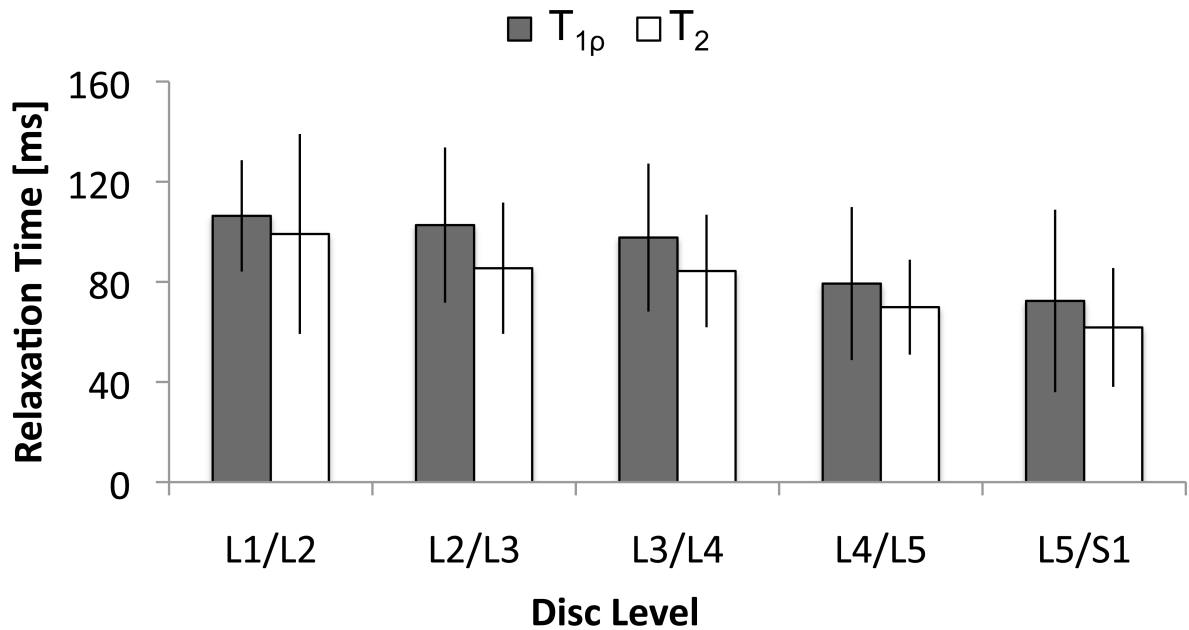


Figure 9.5: Decreasing trends in $T_{1\rho}$ and T_2 values were evident in disc level L1/L2 to L5/S1.

9.4 Discussion and Conclusion

In this study, MR $T_{1\rho}$ and T_2 relaxation were measured in subjects with different grades of disc degeneration and clinical symptoms. This study confirmed the previously reported negative relationship between relaxation time ($T_{1\rho}$ and T_2) and disc degenerative grade (9-13). In addition, $T_{1\rho}$ relaxation time was significantly associated with clinical symptoms quantified using the O.D.I and SF-36 Physical Health questionnaires. A negative relationship between relaxation times ($T_{1\rho}$ and T_2) and age was evident, corroborating results from other studies (9,12,14-16,20). This study suggests that $T_{1\rho}$ relaxation time may be sensitive to early degenerative changes and clinical symptoms in IVDD.

$T_{1\rho}$ relaxation time decreased with increasing severity of disc degeneration, and was lowest in disc L5/S1, compared to other disc levels. It is interesting to note that the $T_{1\rho}$ values in the Pfirrmann grade 2 discs were significantly lower than those in Pfirrmann grade 1 discs, suggesting that *in vivo* $T_{1\rho}$ quantification may detect changes early changes in IVDD.

T_2 relaxation time showed similar trends: T_2 decreased with increasing grade of disc degeneration. Due to the limited number of Pfirrmann grade 4 and 5 discs observed in the study, we were unable to make conclusions about the effects of severely degenerative discs on $T_{1\rho}$ and T_2 values.

The results of this study indicate that $T_{1\rho}$ and T_2 relaxation time are correlated ($r = 0.76$, $p < 0.01$) and are both sensitive to disc degeneration. $T_{1\rho}$ and T_2 relaxation times in structured tissues such as cartilage and intervertebral disc are associated with the slow-motion interaction between bulk water and its macromolecular environment. Previous studies in cartilage have shown that T_2 relaxation time is highly related to collagen integrity (due to a strong dipole-dipole interaction) (21,22), while not very sensitive to changes in macromolecules such as proteoglycan (23). Spin-lock techniques used in $T_{1\rho}$ quantification sequences have shown to reduce residue dipolar interaction, thus enabling a larger dynamic range and less dependence on collagen fibers (24). Consequently, $T_{1\rho}$ has shown to be more sensitive than T_2 to macromolecular changes, such as PG loss (23). Some investigators have suggested that proton exchange between the protein side-chain groups of GAG and bulk water contribute significantly to the $T_{1\rho}$ relaxation in cartilage (25,26). The relationship between $T_{1\rho}$ and T_2 relaxation times and the composition of the extracellular matrix in disc is not clear and warrants further investigation. The reduction of $T_{1\rho}$ and T_2 with degenerated discs observed in this study may be caused by reduced water content (15). In addition, visual differences in the $T_{1\rho}$ and T_2 colormaps are evident. Representative $T_{1\rho}$ and T_2 colormaps of two discs from one subject are shown in Figure 9.6. Changes in both the range and spatial distribution of $T_{1\rho}$ and T_2 values are visible, suggesting that $T_{1\rho}$ and T_2 may provide complementary information about the integrity of the disc. The spatial distribution

of $T_{1\rho}$ and T_2 values has been previously investigated in cartilage: A study by Li et al. (27) assessed the relationship between $T_{1\rho}$ and T_2 values in osteoarthritic cartilage: although mean $T_{1\rho}$ and T_2 values were elevated in OA cartilage, the spatial distribution of these values was different. Moreover, $T_{1\rho}$ has an elevated dynamic range as compared to T_2 (27,28), which may impact the sensitivity of measurement to subtle changes. These studies suggest that although $T_{1\rho}$ and T_2 are correlated, they provide differing information regarding the integrity of the IVD, as evidenced by differences in spatial distribution, dynamic range, and sensitivity to macromolecular composition.

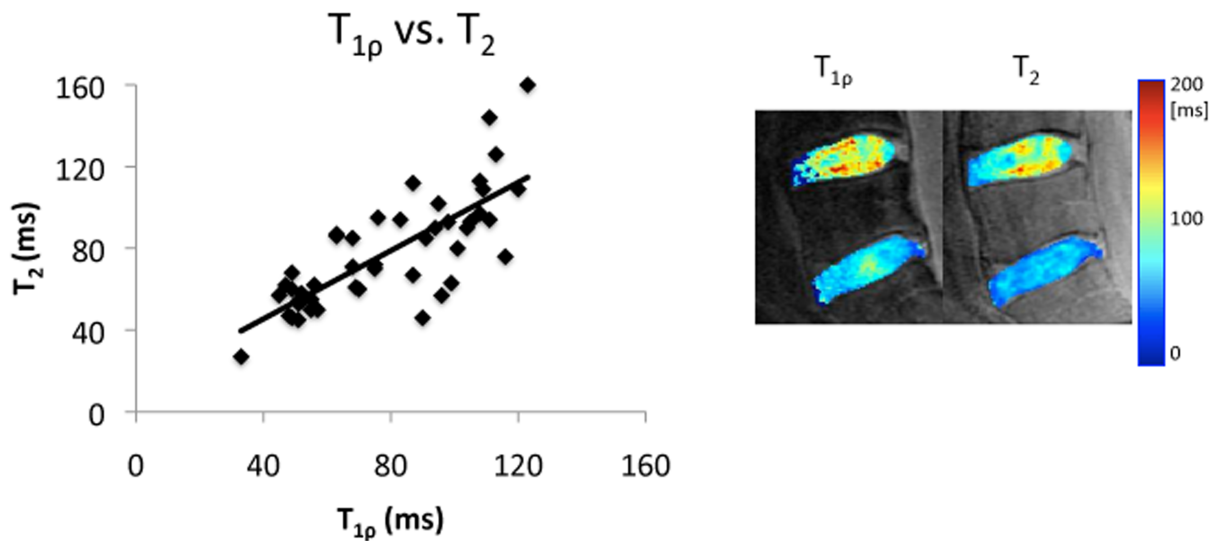


Figure 9.6: The correlation between $T_{1\rho}$ and T_2 values was $r = 0.76$ ($p < 0.01$). The figure shows a $T_{1\rho}$ and T_2 map in the same subject. The disparity between the $T_{1\rho}$ and T_2 values is evident by the differences in the spatial distribution and range of values in the discs.

Studies have shown that the relationship between relaxation times ($T_{1\rho}$ and T_2) in IVDD is in the opposite direction to that of cartilage degeneration (10,29-34). While the mechanisms for degenerative changes in these tissues is still under investigation, the

differences in relaxation times may be linked to the varying tissue compositions and material properties. Cartilage is a laminar structure composed of three primary layers with varied concentrations of macromolecules, while the intervertebral disc is composed of hydrated-gel center (nucleus pulposus), which is surrounded by rows of concentric collagen lamellae (annulus fibrosus). Since cartilage and intervertebral disc tissues vary in composition and size, their intrinsic relaxation properties may differ with degeneration. Previous studies have also suggested that decreases in $T_{1\rho}$ relaxation time in IVDD may be due to fibrosis and cross-linking with degeneration (9). Additional in vitro studies are warranted to further evaluate the pathogenesis of IVDD and the role of MR relaxometry in its non-invasive assessment.

This study examined the relationship between MR $T_{1\rho}$ relaxation time and clinical symptoms in degenerative disc disease. The strong and significant correlations between $T_{1\rho}$ and SF-36 physical health and O.D.I scores suggest that $T_{1\rho}$ may be a useful biomarker for clinical symptoms related to degenerative disc disease. While this study demonstrates a relationship between $T_{1\rho}$ and physical symptoms in subjects with low back pain, the mechanism by which disc degeneration causes low back pain is unclear. Studies have suggested various causes for discogenic back pain: innervations of the inner portion of the disc can occur during degeneration and may be responsible for discogenic back pain (35); the outer annulus has been reported to be the origin of pain reproduced during discography (36). MR imaging studies have identified characteristics of discs in subjects which include decreases in the signal intensity of the disc (37). Thus, a variety of discogenic changes are linked to low back pain, however the mechanisms behind this relationship remain to be determined.

The reproducibility of $T_{1\rho}$ quantification at 3 Tesla using a spiral readout acquisition has been previously reported (16). The coefficient of variation (CV) for phantoms was less than 3% and the CV for *in vivo* quantification was less than 5%. The current study used the same $T_{1\rho}$ preparation pulses as Blumenkrantz et al. (16), however, an FSE readout instead of spiral readout was implemented. A FSE readout was desirable because a spiral readout lacks an anti-aliasing filter and thus cannot be used to acquire sagittal images of the spine. Moreover, sagittal scans minimize partial volume effects, which were often encountered in the axial scans of the disc.

While a single spin-lock power of 300Hz was implemented in this study, previous work by Regatte et al. has demonstrated $T_{1\rho}$ dispersion (over a range of 0 to 3000 Hz) in bovine intervertebral discs (38). Their study also reported that $T_{1\rho}$ has a higher dynamic range than T_2 . Therefore, it is suspected that varying the RF field strength would directly impact image contrast and relaxation time measurement.

The primary limitations of this study were the small sample size (especially for T_2 quantification), the lack of T_2 data for early stages of disc degeneration, and the fact that a spin locking (SL) power of 300 Hz was used in the $T_{1\rho}$ sequence; in $T_{1\rho}$ imaging, a high SL power is desirable, however, is it limited by specific absorption rate (SAR). An SL power of 300Hz was the maximum SL power that could be obtained given our scanning hardware without exceeding the SAR limit.

In this study $T_{1\rho}$ and T_2 relaxation times were calculated in subjects with IVDD and clinical symptoms. This study demonstrates that MRI relaxation time ($T_{1\rho}$ and T_2) decreases with increasing grade of disc degeneration, and that $T_{1\rho}$ values were related to clinical symptoms, as measured by the O.D.I and SF-36 Physical Health questionnaires. This study

shows a potential for the future use of MR imaging markers in the evaluation of treatment efficacy.

9.5 References:

1. Ware JE, Jr., Sherbourne CD. The MOS 36-item short-form health survey (SF-36). I. Conceptual framework and item selection. *Med Care* 1992;30(6):473-483.
2. Fairbank JC, Couper J, Davies JB, O'Brien JP. The Oswestry low back pain disability questionnaire. *Physiotherapy* 1980;66(8):271-273.
3. McHorney CA, Ware JE, Jr., Lu JF, Sherbourne CD. The MOS 36-item Short-Form Health Survey (SF-36): III. Tests of data quality, scaling assumptions, and reliability across diverse patient groups. *Med Care* 1994;32(1):40-66.
4. Fairbank JC, Pynsent PB. The Oswestry Disability Index. *Spine* 2000;25(22):2940-2952; discussion 2952.
5. Pfirrmann CW, Metzdorf A, Zanetti M, Hodler J, Boos N. Magnetic resonance classification of lumbar intervertebral disc degeneration. *Spine* 2001;26(17):1873-1878.
6. Marinelli NL, Haughton VM, Munoz A, Anderson PA. T2 relaxation times of intervertebral disc tissue correlated with water content and proteoglycan content. *Spine* 2009;34(5):520-524.
7. Xia Y. Magic-angle effect in magnetic resonance imaging of articular cartilage: a review. *Invest Radiol* 2000;35(10):602-621.
8. Weidenbaum M, Foster RJ, Best BA, Saed-Nejad F, Nickoloff E, Newhouse J, Ratcliffe A, Mow VC. Correlating magnetic resonance imaging with the biochemical content of the normal human intervertebral disc. *Journal of Orthopaedic Research* 1992;10(4):552-561.
9. Nguyen AM, Johannessen W, Yoder JH, Wheaton AJ, Vresilovic EJ, Borthakur A, Elliott DM. Noninvasive quantification of human nucleus pulposus pressure with use of T1rho-weighted magnetic resonance imaging. *J Bone Joint Surg Am* 2008;90(4):796-802.

10. Auerbach JD, Johannessen W, Borthakur A, Wheaton AJ, Dolinskas CA, Balderston RA, Reddy R, Elliott DM. In vivo quantification of human lumbar disc degeneration using T(1rho)-weighted magnetic resonance imaging. *Eur Spine J* 2006.
11. Kerttula L, Kurunlahti M, Jauhiainen J, Koivula A, Oikarinen J, Tervonen O. Apparent diffusion coefficients and T2 relaxation time measurements to evaluate disc degeneration. A quantitative MR study of young patients with previous vertebral fracture. *Acta Radiol* 2001;42(6):585-591.
12. Perry J, Houghton V, Anderson PA, Wu Y, Fine J, Mistretta C. The value of T2 relaxation times to characterize lumbar intervertebral disks: preliminary results. *AJNR Am J Neuroradiol* 2006;27(2):337-342.
13. Chiu EJ, Newitt DC, Segal MR, Hu SS, Lotz JC, Majumdar S. Magnetic resonance imaging measurement of relaxation and water diffusion in the human lumbar intervertebral disc under compression in vitro. *Spine* 2001;26(19):E437-444.
14. Karakida O, Ueda H, Ueda M, Miyasaka T. Diurnal T2 value changes in the lumbar intervertebral discs. *Clin Radiol* 2003;58(5):389-392.
15. Johannessen W, Auerbach JD, Wheaton AJ, Kurji A, Borthakur A, Reddy R, Elliott DM. Assessment of human disc degeneration and proteoglycan content using T1rho-weighted magnetic resonance imaging. *Spine* 2006;31(11):1253-1257.
16. Blumenkrantz G, Li X, Han ET, Newitt DC, Crane JC, Link TM, Majumdar S. A feasibility study of in vivo T1rho imaging of the intervertebral disc. *Magn Reson Imaging* 2006;24(8):1001-1007.
17. Maier CF, Tan SG, Hariharan H, Potter HG. T2 quantitation of articular cartilage at 1.5 T. *Journal of Magnetic Resonance Imaging* 2003;17(3):358-364.
18. McCulloch CE, Searle SR. *Generalized, linear, and mixed models*: Wiley-Interscience; 2004.
19. Littell RC, Milliken GA, Stroup WW, Wolfinger RD. *SAS system for mixed models*: SAS Institute, Cary, NC; 1996.
20. Wang C, Auerbach JD, Witschey WR, Balderston RA, Reddy R, Borthakur A. *Advances in Magnetic Resonance Imaging for the assessment of degenerative disc disease of the lumbar spine*. *Semin Spine Surg* 2007;19(2):65-71.

21. Mosher TJ, Smith H, Dardzinski BJ, Schmithorst VJ, Smith MB. MR imaging and T2 mapping of femoral cartilage: in vivo determination of the magic angle effect. *AJR Am J Roentgenol* 2001;177(3):665-669.
22. Yang X, Tony F, Nancy B-W, George L. Origin of cartilage laminae in MRI. *Journal of Magnetic Resonance Imaging* 1997;7(5):887-894.
23. Regatte RR, Akella SV, Borthakur A, Kneeland JB, Reddy R. Proteoglycan depletion-induced changes in transverse relaxation maps of cartilage: comparison of T2 and T1rho. *Acad Radiol* 2002;9(12):1388-1394.
24. Akella SV, Regatte RR, Wheaton AJ, Borthakur A, Reddy R. Reduction of residual dipolar interaction in cartilage by spin-lock technique. *Magn Reson Med* 2004;52(5):1103-1109.
25. Makela HI, Grohn OH, Kettunen MI, Kauppinen RA. Proton exchange as a relaxation mechanism for T1 in the rotating frame in native and immobilized protein solutions. *Biochem Biophys Res Commun* 2001;289(4):813-818.
26. Duvvuri U, Goldberg AD, Kranz JK, Hoang L, Reddy R, Wehrli FW, Wand AJ, Englander SW, Leigh JS. Water magnetic relaxation dispersion in biological systems: the contribution of proton exchange and implications for the noninvasive detection of cartilage degradation. *Proc Natl Acad Sci U S A* 2001;98(22):12479-12484.
27. Li X, Benjamin Ma C, Link TM, Castillo DD, Blumenkrantz G, Lozano J, Carballido-Gamio J, Ries M, Majumdar S. In vivo T(1rho) and T(2) mapping of articular cartilage in osteoarthritis of the knee using 3T MRI. *Osteoarthritis Cartilage* 2007.
28. Regatte RR, Akella SV, Lonner JH, Kneeland JB, Reddy R. T1rho relaxation mapping in human osteoarthritis (OA) cartilage: comparison of T1rho with T2. *J Magn Reson Imaging* 2006;23(4):547-553.
29. Regatte R, Akella S, Lonner J, Kneeland J, Reddy R. T1rho relaxation mapping in human osteoarthritis (OA) cartilage: comparison of T1rho with T2. *J Magn Reson Imaging* 2006;23(4):547-553.
30. Li X, Benjamin Ma C, Link TM, Castillo DD, Blumenkrantz G, Lozano J, Carballido-Gamio J, Ries M, Majumdar S. In vivo T(1rho) and T(2) mapping of

- articular cartilage in osteoarthritis of the knee using 3 T MRI. *Osteoarthritis Cartilage* 2007;15(7):789-797.
31. Li X, Han E, Ma C, Link T, Newitt D, Majumdar S. In vivo 3T spiral imaging based multi-slice T(1rho) mapping of knee cartilage in osteoarthritis. *Magnetic resonance in medicine* 2005;54(4):929-936.
 32. Li X, Ma C, Link T, Castillo D, Blumenkrantz G, Lozano J, Carballido-Gamio J, Ries M, Majumdar S. In vivo T1rho and T2 mapping of articular cartilage in osteoarthritis of the knee using 3 Tesla MRI. *Osteoarthritis and Cartilage* 2007;15(7):789-797.
 33. Duvvuri U, Reddy R, Patel SD, Kaufman JH, Kneeland JB, Leigh JS. T1rho-relaxation in articular cartilage: effects of enzymatic degradation. *Magn Reson Med* 1997;38(6):863-867.
 34. Antoniou J, Mwale F, Demers CN, Beaudoin G, Goswami T, Aebi M, Alini M. Quantitative magnetic resonance imaging of enzymatically induced degradation of the nucleus pulposus of intervertebral discs. *Spine* 2006;31(14):1547-1554.
 35. Coppes MH, Marani E, Thomeer RT, Groen GJ. Innervation of "painful" lumbar discs. *Spine* 1997;22(20):2342-2349; discussion 2349-2350.
 36. Moneta GB, Videman T, Kaivanto K, Aprill C, Spivey M, Vanharanta H, Sachs BL, Guyer RD, Hochschuler SH, Raschbaum RF. Reported pain during lumbar discography as a function of annular ruptures and disc degeneration. A re-analysis of 833 discograms. *Spine* 1994;19(17):1968-1974.
 37. Luoma K, Riihimaki H, Luukkonen R, Raininko R, Viikari-Juntura E, Lamminen A. Low back pain in relation to lumbar disc degeneration. *Spine* 2000;25(4):487-492.
 38. Regatte RR, Akella SV, Borthakur A, Reddy R. High Resolution T1rho Relaxation and Dispersion Imaging of the Intervertebral Disc. *Proceedings of the ISMRM*. Kyoto, Japan; 2004. p 1544.

Chapter 10: Summary and Conclusions

10.1 Summary

This thesis described the development of a methodology for non-invasive characterization of early biochemical changes in the extracellular matrix in cartilage and the intervertebral disc. The results demonstrate that MR $T_{1\rho}$ and T_2 times can be used to investigate the changes in the ECM during IVDD and OA. The research studies performed highlights that not only mean values of MR $T_{1\rho}$ and T_2 times are valuable for the assessment of the ECM – the quantification of their spatial distribution is essential for the comprehensive characterization of tissue properties in disease progression.

10.2 Conclusions

10.2.1 MR Relaxation Time Mapping Technique Development

Chapter 4 described the impact of signal to noise ratio and T_2 fitting algorithms on the T_2 quantification. Simulations were performed determine the minimum SNR that can be used to distinguish healthy cartilage from degenerative cartilage in the Osteoarthritis Initiative. The results demonstrated that a minimum SNR (of the first echo) of 12 could be used to accurately calculate and distinguish healthy from degenerate cartilage. In addition, the choice of fitting algorithm (noise correction vs. no noise correction) did not impact the accuracy of T_2 quantification, even though the goodness of fit was improved using the noise correction algorithm.

10.2.2 MR T_2 Relaxation Time Mapping in Osteoarthritis

Chapter 5 examined the relationship between structural changes of trabecular bone and cartilage in patients with varying degrees of OA over two years, using MR imaging. MR

images were acquired for assessing trabecular bone structure and cartilage structure, in addition to measuring T_2 relaxation time. A total of thirty-eight subjects were scanned at baseline and twelve months. Of these subjects, twenty-one were scanned again at twenty-four months (drop-outs due to death, knee replacement, and unwillingness to continue). The severity of each subject's OA at baseline was evaluated using the x-ray based Kellgren-Lawrence (KL) scale (17): KL scores of 1 and 2 were considered mild OA ($n = 13$); KL scores of 3 and 4 were considered severe OA ($n = 17$). Additionally, a group of control subjects with no radiographic evidence of OA ($n = 8$) was included in the study. Cartilage parameters, including thickness, volume, and T_2 were calculated in various cartilage compartments including the medial and lateral tibia, and medial and lateral femur. Trabecular bone parameters, including volume fraction, trabecular number, trabecular spacing, and trabecular thickness were calculated at each time point.

The results demonstrated trends of decreasing bone and cartilage parameters in osteoarthritic subjects (especially in mild OA subjects) over time. The mean T_2 increased significantly ($p < 0.05$) between the baseline and follow-up exams for all cartilage compartments except the lateral tibia. A positive relationship was established between cartilage changes and localized bone changes closest to the joint line, while a negative relationship was established between cartilage changes and global bone changes farthest from the joint line. This study demonstrated a longitudinal relationship between the changes in bone and cartilage structure in patients with varying degrees of OA.

Chapter 6 focused on the evaluation of cartilage T_2 in subjects with and without OA. Specifically, the goals of this study were to characterize the spatial distribution of cartilage T_2 in postmenopausal OA patients and age-matched healthy subjects using second order

texture measures at baseline, and analyze changes in the texture of cartilage T_2 after 9 months in both groups. 3 Tesla-MRI of the knee was performed in 8 mild OA patients and 10 age-matched controls at baseline and after 9 months. Cartilage T_2 maps, volume and average thickness were calculated in all patients. Texture analysis was performed on the cartilage T_2 maps using the grey level co-occurrence matrix method. Texture parameters, including entropy and angular second moment, were calculated at 0° (corresponding to the anterior-posterior axis) and at 90° (corresponding to the superior-inferior axis), with pixel offsets ranging from 1-3 pixels.

Least square means analysis showed that mean T_2 values, their standard deviation, and their entropy were greater ($p < 0.05$) in OA patients than in controls. Over 9 months, the standard deviation and entropy of cartilage T_2 significantly ($p < 0.05$) decreased in OA patients, while no significant changes were evident in cartilage thickness or volume. The mean T_2 values, their standard deviation, and their entropy were greater in OA patients than in controls, indicating that the T_2 values in osteoarthritic cartilage are not only elevated, but also more heterogeneous than those in healthy cartilage. The longitudinal results demonstrate that changes in texture parameters of cartilage T_2 may precede morphological changes in thickness and volume in the progression of OA.

Chapter 7 focused on the longitudinal changes in the spatial distribution of cartilage T_2 values in subjects with OA. This study evaluated both the morphologic and biochemical changes in cartilage using MR imaging as well as clinical data from the OAI. The purpose of this study is to [1] examine changes in MR knee cartilage parameters including thickness, T_2 , and spatial distribution of cartilage T_2 and [2] examine whether these baseline MR

parameters predict change in knee pain. Western Ontario and McMaster Universities (WOMAC) pain score was assessed in each patient (n = 13) at baseline, year 1, and year 2.

Median cartilage T_2 was calculated in each region. Texture analysis was used to examine the spatial distribution of T_2 relaxation times in an image. Texture parameters including angular second moment (ASM), entropy, homogeneity, and contrast were calculated from the GLCM. Longitudinal decreases in mean cartilage thickness were evident in all cartilage compartments over two years. The annual rate of cartilage loss was significant ($p < 0.05$, Table 7.1) in the lateral femur (-2.66% per year), lateral tibia (-1.41% per year), and medial tibia (-3.63% per year). The mean cartilage T_2 showed little change over time, with exception of the lateral tibia, which decreased -4.00% annually ($p < 0.05$). Entropy of cartilage T_2 at baseline (all compartments combined except the lateral tibia) was associated with an increase in WOMAC pain score over 2 years ($p < 0.05$). This study demonstrated that the baseline heterogeneity of cartilage T_2 is associated with changes in clinical pain scores.

10.2.3 MR T_2 and $T_{1\rho}$ Relaxation Time Mapping in Degenerative Disc Disease

Chapter 8 assessed novel MRI methods for non-invasive detection of disc degeneration. The purpose of this study was to test the feasibility of quantifying $T_{1\rho}$ relaxation time in phantoms and to apply the technique to intervertebral discs of healthy volunteers using *in vivo* MR imaging at 3T. A multi-slice $T_{1\rho}$ spiral sequence was used to quantify $T_{1\rho}$ relaxation time in phantoms with different agarose concentrations and in the intervertebral disc of eleven healthy volunteers (mean age = 31.3 years, age range = 23-60 years, gender: 5 females, 6 males).

The phantom studies demonstrate the feasibility of using spiral imaging at 3T. The *in vivo* results indicate that the median $T_{1\rho}$ value of the nucleus (116.6 ± 21.4 ms) is significantly greater ($p < 0.05$) than that of the annulus (84.1 ± 11.7 ms). The correlations between age of the volunteers and $T_{1\rho}$ relaxation time in the nucleus ($r^2 = -0.82$, $p = 0.0001$) and annulus ($r^2 = -0.37$, $p = 0.04$) were significant. A trend of decreasing $T_{1\rho}$ values from L3-L4 to L4-L5 to L5-S1 was evident. The results of this study suggest that *in vivo* $T_{1\rho}$ quantification is feasible and may potentially be a clinical tool to identify early degenerative changes in the intervertebral disc.

Chapter 9 built upon the results from the third study, by evaluating $T_{1\rho}$ and T_2 in subjects with varying degrees of disc degeneration. Specifically, the goals of this study were to [1] determine the relationship between $T_{1\rho}$ & T_2 relaxation time and degenerative grade in intervertebral discs using *in vivo* 3.0 Tesla MR imaging, and to [2] determine the relationship between $T_{1\rho}$ & T_2 relaxation time and clinical findings as quantified by the SF-36 Questionnaire and Oswestry Disability Index (O.D.I). Sixteen subjects participated in this study, and each completed SF-36 and O.D.I questionnaires. MRI $T_{1\rho}$ and T_2 mapping were performed to determine $T_{1\rho}$ and T_2 relaxation times in the nucleus of the intervertebral disc, and T_2 -weighted images were acquired for Pfirrmann grading (80 discs total).

Pfirrmann grade was correlated with both $T_{1\rho}$ ($r = -0.84$, $p < 0.01$) and T_2 ($r = -0.61$, $p < 0.01$). A positive relationship was evident between MR parameters ($T_{1\rho}$, T_2 , Pfirrmann Grade) and clinical questionnaire scores. Only the correlations between $T_{1\rho}$ and the clinical questionnaire scores were significant ($p < 0.05$). A negative relationship between degenerative grade and relaxation time was demonstrated in this study. In addition, $T_{1\rho}$ was significantly associated with clinical symptoms. This study suggests that $T_{1\rho}$ relaxation time

may be sensitive to early degenerative changes and clinical symptoms in intervertebral disc degeneration.

The results of this project suggest that quantifying the spatial distribution of $T_{1\rho}$ and T_2 relaxation times improve the clinical assessment of IVDD and OA, as they provide a non-invasive evaluation of biochemical composition in the intervertebral disc and cartilage tissues. The trends in degenerative changes in the ECM vary between OA and IVDDD, and are specific to the tissue biochemical characteristics. $T_{1\rho}$ and T_2 relaxation times are not only sensitive to biochemical changes in OA and IVDD, they are also valuable for the prediction of pain.

10.3 Future Directions

In addition to investigating subjects with mild and severe osteoarthritis (as performed in this dissertation), it would be valuable to assess MR relaxation time parameters in subjects at risk for OA and develop pain over time. At baseline, it would be interesting to evaluate the relationship between cartilage biochemical composition as quantified using the mean, spatial distribution, and laminar organization of T_2 relaxation time, and morphologic knee joint degeneration in the cartilage, meniscus and bone marrow in subjects at risk for the development of OA. In addition, a prospective analysis would help determine whether baseline cartilage biochemical composition can predict the presence of symptomatic knee OA, defined as development of pain and an increase in morphologic degeneration in the cartilage, meniscus, and bone marrow after two years. Finally, a longitudinal analysis would determine whether changes in cartilage biochemical composition are related to the presence of symptomatic knee OA.

UCSF Library Release

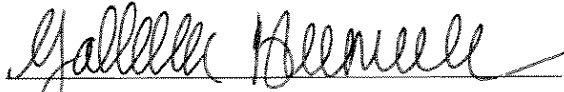
The last page of your dissertation must have the following language:

Publishing Agreement


It is the policy of the University to encourage the distribution of all theses, dissertations, and manuscripts. Copies of all UCSF theses, dissertations, and manuscripts will be routed to the library via the Graduate Division. The library will make all theses, dissertations, and manuscripts accessible to the public and will preserve these to the best of their abilities, in perpetuity.

Please sign the following statement:

I hereby grant permission to the Graduate Division of the University of California, San Francisco to release copies of my thesis, dissertation, or manuscript to the Campus Library to provide access and preservation, in whole or in part, in perpetuity.



Author Signature



Date

(This page must be signed and dated by the author and include the correct pagination – the last page number of your document.)